INVESTIGATIONS OF CARBON NANOTUBE BASED ELECTRONIC DEVICES WITH FOCUS ON METAL AND CARBON NANOTUBE CONTACTS

HUANG LEIHUA

NATIONAL UNIVERSITY OF SINGAPORE

2011

INVESTIGATIONS OF CARBON NANOTUBE BASED ELECTRONIC DEVICES WITH FOCUS ON METAL AND CARBON NANOTUBE CONTACTS

HUANG LEIHUA

(*B. Sci. (Hons.), Fudan University*)

A THESIS SUBMITTED

FOR THE DEGREE OF DOCTOR OF PHILOSOPHY

DEPARTMENT OF ELECTRICAL AND COMPUTER ENGINEERING

NATIONAL UNIVERSITY OF SINGAPORE

2011

ACKNOWLEDGMENTS

Many individuals deserved to be appreciated for their contributions and support to the completion of the work within this dissertation.

First and foremost, I would like to express my deep gratefulness to my thesis advisor, Prof. Chor Eng Fong who made the whole work possible. My experience of working as a student of Prof. Chor is an invaluable treasure, which will benefit my whole life. Her experience, knowledge and side by side guidance have been invaluable throughout my graduate career. I feel lucky to have her as mentor, and will always cherish these years being a student of hers.

I would also like to express my appreciation to my co-supervisor Prof. Wu Yihong for providing insightful suggestions and devoting a lot of his precious time to my work. He creates every opportunity to help me to connect, learn, and benefit from other researchers in the field. I have been truly benefited from his valuable opinions, encouragement, and the collaboration with his lab.

I am also deeply indebted to my co-supervisor Dr. Guo Zaibing in Data Storage Institute (DSI) for extensive discussions for my work and creating a lot of opportunities for me to use the equipments of DSI which is extremely helpful to my research work. I have learned much knowledge and skills about process and

characterization of semiconductors from Dr. Guo, which leads me to a better understanding on my own and other people's research work.

I would also especially like to thank Ms. Musni bte Hussain and Mr. Tan Beng Hwee who have provided me a joyful working environment and much great help in centre for optoelectronics (COE). My gratitude also goes to Mr Loh Suan Bin who was an undergraduate in Prof Chor's group. He helped optimize the dispersion process of carbon nanotube solution which has been a great help on my dissertation projects.

Finally I want to thank my parents for their unconditional love and always standing by me and my wife, Dr. Li yanfeng, for her enormous sacrifice to support my work.

Table of Contents

Page

ACKNOWLEDGEMENT i

TABLE OF CONTENTS.. iii

SUMMARY ix

LIST OF TABLES xii

LIST OF FIGURES xiii

LIST OF SYMBOYS..xx

LIST OF ABBREVIATIONS..xxii

CHAPTER

1 INTRODUCTION 1

1.1 The transport characteristic of single wall carbon nanotube 2

1.2 Carbon nanotube and metal contact 4

1.2.1 Atomic structure of carbon nanotube and metal contacts 4

1.2.1.1 Carbon nanotube and metal contact with side-contact structure........6

1.2.1.2 Carbon nanotube and metal contact with end-contact structure.........7

1.2.1.3 Summary of the atomic structure of carbon nanotube and metal contacts 8

1.2.2 Charge transfer between metals and carbon nanotube contacts 9

1.3 Carbon Nanotube based devices 12

1.3.1 Carbon nanotube field effect transistors (CNTFET) 13

1.3.1.1 *p*-type carbon nanotube field effect transistors 13

1.3.1.2 Ambipolar carbon nanotube field effect transistors 16

1.3.1.3 *n*-type carbon nanotube field effect transistors 17

1.3.1.4 The challenges of CNTFET.. 19

1.3.2 Carbon nanotube diodes.. 22

1.4 Motivation and Synopsis of Thesis 24

1.4.1 Ohmic metal carbide and SWCNT contacts 26

1.4.2 Random network carbon nanotube transistor 27

1.4.3 Schottky carbon nanotube diodes by contact engineering..................... 30

1.4.4 Double-Wall carbon nanotube field effect transistors 31

1.5 Outline of thesis 33

2 EXPERIMENTAL PROCEDURE FOR THE FABRICATION AND CHARACTERIZATION OF CARBON NANOTUBE BASED DEVICES 35

2.1 Preparation of carbon nanotube solution for device fabrication 35

2.1.1 Dispersion of carbon nanotubes 35

2.1.2 Purification of carbon nanotube solutions 40

2.2 Fabrication procedure of individual single wall carbon nanotube field effect transistor 42

2.2.1 Alignment of carbon nanotubes 42

2.2.1.1 Floating potential AC dielectrophoresis 42

2.2.1.2 Large scale AC dielectrophoresis 49

2.2.2 The formation of metal and carbon nanotube contacts 51

2.2.3 Removal of metallic carbon nanotubes 54

2.3 characterization of carbon nanotube based devices 59

2.3.1 Morphological characterization of carbon nanotube devices 59

2.3.2 Electrical characterization of carbon nanotube devices 61

2.4 Summary 62

3 HIGH PERFORMANCE CNTFET WITH NIOBIUM CARBIDE CONTACT 64

3.1 Advantages of metal carbides 64

3.2 The formation of niobium carbide at SWCNT and Niobium contacts 66

3.3 XRD characterization of niobium carbides 69

3.4 Electrical properties of niobium carbide in CNTFET 72

3.5 Comparison of niobium carbide contacts with titanium carbide and palladium contacts 81

3.6 summary 86

4 *n*-TYPE RANDOM NETWORK SINGLE-WALL CARBON NANOTUBE FIELD EFFECT TRANSISTOR WITH YTTRIUM CONTACTS 88

4.1 The advantages of carbon nanotube thin film transistors 88

4.2 The status of *n*-type rn-SWCNT FET 89

4.3 Fabrication procedure of Yttrium contacted rn-SWCNT FET 91

4.4 The electrical characterization of rn-SWCNT FET with Yttrium contacts
.... 93

4.5 Optimization of rn-SWCNT FET by chemical etching 102

4.6 Summary 110

5 THE SEMICONDUCTING-SEMICONDUCTING DOUBLE WALL
CARBON NANOTUBE FIELD EFFECT TRANSISTORS 112

5.1 The unique electrical properties of double wall carbon nanotube 112

5.2 The Status of DWCNT FET 113

5.3 The fabrication procedure of DWCNT FET 114

5.4 The electrical characteristics of DWCNT FET 116

5.4.1 The relationship between DWCNT FET characteristics and the structure
of DWCNT 116

5.4.2 Comparison between *s*-*s* DWCNT FET and *s*-SWCNT FET 118

5.4.2.1 For large diameter nanotubes (d ≥ 2 nm) 120

5.4.2.2 For intermediate diameter nanotubes (2 > d ≥ 1.6 nm) 126

5.4.2.3 For small diameter nanotubes (d < 1.6 nm) 128

5.5 The Ruthenium contacted DWCNT FET 130

5.6 Summary 133

6 FABRICATION OF SINGLE-WALL CARBON NANOTUBE SCHOTTKY DIODE WITH ASYMMETRIC THIOLATE MOLECULES MODIFIED GOLD CONTACTS 135

6.1 Carbon nanotube Schottky diodes 135

6.2 The fabrication procedure of SWCNT Schottky diodes with thiolate molecules 139

6.3 The electrical characteristic of the SWCNT Schottky diodes 142

6.3.1 The modification effect of thiolate molecules on the SWCNT and Au contacts 142

6.3.2 The working mechanism of the SWCNT Schottky diodes 149

6.3.3 Enhancing SWCNT Schottky diode performance using asymmetric thiolate molecules modified gold contacts 154

6.3.4 The effect of back gate voltage on the electrical characteristic of the SWCNT Schottky diodes 157

6.3.5 The stability of SWCNT Schottky diodes by thiolate molecules 159

6.4 Summary 161

7 CONCLUSIONS AND SUGGESTED FUTURE WORK 162

7.1 Conclusion 162

7.1.1 High performance CNTFET with niobium carbide contact 162

7.1.2 *n*-type random network single-wall carbon nanotube field effect transistor with Yttrium contacts 163

7.1.3 Fabrication of single-wall carbon nanotube Schottky diode with gold contacts modified by asymmetric thiolate molecules 164

7.1.4 Semiconducting-semiconducting double-wall carbon nanotube field effect transistors 165

7.2 Suggested future work on carbon nanotube electronics 167

7.2.1 Other metal carbide contacts for CNTFET application 167

7.2.2 Metal gate engineering 168

7.2.3 Graphene FETs 169

7.2.3.1 Brief comparison between graphene and CNT 169

7.2.3.2 Comparison between graphene FET and CNTFET 170

7.2.3.3 Future work on graphene and metal contact 172

Reference 174

List of publications 195

Summary

Carbon nanotube field effect transistors (CNTFETs) have attracted much attention owing to their potential importance to integrated circuits. However, to date, there are still challenges faced by CNTFET, e.g., the optimization of Ohmic contacts between CNT and metal, the precise position and alignment of CNT, and the presence of both metallic and semiconducting CNTs during synthesis and the inability to remove all the metallic CNTs during subsequent device fabrication.

In our work, we have developed a thermal solid state reaction method to achieve niobium carbide (Nb_2C) between single wall CNT (SWCNT) and niobium (Nb) electrodes. It is found that the Nb_2C contact exhibits very small Schottky barrier (~18meV) to *p*-type transport which means near Ohmic contact to SWCNT has been achieved. More importantly, the Schottky barrier between SWCNT and Nb_2C contact is almost independent of the tube diameter (d) for d down to 1 nm. The performance of Nb_2C contacted SWCNT FET is as good as that with Pd contacts for $d > 1.6$ nm and better when d is smaller than 1.6 nm. In addition, Nb_2C contact surpasses titanium carbide (TiC) contacts by yielding more unipolar FET characteristic.

In order to overcome the challenges of alignment and positioning issues of CNT and of removing metallic CNTs in device fabrication, we have also developed thin film FET based on random network of SWCNT. Owing to the lack of study on *n*-type random network SWCNT FETs (rn-SWCNT FETs), we focus

on their fabrication by means of contact engineering, using low work function metal Yttrium. As expected, the rn-SWCNT FETs have better reproducibility than FETs based on individual SWCNT. By employing 2,4,6-triphenylpyrylium tetrafluoroborate (2,4,6-TPPT) to selectively etch the metallic nanotubes in the rn-SWCNT, the FETs achieve high on/off current ratio up to $\sim 10^5$, good unipolar characteristic with n-/p-branch current ratio $\sim 10^3$-10^4, high mobility $\sim 25\ cm^2 v^{-1} s^{-1}$, and transconductance ~0.12 μS/μm. Moreover, they have demonstrated air-stable *n*-type characteristics.

We have also demonstrated that SWCNT Schottky diodes can be fabricated by asymmetrically modifying the Schottky barrier at the two Au/SWCNT contacts. In our work, thiolate molecules methanethiol (CH_3SH) and trifluoroethanethiol (CF_3CH_2SH) are used to achieve such modification and the characterizations have revealed that the highly asymmetrical contacts with Schottky barrier heights of ~190 and ~40 meV, respectively, can be achieved for the modified Au/SWCNT contacts. The SWCNT Schottky diodes exhibit good performance: forward and reverse current ratio higher than 10^4, forward current as high as ~5 μA, reverse leakage current as low as ~100 pA, and current ideality factor as low as ~1.42. This is at least comparable to SWCNT Schottky diodes fabricated with asymmetrical metals which have been well developed.

In addition to the study on CNT and metal contacts, we have investigated the transport characteristics of double wall carbon nanotube with both

semiconducting tubes (*s-s* DWCNT). It has been found that the tube-tube interaction in *s-s* DWCNT is important to the transport characteristic of DWCNT and is dependent on the diameter of DWCNT. Hence, the *s-s* DWCNT FET can behave differently from SWCNT FET as a result of the variation of the inter-tube interactions. In general, the conductance of *s-s* DWCNT is found to be larger than that of SWCNT with the same diameter, owing to the weaker electron–phonon scattering in the DWCNT than that in SWCNT as a result of inter-tube interaction. However, when the tube diameter is very small (<1.6 nm), the bandgap of *s-s* DWCNT is greatly reduced owing to the π-σ rehybridization of the even smaller inner tube. Therefore, it is suggested that DWCNT FET can be one promising candidate of CNT based devices in addition to SWCNT FET. In the study of DWCNT FETs, it has also been found that ruthenium oxide (RuO_2) can form near-Ohmic contact with DWCNT owing to its high work function and good wetting properties with DWCNT.

List of tables

Table 1.1 CNFET Technology Challenges and Outlook

Table 2.1: Suppliers and parameters of CNT (SWCNT & DWCNT) samples used in our experiments.

List of Figures

Fig. 1.1: Two types of interface between a metal crystal and a carbon nanotube: end-contact (top) and side-contact (bottom).

Fig. 1.2: Schematic of a back-gated SWCNT FET

Fig. 1.3: Band structure diagram of a *p*-type SB-CNTFET. (a) With no bias on the gate, a large Schottky barrier exists between the valence band of the CNT and the Fermi level (Ef) of the source contact. A positive bias on the source lowers the Fermi level of the source and raises the level of the drain. (b) A negative bias on the gate raises the conduction and valence band of the CNT. The shift in bands leads to a narrower Schottky barrier at the source/CNT interface and allows holes to be transported from the source to the valence band of the CNT.

Fig. 1.4: Schematics of a rn-SWCNT FET.

Fig. 2.1: Dispersed CNT solution by NaDDBS (~ 0.1 M), after homogenization for 20 minutes (left), and after 2 weeks on storage (right).

Fig. 2.2: (a) Schematic diagram of the centrifugation process for removal of impurities in the CNT solution. (b) The CNT solution before and after the centrifugation process.

Fig. 2.3: Schematic of AC dielectrophoresis setups: normal AC dielectrophoresis (top figure) and floating potential AC dielectrophoresis (bottom figure), which has additional floating electrode compared to the normal AC dielectrophoresis.

Fig. 2.4: (a) The schematic layout of floating-potential AC dielectrophoresis (FPD) - region I is the controlled region and region II is the floating region. The arrows in the figure indicate the distribution of electric field in these regions. (b) Schematic layout of wafer scale floating- potential

AC dielectrophoresis, and the experiment setup (top view): one probe is put on the biased electrode (BE) and another probe on the substrate of the probe station (GE).

Fig. 2.5: SEM pictures showing the results of floating potential dielectrophoresis: (a) the controlled region (I), where both SWCNT bundles and amorphous carbons are attracted to the electrodes, and (b) the floating region (II), where only one individual SWCNT is aligned across the electrodes.

Fig. 2.6: SEM picture of device based on individual SWCNT fabricated by wafer scale AC dielectrophoresis. The arrow indicate the positon of the SWCNT.

Fig. 2.7: Fabrication process of CNTFETs with CNTs lying on top of metal electrodes: (a) high doping *n*-type silicon substrate is used as the back gate, (b) SiO_2 is grown as the gate insulator by means of thermal oxidation, (c) resist is spin-coated onto the surface of substrate, (d) lithography is carried out to define the shape and position of the metal electrodes, (e) exposed resist is removed by the appropriate developer, (f) metals are deposited by electron beam evaporation, g) metal lift-off is performed with the help of ultra-sonicator, h) CNTs in the solution are deposited onto the top surface of metal electrodes, and the fabricated devices are cleaned by rinsing in DI water and dried by nitrogen gas.

Fig. 2.8: the I_{DS}-V_{GS} curves of a CNTFET with a bundle of SWCNTs as the channel, before and after the electrical breakdown process (V_{DS} = 8 V and V_{GS} = 10 V).

Fig. 2.9: I_{DS}-V_{GS} curves of a CNTFET whose channel has both metallic and semiconducting SWCNTs, before and after the chemical etching process using 2,4,6-TPPT molecules (V_{DS} = 0.1 V).

Fig. 2.10: Electrical measurement setups for (a) CNTFET, and (b) CNT diode.

Fig. 3.1: SEM picture of a typical Nb contacted SWCNT FET, the alignment of one individual SWCNT between two Nb electrodes is achieved by using AC dielectrophoresis with applied AC voltage $V_{P\text{-}P}$ ~ 8 V, frequency f ~ 1 MHz and duration time t ~ 1 minutes.

Fig. 3.2: SEM pictures of a typical Nb and SWCNT contact: (a) before, and (b) after annealing in vacuum at 700 ^{o}C for 1 *hr* (resulted in the formation of niobium carbide, Nb_2C). The SWCNT lying on the Nb electrode becomes invisible after the formation of Nb_2C, signifying that the SWCNT has embedded into the electrode.

Fig. 3.3: XRD spectra of SWCNT thin film deposited on 50 nm Nb layer: (a) before annealing. (b) after vacuum annealing at 700 ℃ for 1 *hr* (resulted in Nb_2C formation), and (c) after vacuum annealing at 900 ℃ for 1 *hr* (resulted in additional NbC formation). The spectrum after annealing at 400 ^{o}C is similar to that without annealing.

Fig. 3.4: (a) I_{DS}-V_{GS} curves (V_{DS} = 0.1 V) for the SWCNT FET with Nb contacts before and after vacuum annealing at 400, 700, 900 ^{o}C for 1 hr. (b) Corresponding I_{DS}-V_{DS} curves of the SWCNT FET at V_{GS} = 0 V and the inset is an expanded curve of the SWCNT FET after vacuum annealing at 400 ^{o}C for 1 hr. The diameter of the SWCNT in the CNTFET is ~ 1.5 nm.

Fig. 3.5: Plots of (a) $\ln(I/T^2)$ versus $1/T$ from 200 to 300 K for different bias voltages, V = 0.1 to 0.5 V in steps of 0.1 V, to determine the contact effective Schottky barrier height (Φ_e) for hole transport, gate bias V_{GS}=0V, and (b) effective SBH as a function of the square root of bias voltage ($V^{1/2}$). Schottky barriers at zero bias voltage (Φ_b) are attracted for devices after annealing at 400, 700 and 900 ^{o}C, respectively.

Fig. 3.6: I_{DS}-V_{GS} curves (V_{DS} = 0.1 V) of Nb_2C contacted SWCNT FET immediately after the formation of Nb_2C and after exposure to air for 10 days

Fig. 3.7: I_{DS}-V_{GS} curves (V_{DS} = 0.1V) for Nb_2C, TiC and Pd contacted SWCNT FETs (SWCNT diameter ~1.5 nm). Inset shows the corresponding I_{DS}-V_{DS} curves (V_{GS} = 0 V).

Fig. 3.8: I_{DS}-V_{DS} curves (V_{GS} = 0 V) for (a) Pd contacted SWCNT FETs with 1.53 and 1 nm SWCNTs, and (b) Nb_2C contacted SWCNT FETs with 1.6 and 1 nm. Insets show the I_{DS}-V_{GS} curves (V_{DS} = 0.1 V) for SWCNT FETs.

Fig. 4.1: SEM picture of random network of SWCNTs on the SiO_2 substrate.

Fig 4.2: (a) SEM picture of a RN-SWCNT FET with Yttrium source and drain contacts (the lighter shade regions in figure), and (b) radial breathing mode Raman characteristic of the RN-SWCNT on the SiO_2 substrate.

Fig. 4.3: IV characteristics of a rn-SWCNT FET (channel length, L_C = 4 μm; channel width, W_C = 10 μm): (a) I_{DS}-V_{GS} curve at V_{DS} = 0.1 V in linear scale for V_{GS} from -10 to 10 V, and the inset shows the curve in semi logarithmic scale; and (b) I_{DS}-V_{DS} curves at V_{GS} = 10, 5, and -5 V for V_{DS} From 0 to 1 V.

Fig. 4.4: The effects of rn-SWCNT FET channel length on transistor characteristics: (a) *n*-branch On-current (I_{ON}), (b) Off-current (I_{OFF}), (c) *p*-branch on-current (I_p), (d) on/off current ratio (I_{ON}/I_{OFF}) and (e) *n*-/*p*-branch current ratio (I_{ON}/I_p). The channel width, W_C = 10 μm and the data indicated are averages of 20 devices.

Fig. 4.5: Schematics showing the 4 simplified types (I, II, III, IV) of transport routes in the RN-SWCNT FET channel. An example of combination transport route (Type II-IV) is also shown.

Fig. 4.6: (a) I_{DS}-V_{GS} curves (V_{DS} = 0.1 V) of Y contacted rn-SWCNT FET (L_C = 4 μm, W = 10 μm) before and after the reaction with 2,4,6-TPPT, (b) I_{DS}-V_{GS} curves (V_{DS} = 0.1 V) of 20 RN-SWCNT FETs (L_C = 4 μm, W = 10 μm) after reaction with 2,4,6-TPPT, demonstrating the small deviation in the On-current of RN-SWCNT FETs, and (c) the effect of reaction time on the I_{DS}-V_{GS} curve of Y contacted rn-SWCNT FET (L_C = 2 μm, W = 10 μm).

Fig. 4.7: The effects of chemical etching by 2,4,6-TPPT on the distribution of (a) on/off current ratio (I_{ON}/I_{OFF}), and (b) *n-/p*-branch on-current ratio (I_{ON}/I_p) of rn-SWCNT FETs (L_C = 4 μm, W = 10 μm).

Fig. 4.8: I_{DS}-V_{GS} (V_{DS} = 0.1 V) curves of a rn-SWCNT FET (L_C = 4 μm, W = 10 μm and after reaction with 2,4,6-TPPT,) with Y/Au (50/30 nm) electrodes, immediately after fabrication, and after 1 day and 7 days exposure to air.

Fig. 5.1: (a) Schematic layout of a back-gated carbon nanotube FET, where the carbon nanotube was deposited on the top of Ti/Au electrodes by AC dielectrophoresis, and (b) SEM picture of a typical DWCNT FET, (c) TEM picture of DWCNTs.

Fig. 5.2: (a) I_{DS}-V_{GS} curves of three types of DWCNT-FETs: metallic (*m-m*/*m-s*), semi-metallic (*s-m*) and semiconducting (*s-s*) characteristics. The diameter of the DWCNTs exhibiting metallic, semi-metallic and semiconducting characteristics are 2.4, 2.37 and 2.34 nm, respectively. (b) I_{DS}-V_{GS} curves of two types of SWCNT-FETs: semiconducting (*s*) and metallic (*m*). The diameter of the SWCNTs exhibiting metallic and semiconducting characteristics are 1.96 and 2 nm, respectively.

Fig. 5.3: The I_{DS}-V_{GS} (V_{DS} = 0.1 V) comparison between DWCNT and SWCNT FETs. The diameters of DWCNT and SWCNT are respectively: a) 2.34 and 2.31 nm, b) 1.62 and 1.6 nm, and c) 1.38 and 1.34 nm.

Fig. 5.4: The On-current (I_{ON}) and Off-current (I_{OFF}) of DWCNT and SWCNT FETs as a function of the nanotube diameter. I_{ON} is I_{DS} at V_{GS} = -10 V and V_{DS} = 0.1 V, while I_{OFF} is the lowest I_{DS} in the range of V_{GS} from -10 to 10 V. the solid red lines are the polynomial fitted curves and the symbols are the experimental data.

Fig. 5.5: (a) Plots of ln(I/T^2) versus 1/T for T from 200 to 300 K for different bias voltages (V = 0.1 to 0.5 V in steps of 0.1 V) for DWCNT and Au Schottky contact, V_{GS}=0V. The biased dependent SBH (Φ_e) is extracted and plotted in (b) as a function of bias voltage ($V^{1/2}$) to yield the Schottky barrier height at zero bias voltage: Φ_b. The data for SWCNT and Au Schottky contact are also shown in (b).

Fig. 5.6: Effect of the drain field on the I_{DS}-V_{GS} characteristics of DWCNT FET and SWCNT FETs, V_{DS}= 0.1 V, 1 V and 3 V.

Fig. 5.7: The I_{DS}-V_{GS} (V_{DS} = 10 mV) characteristics of Ru contacted DWNT FETs annealed in vacuum or O_2 ambient at 400°C for 15 mins, in comparison with that of transistor without annealing, the diameter of DWCNT is about 2.5 nm.

Fig. 6.1: Fabrication of SWCNT Schottky diodes by asymmetrically tuning the Fermi level lineup at the two Au/SWCNT contacts using different thiolate molecules: (a) methanethiol (CH_3SH) and (b) trifluoroethanethiol (CF_3CH_2SH). The Au/SWCNT contact structure and the dipole direction (indicated by arrows) formed between Au and the absorbed self-assembled thiolate molecules are shown in (c) for CH_3SH and (d) for CF_3CH_2SH.

Fig. 6.2: I_{DS}-V_{GS} curves (V_{DS} = 0.1 V) for back-gated SWCNT FETs as a function of modification duration by (a) methanethiol (CH_3SH) and (b) trifluoroethanethiol (CF_3CH_2SH).

Fig. 6.3: *I-V* curves of Au-SWCNT-Au structures before and after modification by different thiolate molecules: methanethiol (CH_3SH) and trifluoroethanethiol (CF_3CH_2SH) in (a) linear scale; (b) semi-log scale.

Fig. 6.4: I_{DS}-V_{GS} curves (V_{DS} = 0.1 V) for SWCNT FETs with only SWCNT channels modified by thiolate molecules and SWCNT/Au contacts are protected by resist: (a) by CH_3SH; (b) by CF_3CH_2SH.

Fig. 6.5: Energy band diagrams of Au-SWCNT-Au structure under forward and reverse bias: (a), (b) before modification; (c), (d) after modification by thiolate molecules, CH_3SH and CF_3CH_2SH. In the Figure, solid arrow indicates thermionic emission current and dashed arrow indicates tunneling current.

Fig. 6.6: (a) Plots of ln (I/T^2) versus 1/T for T from 200 to 300 K for different bias voltages (V = 0.1 to 0.5 V in steps of 0.1 V) for SWCNT and Au Schottky contact, V_{GS}=0V. The biased dependent SBH (Φ_e) is extracted and plotted in (b) as a function of bias voltage ($V^{1/2}$) to yield the Schottky barrier height at zero bias voltage: Φ_b.

Figure 6.7: I-V characteristics of SWCNT Schottky diode at different gate voltages (V_{GS}= -10, 0 and 10 V) in semi-log scale.

Figure 6.8: *I-V* curves of SWCNT Schottky diode fabricated by SAM technology after fabrication and after 5 days of exposure to air.

List of Symbols

Symbol	Meaning
A	Ampere
Al	Aluminum
Ag	Silver
Au	Gold
C	capacitance
Ca	Calcium
cm	centimeter
Co	Cobalt
Cr	Chromium
d	diameter of carbon nanotube
e	elementary charge
$\vec{E}$	Electric field
E_g	energy bandgap
$\vec{F}$	Coulombic force
f	frequency
f_T	cut-off frequency
Fe	Iron
Gd	Gadolinium
g_m	transconductance
h	Planck's constant
Hf	Hafnium
Hz	hertz
I_{DS}	source-drain current
$I_{forward}$	forward current
$I_{reverse}$	reverse current
I_n	*n*-branch On-current
I_p	*p*-branch On-current
I_s	reverse saturation current
I_{OFF}	off current
I_{ON}	on current
k	Boltzmann's constant
L	liter
L_C	channel length
m-	metallic
Mg	Magnesium
Mn	Manganese
µm	micron-meter

Mo	Molybdenum
n	current ideality factor
N_2	Nitrogen
Nb	Niobium
Ni	Nickel
nm	nano-meter
O_2	Oxygen
$\vec{P}$	dipole moment
Pd	Palladium
Pt	Platinum
q	Electronic charge
R_S	lumped series resistance
Rh	Rhodium
Ru	Ruthenium
s	seconds
S	Siemens
s-	semiconducting
Sc	Scandium
Si	Silicon
T	time
T_{ox}	oxide thickness
Ti	Titanium
V	Volts
V_{TH}	threshold voltage
V_{DS}	source-drain voltage
V_{GS}	gate-source voltage
W	Tungsten
W_C	channel width
Y	Yttrium
Zr	Zirconium
ε_0	Permittivity of free space
ε_{SiO2}	Permittivity of SiO_2
Φ_m	metal work function
Φ_b	Schottky barrier height at zero bias
Φ_e	Schottky barrier height for electrons
Φ_h	Schottky barrier height for holes
Ω	Ohm

List of abbreviations

1D	one dimensional
2D	two dimensional
3D	three dimensional
2,4,6-TPPT	2,4,6-triphenylpyrylium tetrafluoroborate
AC	alternating current
AFM	atomic force microscopy
BE	biased electrode
CE	counter electrode
CF_3CH_2SH	trifluoroethanethiol
CH_3SH	methanethiol
CMOS	Complementary metal–oxide–semiconductor
CNT	carbon nanotube
CNTFET	carbon nanotube field effect transistor
CVD	chemical vapor deposition
CCVD	catalytic chemical vapor deposition
DC	direct current
dec	decade
DOS	density of states
DWCNT	double wall carbon nanotube
EBL	electron beam lithography
Fe_3C	Iron carbide
FPD	floating-potential AC dielectrophoresis
GE	gate electrode
GFET	graphene field effect transistor
GNR	graphene nanoribbon
H_2SO_4	Sulfuric acid
hr	hour
$HSCH_2CH_2NH$	2-aminoethanethiol
i-SWCNT	individual single wall carbon nanotube
NaDDBS	sodium dodecylbenzene sulfonate
Nb_2C	niobium carbide
PEI	Polyethyleneimine
RBM	radial breathing mode
rf	radio frequency

rn-SWCNT	random network single wall carbon nanotube
rpm	round per minute
RuO_2	ruthenium oxide
SAM	self-assembled monolayers
SB	Schottky barrier
SBFET	Schottky barrier field effect transistor
SBH	Schottky barrier height
SEM	Scanning Electron Microscope
Si_3N_4	silicon nitride
SiO_2	silicon dioxide
SWCNT	single wall carbon nanotube
TEM	transmission electron microscopy
TFT	thin film transistor
TiC	titanium carbide
VLSI	Very-large-scale integration
XRD	X-ray diffraction

Chapter 1

Introduction

In the past few decades, exciting developments in electronics have been achieved as a result of the continuous miniaturization of silicon based electronic devices. However, with devices becoming smaller and smaller, the limitations in both fundamental physics and technologies have been realized to be the significant challenges to modern electronic devices. The realization of the approaching limits sparked an intense search for alternative technologies. The effort involves searching for new device principles or new materials. Some approaches abandon traditional electron transport-based electronics but take use of other physical principles: for example, developing devices based on spin transport. Another approach maintains the operating principles of the currently used electronic devices, primarily that of the field-effect transistor, but replaces a key component of the device — the conducting channel (silicon), with new materials (Avouris et al., 2007). Among these materials, carbon nanotube (CNT) is considered one of the promising candidates owing to its superior physical and electronic properties (Avouris et al., 2003).

In this chapter, we will first examine briefly the electronic structure and electrical transport properties of CNTs, mainly that of the single wall carbon nanotube (SWCNT), which is the simplest form of CNT. The focus is on the

physical phenomena involved, which will help us better understand how the CNT based devices work. In the latter part, a brief review of the CNT based devices, e.g., field effect transistors and diodes will be presented with particular emphasis on the CNT and metal contacts. Finally, the motivation of this dissertation will be presented.

1.1 The transport characteristic of single wall carbon nanotube

One of the most attractive properties of CNT is its ballistic characteristic owing to its long elastic mean free path at room temperature, which is of the order micrometer (Kajiura et al., 2005). The ballistic transport makes high speed and low power consumption devices possible, and is a reason for CNT to be considered a promising candidate to replace silicon in the next generation electronic devices. The length over which a CNT can behave as a ballistic conductor depends on its structural perfection, temperature and the strength of the driving electric field. In general, ballistic transport can be achieved over lengths typical of a modern scaled electronic device that is ≤ 100 nm. However, this can be extremely long, up to 10 micron in CNTs (White and Todorov, 1998)], i.e., as much as 1,000 times higher than that in bulk silicon.

Under high bias conditions, optical phonon scattering becomes very strong in CNTs and such processes were first observed in metallic tubes (Javey et al.,

2004b; Ji-Yong et al., 2004; Zhen et al., 2000) and later in semiconducting tubes (Yung-Fu and Fuhrer, 2005). Owing to the short optical phonon mean-free-path, of the order of 10–20 nm, the current in SWCNTs is found to saturate at about 25 μA (Javey et al., 2003; Mann et al., 2003), meaning for FETs based on individual SWCNT, the highest output current in principle would be 25 μA. For long CNTs (i.e., with length much longer that the mean free path), many scattering collisions can take place and the carrier transport in CNT is diffusion limited, similar to conventional conductors, and in this regime, the carriers in CNT have finite mobility.

It should be noted that the resistance of a ballistic CNT is not zero, even though there is no scattering in the conduction channel in principle. This is because there is a mismatch of the number of states between one dimensional (1D) CNT and three-dimensional (3D) metal electrodes. And this mismatch of number of states would lead to a quantized resistance at CNT and metal contacts. (Buttiker, 1988; Landauer, 1996). The size of the quantized resistance is: $R_Q = h/(2e^2) \approx 6.5k\Omega$ (Javey et al., 2003). In addition to quantum resistance, a contact resistance owing to the Schottky barrier at the CNT/metal interfaces always exist in practical CNT based devices, and it could play a more important role in the transport characteristic of CNT based devices (Heinze et al., 2002). The Schottky barrier resistance of a CNT and metal contact is dependent on almost all the factors of the contact system, e.g., the nanotube properties (Tseng et

al., 2006), the atomic structure of metal electrodes (Shan et al., 2004) and the contact structures (Vitale et al., 2008). Moreover, ‘parasitic’ resistance, which is simply owing to ‘bad’ contacts and resulting from the process issues of the device manufacture process, could also exist and affect the transport characteristics of CNT (Zhang et al., 2006).

In conclusion, the unique structure of CNT would significantly impact its electrical transport properties and in the following sections we will discuss the electrical characteristic of CNTs based devices.

1.2 Carbon nanotube and metal contact

As with any electronic device, contacts need to be established for CNT electronics and creating good connection between CNT and metal is a challenging field in modern nanotechnology. In this section, we will analyze the characteristics of CNT and metal contacts which dominate the transport mechanism of CNT based devices such as field-effect transistors (FETs) and Schottky diodes. Moreover, the study of CNT and metal contact is the main focus of this dissertation.

1.2.1 Atomic structure of carbon nanotube and metal contacts

CNT can be regarded as rolled-up of graphene and owing to the anisotropy of graphene, there are two completely different interfaces between a CNT and a

metal crystal, as shown in Figure 1.1. The CNT may constitute an end-contact to the metal, involving covalent bonds at the interface, or a side-contact where the metal forms a weakly bonded interface with the surface of the tube (Banhart 2009). To date, more experimental work has been devoted to the side-contact interface. This is because the main method to make electrical contacts to CNTs is to deposit a metal strip from above or depositing CNTs on top of metal electrodes. However, a large contact resistance has always been measured, in particular when the CNT is just lying on a metal electrode without any 'soldering' (Chen et al., 2006). Therefore, the full utilization of the ballistic transport characteristic of CNT is still a big challenge for CNT electronic devices owing to the contact issue.

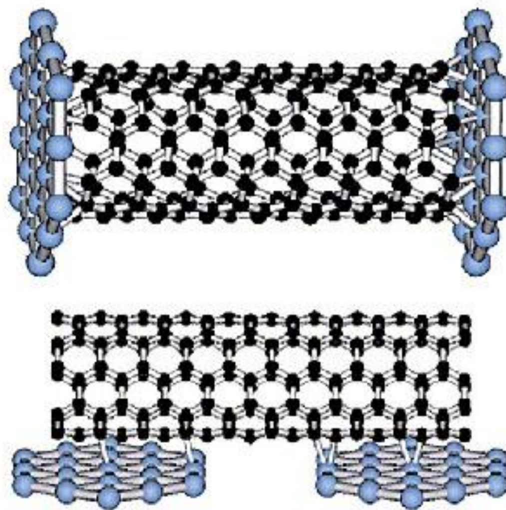

Figure 1.1: Two types of interface between a metal crystal and a carbon nanotube: end-contact (top) and side-contact (bottom) (Banhart 2009).

1.2.1.1 Carbon nanotube and metal contact with side-contact structure

As the (0001) surface of graphene is chemically rather inert, it is assumed that weakly bonded metals are attached to the graphene surface by the Van der Waals bonding, and covalent chemical bonds are absent (Banhart 2009). Therefore, the interface between a CNT and a metal with side-contact structure is determined by the surface wetting of metal electrodes to CNTs (Maiti and Ricca, 2004). It has been reported that there is dramatic difference in the wetting properties of metals to CNTs, e.g., Ti, Ni and Pd have good wetting properties with CNT, while Al, Fe and Au have bad wetting properties (Zhang et al., 2000). Good wetting means the deposition of metal layers on CNTs is continuous whereas poor wetting leads to isolated metal islands deposited on CNT surface. The binding energy between a metal atom and a CNT surface is one parameter that identifies the wetting properties of metal. This is because the binding energy between a metal atom and a CNT surface determines which metal sticks best to the surface.

However the wetting property is not the only factor that is critical to the electrical properties of the CNT and metal contact (Maiti and Ricca, 2004). For example, Ti has higher cohesion energy on the surface of CNT than Pd and therefore a better wetting property. However Ti forms a poorer (mostly non-Ohmic) electrical contact, while Pd can form Ohmic contacts with CNTs. In the simulation study (an *ab* initio study) of carrier injection at the Ti (Pd)/CNT

contact, the charge density redistribution at Ti/CNT contact suggests that charge accumulation in the atomic layers, depopulation of the interlayer region, and thus an increase of the interlayer scattering potential. On the other hand, the populated interlayer state and the lower scattering potential and at the Pd⁄CNT junction is found (Nemec et al., 2006). The lower scattering potential leads to more efficient injection of charges from metal contacts into the CNTs. Therefore, the Pd⁄CNT contact is superior to the Ti⁄CNT contact.

Besides the charge transfer, the contact electrical quality also depends on the nanotube-metal hybridization. Based on Landauer transport calculations, the ‘optimum’ metal-nanotube contact generally involves a weak hybridization between metal contacts and CNTs (Nemec et al., 2006). This on the other hand identifies that Pd/CNT contact is a better electrical contact than Ti/CNT contact, owing to the much stronger band shift at Ti/CNT junctions (Nemec et al., 2006).

1.2.1.2 CNT and metal contact with end-contact structure

Owing to the stronger bonding and the better coupling at the interface, an end-contact structure should be favorable for CNT and metal contacts. One promising way to achieve CNT and metal end-contact is by forming metal carbide at the CNT and metal interface (Zhang et al., 1999).

In experiments, transition metals are often employed for CNT contacts. The bonding between transition metal and CNT is dependent on the number of unfilled *d*-orbitals in the transition metal (Andriotis et al., 2000). This is because the hybridization for a CNT and metal side-contact is determined by the overlap of the p_z-orbitals of carbon (normal to the surface of CNTs) and the *d*-orbitals of transition metals. For example, Au or Pd has no unfilled *d*-orbitals and therefore exhibit a low affinity for carbon. Metals with a few vacant *d*-orbitals (Ni, Fe, Co) have a higher affinity, which is also reflected by the fact that these metals have a certain (yet low) solubility for carbon. Metals of 3*d*- and 4*d*-type with vacant *d*-orbitals (Ti, Nb) form strong bonds with carbon (Andriotis et al., 2000). Strong metal–carbon bonds can lead to a sufficient solid-state reaction and to the formation of stable carbides. Therefore, the number of unfilled *d*-orbitals is a very important parameter for selecting metals to form CNT and metal carbide contacts for the application of CNT based devices.

1.2.1.3 Summary of the atomic structure of carbon nanotube and metal contacts

In conclusion the nature and geometry of the metal and CNT contact can drastically change its electrical behavior. In theory, end-contact structure is preferred to side contact structure for the formation of Ohmic metal and CNT

contacts. Solid state formation of metal carbide is one promising way to achieve end-contacts, and transition metals with more unfilled *d*-orbitals are preferred candidate for the formation of carbide contacts.

However, side-contact structure is much more commonly used in CNT based devices owing to its simpler processing. Therefore, it is also important to understand the properties of such contact structure and to optimize its electrical performance. It has been found that for good electrical side-contact, metals with both good wetting and weak hybridization with CNT are preferred, e.g., Pd.

It should be noted that the metal and CNT contact is a very complex system with properties determined by a combination of factors, including the atomic structure of metal electrode, the interface structure, etc. As the CNT and metal contact is not yet fully understood, it is the main focus of this dissertation.

1.2.2 Charge transfer between metals and CNTs contacts

Schottky barriers in a 1D system differ in one crucial aspect from that in three dimensional (3D) system: they are much thinner (on the nanometer scale), and tunneling or thermally activated tunneling through the barrier is more important than thermal emission over the barrier. This has important consequences for the charge transport at the CNT and metal contacts.

In a 3D system, metal-induced gap states appear in the semiconductor and behave similar to surface states, and the Fermi level of the metal is pinned close to

the middle of the semiconductor band gap and this is known as 'Fermi pinning'. However, for a CNT and metal system, Fermi level pinning owing to metal-induced gap states is not as effective as conventional semiconductor (Leonard and Tersoff, 2000). This is because of the point-like contact between CNT and metal electrodes and therefore potential shifts at the CN/metal interface decay rapidly in a direction normal to the interface and disappear within a few nanometers (Martel et al., 2001). Therefore, for CNT and metal contacts, the Schottky barrier has a width of a few nanometers only, and electrons can tunnel through the barrier easily. As the Fermi pinning is not important in the CNT-metal contact, the Schottky barrier height (SBH) is very sensitive to the work function of the metal. By employing small work function metals, e.g., Ca (Nosho et al., 2005), Gd (Kim et al., 2008), Y (Ding et al., 2009) and Sc (Jiao et al., 2008), *n*-type Schottky contacts were formed; while by using high work function metals, e.g., Au (Martel et al., 1998), Pd, Rh (Kim et al., 2005) and Pt (Tans et al., 1998), *p*-type Schottky contacts were formed. As for metals with intermediate work function values such as Ti (Martel et al., 2001) and Mg (Nosho and et al., 2006), the Schottky barrier heights for hole and electron transport are similar, as the Fermi level of metal is near the middle of the bandgap of carbon nanotube, and lead to ambipolar characteristic.

In addition to the work function of metal, the diameter of CNT (*d*) is another important parameter that affects the Schottky barrier at the CNT and

metal contacts. This is because the bandgap of semiconducting CNT is a function of its diameter. The larger the tube diameter, the smaller the Schottky barrier height for both hole and electron transport. Therefore, a CNT of small diameter always leads to unipolar contact characteristic, while a CNT of large diameter leads to ambipolar contact characteristic.

Ohmic contact, on the other hand, is established when the metal work function is within the valence or conduction band of a semiconducting CNT. Ohmic side-contact has been obtained for Pd on a semiconducting CNTs (Javey et al., 2003). However, this can only be achieved for semiconducting SWCNTs (*s*-SWCNTs) with large diameter (>1.6 nm). For small diameter SWCNT, the Schottky barrier still exists at the contacts (Kim et al., 2005), which means there is a limitation with Pd yieding Ohimic contact to CNT. To date, several techniques have been investigated to achieve Ohmic CNT and metal contact, in addition to Pd, e.g., using metal carbides (Martel et al., 2001) or doping at contact region (Chen et al., 2005). Currently, there are still a lot of research efforts on CNT/metal contacts aiming to improve the CNT based devices further.

In conclusion, establishing reliable electrical metal contacts on CNTs is a goal that should be achieved. Contacts with very low Ohmic resistance are important to achieving outstanding electrical properties of CNTs such as ballistic transport. However, this does not mean that Schottky contact is bad and in fact high performance Schottky contacted devices, e.g., FETs (Yu-Ming et al., 2005a)

and diodes (Manohara et al., 2005) have been achieved. In addition, Schottky contact is critical to achieving some new concept devices, such as single electron FET where the existence of coulomb blockade results from large Schottky barriers at the contacts [(Matsuoka et al., 2006)]. As a result, both Schottky and Ohmic metal and CNT contacts have important applications for CNT based devices and would be the objectives of this dissertation.

1.3 Carbon Nanotube based devices

Carbon nanotube based devices have been extensively researched since the first demonstration in 1998 of the carbon nanotube field effect transistors (CNTFETs) (Martel et al., 1998; Tans et al., 1998). The CNTFETs use semiconducting *s*-SWCNTs as the channel and the reason is owing to the superior properties of *s*-SWCNT compared with the conventional semiconductor — Si. Moreover, many of the problems that silicon technology is or will be facing are not present in CNTs. The main advantages of *s*-SWCNT over Si as the FET channel are summarized as follows:

[1] Ultra small scale (1~2 nm diameters). The strong 1D electron confinement and full depletion in the nanoscale diameter of the SWCNTs (1-2 nm) lead to a suppression of short-channel effects in CNT transistor devices (Slava V. Rotkin, 2005).

[2] No dangling bond states at the surface of CNTs. Therefore there is almost no surface roughness scattering at SWCNT/high-*k* insulator surface. This means in CNTFET, both high mobility and ultra-thin body channel of dimension of several nanometers can be achieved simultaneously, which has not been demonstrated in conventional semiconductor devices (Javey et al., 2004a).

[3] High mobility of CNT (Durkop et al., 2003). This means much higher speed electronic devices can be achieved.

[4] Long-range ballistic transport of electrons in CNT. Ballistic electron transport means that SWCNT based transistors will exhibit higher ON currents and therefore lower power consumption.

In this dissertation, the focus is on two important types of CNT based devices, CNTFET and diodes, which form the bases of other CNT electronics, and they will be briefly reviewed in the following sections.

1.3.1 Carbon nanotube field effect transistors (CNTFET)

1.3.1.1 *p*-type Carbon nanotube field effect transistors

The first devices (Martel et al., 1998; Tans et al., 1998) as well as most of the SWCNT-FETs realized so far are fabricated in a back-gate configuration, as it

is easier to fabricate. However, it has the disadvantage of not being able to control individual transistors because the substrate is shared by all transistors. This configuration is probably not a realistic candidate for commercialization but it is good for research. In such devices, a single *s*-SWCNT is contacted by metal electrodes, with the standard substrate being heavily doped silicon covered by a thermally grown silicon oxide (SiO_2) of thickness in the range of 100 nm to 1 μm that serves as the gate insulator (see Figure 1.2).

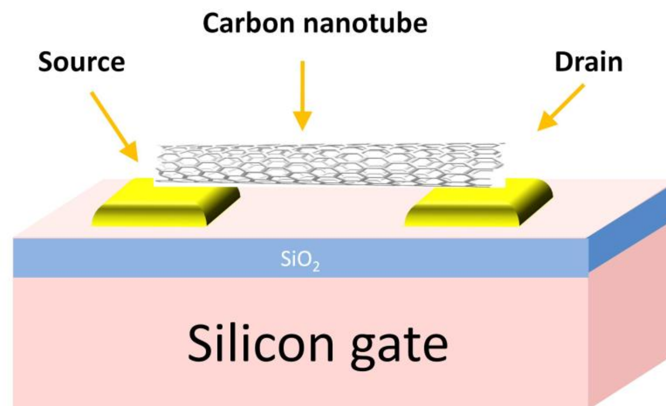

Figure 1.2: Schematic of a back-gated SWCNT FET

Unlike conventional MOSFETs, the SWCNT FET functions like a Schottky barrier FET (SBFET) (Heinze et al., 2002; Leonard and Tersoff, 2000; Martel et al., 2001), owing to the Schottky barriers existing at the CNT/metal contacts, in which switching occurs primarily by modulation of the contact

resistance rather than the channel conductance. Carrier injection thus takes place through thermionic emission and tunneling across the Schottky barriers, whose width depends on the applied gate voltage. CNTFETs normally exhibit *p*-type characteristic and this is attributed to the oxygen absorption on the sidewall of CNT (Donghun and et al., 2005; Sumanasekera et al., 2000) and/or the Schottky barrier at the CNT and metal contact (Tans et al., 1998; Heinze et al., 2002). As depicted in Figure 1.3, a variation in the gate potential shifts the CNT energy band and changes the width of the Schottky barrier at the CNT/source interface. For *p*-type FET, when a negative gate is applied, the valence band is pulled above the Fermi level of the source. This means that the Schottky barrier becomes narrower, and electrons can then easily tunnel from the valence band to the source. However, when no bias is applied to the gate, the Fermi level of the source is higher than the energy level of the holes in the valence band of the CNT. Therefore, very few holes can move from the CNT to the source, even though an electric field exists between the source and drain. The FET therefore operates in the OFF states.

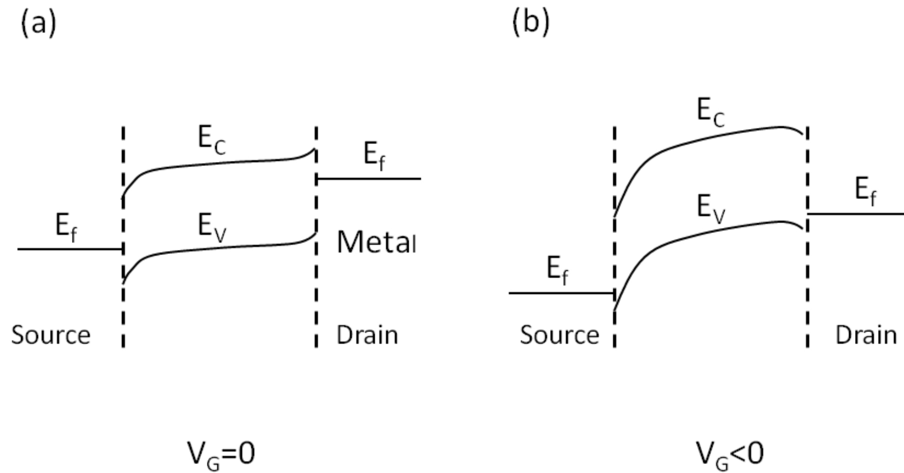

Figure 1.3: Band structure diagram of a *p*-type SB-CNTFET. (a) With no bias on the gate, a large Schottky barrier exists between the valence band of the CNT and the Fermi level (E_f) of the source contact. A positive bias on the source lowers the Fermi level of the source and raises the level of the drain. (b) A negative bias on the gate raises the conduction and valence band of the CNT. The shift in bands leads to a narrower Schottky barrier at the source/CNT interface and allows holes to be transported from the source to the valence band of the CNT.

1.3.1.2 Ambipolar Carbon nanotube field effect transistors

For SB-CNTFET, when both the Schottky barriers at the two contacts become very thin, they pose almost no barrier for transport. Therefore, a large leakage current flows in the OFF state. In devices with a *p*-type characteristic, for example, this leakage current is carried by electrons that are injected at the drain when the drain voltage exceeds the gate voltage. Such a phenomenon can be observed in three situations: 1) with ultra-thin gate insulator (Heinze et al., 2003),

2) when the Fermi level of metal lines up close to the mid-gap of CNT (Nosho et al., 2006), 3) large-diameter CNTs owing to a small bandgap (Javey et al., 2002). Such a phenomenon is known as ambipolar transport. For complementary circuit applications, ambipolar transport is undesirable. This is because high-performance FETs require low OFF current.

1.3.1.3 *n*-type Carbon nanotube field effect transistors

For the development of CNT based CMOS circuits, high performance *n*-type FETs are as important as *p*-type FETs. It has been discussed in the previous section that, unless subjected to further treatment, e.g., electron doping (Izumida et al., 2006; Javey et al., 2005; Shim et al., 2001), SWCNT-FETs in general show *p*-type characteristics which have been attributed to the Schottky barrier at the CNT and metal contact (Tans et al., 1998) and/or the adsorption of oxygen molecules on the surface of SWCNTs, which causes hole doping of the carbon nanotube (Donghun et al., 2005). In fact, there is still dispute as to which is the exact cause of the *p*-type characteristic of CNTFETs and researchers are still looking for ways to solve this problem.

In essence, doping of CNTFET to convert it to *n*-type characteristic is still a challenge for CNT application. There are mainly two types of dopants that would result in *n*-type CNTFET operating in air ambient. First type of electron

dopants are alkali metals (Kong et al., 2000) and the second type of dopants are polymers (e.g. PEI) (Shim et al., 2001). However, alkali dopants suffer from immediate degradation upon exposure to air which means this is not a stable process and defects would be introduced in the doping process which results in the decrease of the conductance of CNTs. Even though air stable and good performance *n*-type CNTFET can be achieved by PEI doping (Shim et al., 2001), the life-time of such *n*-type FETs is very limited when the devices are stored under ambient, which is a consequence of the low air stability of PEI (Balasubramanian et al., 2008). These results indicate that in order to achieve high performance *n*-type CNTFET, the doping technology has to be optimized. On the other hand, alternative technologies could be the way to solve the problem of *n*-type CNTFET.

In addition to doping, air-stable *n*-type CNTFET can be fabricated by depositing passivation films such as Si_3N_4 (Kaminishi et al., 2005) on the devices. This is because adsorbed oxygen on the CNT sidewalls is removed during the deposition process of the Si_3N_4 passivation films. However, the small energy bandgap of Si_3N_4 (~5 eV) results in large OFF currents and therefore makes it not a good insulator candidate for high performance *n*-CNTFETs. This method hints at the possibility using non-oxide insulator for *n*-CNTFET if an insulator material with large bandgap is used. However, to the best of our knowledge it has not been reported yet.

Based on the discussion in Section 1.2.2, the approach that entails contact engineering to achieve a very small Schottky barrier for electron transport at SWCNT and metal contacts seems a more reasonable and promising technology to fabricate high performance *n*-type CNTFET. Recently, it has been reported that Scandium (Sc ~3.5eV) (Jiao et al., 2008), Yttrium (Ding et al., 2009) and Gadolinium (Gd ~3.1eV) (Kim et al., 2008) contacted SWCNT-FETs can exhibit a long-term air stable high performance *n*-type behavior by forming near Ohmic contacts with SWCNTs, yielding high ON current, high ON/OFF current ratio and large transconductance that are comparable to those of *p*-CNTFETs.

In conclusion, great efforts have been taken to achieve high performance *n*-type CNTFET for complementary circuit application. Even though contact engineering seems a feasible way for device fabrication, there is still a need to optimize the performance of such devices. The *n*-type CNT and metal contacts would be useful to a lot of CNT based devices, e.g., diodes, thin film transistors which would also be discussed in this dissertation.

1.3.1.4 The challenges of CNTFET

CNTFETs offer intrinsic advantages for high-performance logic device applications. To date, high performances of CNTFETs have been achieved: ON resistance as low as 22 Ω/μm (Javey et al., 2004a), ON/OFF current ratio

(I_{ON}/I_{OFF}) ~10^6 (Yu-Ming et al., 2005b), transconductance ~ 17650 μS/μm (Javey et al., 2004a) and subthreshold slope < 60 mV/dec (Appenzeller et al., 2004).

Even though with such promising results obtained in exploratory devices, the challenges that must be met in order to fabricate practical high performance devices and circuits have to be considered. The challenges and outlook of CNTFETs are briefly summarized in Table 1.1.

Table 1.1 CNFET Technology Challenges and Outlook

Challenge	Need for	Possible solutions	Status
CNT alignment and positioning	Correct logic functionality	• AC dielectrophoresis alignment (Vijayaraghavan et al., 2007) • Direct alignment growth (Yuegang et al., 2001) • Mis-positioned-CNT-immune design (Patil et al., 2008a; Patil et al., 2008b)	It is still far away from the requirement for integrated circuits.
% metallic CNTs (*m*-CNTs) grown or deposited on substrate	Small leakage current (Need: >99.99% *m*-CNTs removed)	• 1% *m*-metallic CNTs synthesis (Nougaret et al., 2009) • Solution Based CNT Sorting: 1% Metallic CNTs (Engel et al., 2008) • Electrical breakdown (not VLSI compatible) (Collins et al., 2001) • Selective chemical etching of metallic CNTs (An et al., 2004)	• Tighter control of CNT chirality needed • More VLSI-compatible • metallic CNT removal required
CNT doping	High performance complementary circuits	• *n*-type doping (PEI) (Shim et al., 2001) • *p*-type doping (Triethyloxonium hexachloroantimonate) (Jia et al., 2005)	Air stable CNT doping with controllable doping level required
Source/drain contact metal	High performance complementary circuits	*p*-type: Pd, Rh (Kim et al., 2005) *n*-type: Sc (Zhang et al., 2007), Y (Ding et al., 2009)], Gd (Peng Cheng et al., 2008)	the contacts to small diameter CNTs needs to be achieved
Threshold voltage setting	Cascadable logic circuit	CNT circuit on flexible substrate (Qing et al., 2008)	Air stable CNT doping with controllable doping level required

1.3.2 Carbon nanotube diodes

Diode is another fundamental semiconductor device used widely in rectification, switching, high frequency multiplier and photonic devices. Nano-scale diodes based on CNT have been developed by forming either a *p–n* (Lee et al., 2004; Abdula and Shim, 2008) or metal–semiconductor Schottky (Manohara et al., 2005; Kim et al., 2006; Lim et al., 2008; Lu et al., 2006; Yang et al., 2005) junction. However, as indicated in Table 1.1, the stable doping of CNT is still facing challenges. Therefore, the CNT *p-n* diodes are still far away from practical applications. Compared with *p-n* diodes, CNT Schottky diode developed by contact engineering seems to be a more promising strategy. In addition, rectifying metal-semiconductor Schottky junctions have advantages in their higher switching speeds, lower forward resistance, lower noise level than *p-n* junctions and inherent suitability for low-voltage, high-current applications (Sze, 1981). Therefore in this dissertation, the study will focus on CNT Schottky diodes, but not CNT *p-n* diodes.

The core idea of the CNT Schottky diodes is to form asymmetrical Schottky contacts at the two ends of the CNT. To date, several schemes have been employed to achieve this: 1) depositing dissimilar metals with significantly different work function (Lim et al., 2008; Lu et al., 2006; Yang et al., 2005); 2) asymmetrically modulating the Schottky barrier by modifying the contact structure, e.g., an AFM tip is utilized to create an asymmetric Schottky barrier at

the two contacts of the SWCNTs by selectively modifying the tube-metal interaction or the contact length (Jiao et al., 2008); or 3) asymmetrically modulating the Schottky barrier by adjusting the work function of the metal electrodes, and this method is based on the principle that the work function of contact metal can be modulated by the attachments on its surface of external molecules, e.g., thiolate molecules (Kim et al., 2006).

The different schemes have their own specific advantages and drawbacks. To date, the best CNT Schottky diodes are achieved using the first method. This is because both stable and high performance Ohmic and Schottky barriers can possibly be achieved by using suitable metal electrodes. However, it should be noted in such a device structure, the metal electrodes are normally deposited on top of the carbon nanotube. This is because the low work function metal which is commonly used to form large Schottky barrier contact, e.g., Ti or Al, is easily oxidized with oxides typically formed at the top surface. Therefore, if the CNT is deposited on top of the metal electrodes, the device cannot work properly. However, the contact structure with CNT deposited on top of the metal electrodes is widely used owing to its ease of processing. Therefore, the CNT diodes with the structure of two different metal electrodes cannot be fabricated by using the AC dielectrophoresis method which leads to the deposition of CNTs on top of metal electrodes.

High performance devices can also be achieved by using the second method. However, the fatal drawback of this method is the poor repeatability of the process. In addition, the process is both difficult and time consuming which makes it not feasible to apply on a large scale. Therefore, this technology has very limited development space in the future.

The third method is based on the principle that the work function of metal can be modulated by the adsorption of external molecules. Therefore, there are a lot of choices for this technique by the different combination of metal electrodes and the modification media. To date, both Lithium ions (Choi and Lim, 2008; Lim et al., 2008) and thiolate molecules (Kim et al., 2006) can act as the media to fabricate such diodes. However, the study of this type of diodes is still preliminary and especially the performance of the device needs optimization.

In conclusion, the exploration of CNT diodes is important to CNT based electronics, and in our work, we will explore the fabrication of Schottky CNT diodes by means of contact engineering, in line with the main focus of this dissertation.

1.4 Motivation and Synopsis of Thesis

Based on the discussion in Section 1.2, it is seen that metals are important peripheral materials in the CNT technology. Therefore, it is desirable to study the

interaction of CNTs with as many different metals as possible in a systematic way. Establishing reliable electrical metal contacts on CNTs is a goal that is desired to be achieved. Metal carbide has shown promising results in CNTFET even though in limited studies. The key challenge of this application might be a thorough understanding of the interaction of transition metals (single atoms as well as clusters or crystals) with CNT and identification of the optimal metal carbide which will yield good electrical performance of CNTFET. Therefore in this dissertation, the carbide contact in CNTFET devices will be studied.

In additional to FET devices based on individual SWCNT (i-CNTFET), it is also important to investigate the other possible applications of CNT for electronic devices. In this dissertation, we would conduct such investigation in two ways. Firstly, it is still based on the FET devices, but replacing the channel material with random network of SWCNTs (rn-SWCNT) — thin film transistors (TFTs). In this dissertation the *n*-type rn-SWCNT FET would be the main focus as the research on such devices is still preliminary. Secondly, we also focus on two terminal devices — diodes. Our studies of CNT and metal contacts can be applied for the optimization of Schottky type CNT diodes.

The above research motivation concerns both the contact properties of SWCNT/metal contacts and the device applications based on SWCNT. In this dissertation, we are also interested in the bulk properties of CNT. As the study of SWCNT has been extensively documented, in this dissertation, we would focus

on another important form of CNT — double wall CNT (DWCNT). Compared with SWCNT, the study of DWCNT is significantly lagging behind and it is considered a best form of CNT to study the inter-tube interaction in CNTs, which will be important to understanding the properties of more complicated CNT, the multi wall CNT (CNT). More importantly, we would like to investigate the possibility of using DWCNT as a functional element to fabricate electronic devices, e.g., FET, and evaluate their performance.

In the following sections, we will discuss the motivation of this dissertation in more detail.

1.4.1 Ohmic metal carbide and SWCNT contacts

As summarized in Table 1.1, one essential challenge to overcome is to form stable Ohmic contacts for small diameter carbon nanotubes. Based on the discussion in Section 1.2, application of metal carbide as contacts appears to be a promising route to solve this problem. This is because this scheme is not limited by the nanotube diameter as it converts the contact structure from weak bonded side-contact to end-contact with much better coupling.

In this dissertation, we will focus on niobium (Nb) carbide – Nb_2C which is formed at the Nb electrode and CNT interface during the thermal annealing process. There are 11 transition metals which can form carbides when reacted

with carbon, e.g., Ti, V, Cr, Mn, Fe, Zr, Nb, Mo, Hf, and W (Leroy et al., 2006). Among these metals, Cr, V, Mn and Zr are very sensitive to oxygen and therefore oxides rather than carbides would be formed in the thermal annealing process. Therefore, they are not promising candidates as metal electrodes in our work. Fe is also ruled out as its carbide Fe_3C tends to segregate a graphite layer in the formation process, which may interfere with device operation. In the remaining six transition metals, Nb's carbide, Nb_2C, is known to have the highest work function (~5.25eV) and therefore Nb is chosen in our work. This is because high work function electrode is preferred to form highly unipolar *p*-type characteristic in CNTFETs.

To our knowledge, Nb_2C has never been applied to CNTFETs. In addition, it is necessary to clarify the interaction between the Nb and CNT in the formation process of Nb carbide. This is because the interface between Nb and CNT is sensitive to the annealing temperature which means the electrical properties of the Nb and CNT contact is varying in the carbide formation process. Therefore, it is critically important to relate the electrical properties of carbide contacts with the interaction at the interface.

1.4.2 Random network carbon nanotube transistor

As discussed in the previous section, CNT alignment and positioning, and high percentage of semiconducting SWCNTs are important to the yield of

individual SWCNT FETs (i-SWCNT FETs). Although much research efforts have been devoted to solving these challenges and have achieved substantial developments, it is still far away from the desired situation. To date, the highest concentration of semiconducting SWCNTs during synthesis has been achieved up to 99% (Nougaret et al., 2009). This means the failure yield of i-SWCNT FET is about 1% in principle, which is not acceptable for the future application in industry. If the positioning and alignment yield of individual semiconducting SWCNT onto the metal electrodes, e.g., by using AC dielectrophoresis technology, is also included, the failure yield of i-SWCNT FETs would be worse. This is because the metallic SWCNTs are more likely to be attracted to the metal electrodes in the AC dielectrophoresis process than semiconducting SWCNTs.

Therefore another type of transistor based on CNT, the random network (rn) SWCNT FET, as shown in Figure 1.4., has been developed and attracted more interest recently. This is because the fabrication process of rn-SWCNT FET is relatively simpler, as the rn-SWCNT is normally deposited simply by using spin coating method. Moreover, the alignment issue of SWCNTs in the random network is not critical in this type of devices. In the spin coating process, the semiconducting and metallic SWCNTs are deposited on the substrate with no preference. This means if the concentration of semiconducting SWCNTs in the solution is up to 99%, the ratio of semiconducting to metallic SWCNTs in the channel of rn-SWCNT FET should be very close to 99:1. Therefore, the

possibility of the existence of a transport route in the channel composed entirely of metallic SWCNTs is very low, e.g., <<1%. It is well known that only the transport route which is totally metallic will deteriorate the performance of rn-SWCNT FETs. This means the yield of rn-SWCNT can be much higher than i-SWCNT FET. In other words, rn-SWCNT FETs are more tolerant of metallic SWCNT than i-SWCNT FET.

To date, good performance of *p*-type rn-SWCNT FET has been achieved, e.g., ON/OFF ratios around 10^5 (Izard et al., 2008), field effect mobilities on the order of 10~150 cm^2/Vs (Snow et al., 2005), subthreshold slopes as low as 140 mV/dec and operating voltages less than 5 V together with deterministic control over the threshold voltages (Qing et al., 2008). Taken together, these results suggest that rn-SWCNT is an attractive material for thin film transistors.

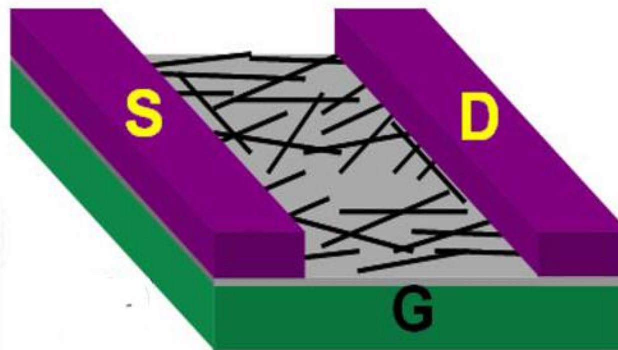

Figure 1.4: Schematic of a rn-SWCNT FET.

However to date, the study of *p*-type rn-SWCNT FETs has significantly preceded the *n*-type devices. Therefore in this work, we would focus on *n*-type rn-SWCNT FETs and try to explore both the working mechanism of *n*-type rn-SWCNT FETs and the way to optimize the performance of such devices. Such study would also be based on the core issue of this dissertation — the CNT and metal contacts. This is because the switching mechanism in rn-SWCNT FETs is owing to modulation of the Schottky barriers between semiconducting tubes and metallic tubes (Kodama et al., 2007; Stadermann et al., 2004) or metal contacts (Merchant and Markovic, 2009).

1.4.3 Schottky carbon nanotube diodes by contact engineering

The method of using surface modification to engineer the Schottky barrier at the CNT/metal contact is still in the developing stage and is suitable for devices with contacts where carbon nanotubes are deposited on top of metal electrodes. Therefore in this work, one of the motivations is to fabricate Schottky CNT diodes by using selected thiolate molecules and to optimize its performance.

Thiolate molecules are known to form self-assembled monolayers (SAMs) on the surface of noble metals (e.g., Au, Ag and Pt), which can modulate the surface work function via dipole formation on its surfaces (Rusu and Brocks, 2006). Different thiolate molecules would lead to different modulation effect of

the work function of metal electrodes. In this work, two different thiolate molecules, methanethiol (CH_3SH) and trifluoroethanethiol (CF_3CH_2SH), are chosen to asymmetrically modulate the two Au/SWCNT contacts to achieve a Schottky diode structure. Based on theoretical studies (Rusu and Brocks, 2006), CH_3SH and CF_3CH_2SH will modulate the Schottky barrier between CNT/Au contact highly asymmetrically and may lead to high performance CNT Schottky diodes being fabricated.

1.4.4 Double-Wall carbon nanotube field effect transistors

To date, SWCNT has been extensively explored both theoretically and experimentally, double-wall carbon nanotube (DWCNT), consisting of two cylinders of graphene, has also garnered some attention for multiple applications recently (Li et al., 2007; Liang and Wang, 2004; Shidong and Grifoni, 2007). This is because its unique structure provides it with characteristics between those of SWCNT and multi-wall carbon nanotube (MWCNT). Therefore, DWCNT can probably reap both the advantages of SWCNT and MWCNT.

In the study of *s-m* DWCNT FETs, where *s* and *m* represents the outer semiconducting tube and inner metallic tube of the DWCNT, respectively (Lu et al., 2007; Shidong and Grifoni, 2005; Wang et al., 2005), it has been found that the inter-tube interaction in the *s-m* DWCNTs is important to the transport characteristic of *s-m* DWCNT FETs. In these studies, when only the outer

semiconducting tube of the DWCNT is contacted with the metal electrodes, its FET characteristic is seriously weakened with the on/off current ratio reduced to about 10 while for semiconducting SWCNT, the on/off current ratio is normally higher than 10^3. This phenomenon has been attributed to inter-tube charge transfer (Wang et al., 2005) or the proximity effect of the metallic phase of inner tube which results in local density of states in the bandgap of the outer semiconducting tube (Lu et al., 2007). Even though it is still not clear which theory better explains the transport mechanism of *s-m* DWCNT FET, it is confirmed that the abnormal FET characteristic of *s-m* DWCNT results from the inter-tube interactions. Therefore, it is logical to consider if such similar or different kind of inter-tube interaction exists in the *s-s* DWCNT and how the inter-tube interaction will influence the transport characteristic of *s-s* DWCNT FET. It is believed that this is an important challenge for DWCNT application and in fact has attracted more and more attention (Jing et al., 2005; Okada and Oshiyama, 2003). This is because from a technology point of view, *s-s* DWCNT FET is more suitable for FET application than *s-m* DWCNT whose on/off current ratio is too low. On the other hand, it has been experimentally demonstrated that the on/off current ratio of *s-s* DWCNT FET is close to that of SWCNT FET (Liu et al., 2009; Wang et al., 2005).

To the best of our knowledge, to date, almost all the studies on the inter-tube interaction in *s-s* DWCNT are based on theoretical calculations (Jing et al.,

2005; Okada and Oshiyama, 2003) and no experimental work has been reported. Based on the theoretical work, it has been inferred that the inter-tube interaction in *s*-*s* DWCNT will give rise to the change of its electronic structure, e.g., the π-σ rehybridization of the inner tube will cause the metallization of the *s*-*s* DWCNT with the bandgap vanishing in the outer semiconducting tube when the inner tube is very thin. However, it is not clear what the effect of inter-tube interaction is in the *s*-*s* DWCNT with large inner tube (the large diameter *s*-*s* DWCNT) and what will be the corresponding behavior of its FET characteristic. In order to answer these questions, we would mainly focus on FETs based on *s*-*s* DWCNT rather than other types of DWCNTs in our dissertation, and we would experimentally investigate the electrical characteristics of FETs based on *s*-*s* DWCNT with different diameters and compare them with SWCNT FETs with same diameter.

1.5 Outline of Thesis

In conclusion, the study of metal and CNT contacts is the core and main line of this dissertation. In the results and discussion part of this dissertation (chapter 3, 4 and chapter 6) even though different CNT based devices are studied, all the aims of these chapters are to investigate different metal and CNT contacts and their applications. And in chapter 5, we focus on the properties of DWCNT. This is because with the studies of CNT deeper and deeper, it has been realized

DWCNT is another important member in CNT family except SWCNT which has significant potential in applications. Moreover we believe the investigation of bulk CNT is as important as the study of metal and CNT contact to optimize the performance of CNT based devices.

Chapter 1 has briefly reviewed the electronic structure and electrical transport properties of CNTs and the CNT based devices, e.g., field effect transistors and diodes with particular emphasis on the CNT and metal contacts. In addition, the motivation of this dissertation has been presented.

Chapter 2 describes the experimental procedures for the fabrication and characterization of carbon nanotube based devices.

Chapter 3 investigates the formation and characterization of niobium carbides in carbon nanotube field effect transistors.

Chapter 4 discusses the working mechanism of *n*-type random network single wall carbon nanotube field effect transistors with yttrium contacts.

Chapter 5 studies the double wall carbon nanotube (DWCNT) field effect transistor and the inter-tube interaction in semiconducting DWCNT.

Chapter 6 describes the fabrication process of carbon nanotube Schottky diodes by using thiolate molecules and investigates their electrical characteristics.

Chapter 7 concludes the thesis and discusses the future work of this dissertation.

Chapter 2

Experimental procedure for the fabrication and characterization of carbon nanotube based devices

In the fabrication of carbon nanotube (CNT) based devices a number of steps are involved. Firstly, there is the need to prepare the CNT solution from the source bought from commercial suppliers. This entails the dispersion of CNTs in a solution, followed by the purification of the CNT solution to remove the impurities in the CNT source, such as metal catalyst particles, amorphous and fullerene-like (non-tube) carbon structures. The preparation of the CNT solution will first be described, following which, the fabrication procedure of individual single wall carbon nanotube field effect transistors (SWCNT FETs) will be presented.

2.1 Preparation of carbon nanotube solution for device fabrication

2.1.1 Dispersion of carbon nanotubes

All the carbon nanotube samples (single-wall and double-wall CNTs) for device fabrication in our experiments were bought from commercial suppliers. Some of the basic while important parameters of these materials are summarized

in Table 2.1, where all the data presented are extracted from the data sheet of the products.

In our work, the first step in the fabrication of CNT devices is to disperse CNTs in a solution, which makes it possible for us to manipulate the location of tubes on the substrate. This is necessary because almost all CNTs are tangled in bundles during their synthesis, owing to the strong Van der Waals force between CNT sidewalls. In addition, there is a mixture of semiconducting and metallic tubes in the synthesized CNTs and this is the reason why tubes need to be separated for device fabrication.

Table 2.1: Suppliers and parameters of CNT (SWCNT & DWCNT) samples used in our experiments.

	Suppliers	**Diameter (*d*)**	**Length (*l*)**	**Purity (%)**	**Form**	**Synthesis Method**
SWCNT	**Helix Material Solutions**	~ 1.3 nm	0.5-40 µm	> 90 %	Powder	Chemical vapor deposition (CVD)
	NANOCYL	~2 nm	Several µm	> 70 %	Powder	Catalytic chemical vapor deposition (CCVD)
	Nanocs (water soluble)	1~2 nm	10 nm – 10 µm	> 90%	Solution	CVD
	SWeNT (SG 76)	0.9 +/- 0.2 nm	~1 µm	~ 90 % (>50% of tubes are (7,6) chirality)	Powder	CoMoCAT (Kitiyanan et al., 2000)
	SWeNT (SG 65)	0.8 +/- 0.1 nm	~1 µm	~ 90 % (>50% of tubes are (6,5) chirality)	Powder	CoMoCAT
	Mer Corporation	1.2-1.4 nm	10-50 µm	~ 12 % (25 wt% metal catalyst particles, 10 wt% fullerenes, 10 wt% MWCNT and other graphitic structures)	Powder	Arc-discharge
DWCNT	**Mer Corporation**	2-5 nm	5-15 µm	~15 % (15 wt% amorphous, 5% graphitic carbon particles, 65 wt% metal particles)	Powder	Arc-discharge
	NANOCYL	~ 3 nm	1-10 µm	>90%	Powder	(CCVD)

The mechanism of solution dispersion is as follows: surfactants would coat the surface of individual CNTs in the solution and therefore making CNTs repulsive from each other in the bundles during the dispersion process. In our work, we have chosen sodium dodecylbenzene sulfonate (NaDDBS) as the dispersion medium. This is because the CNT solutions dispersed by NaDDBS exhibit good stability and homogeneity, and they also yield longer CNTs in the solution, compared to those using other chemicals (Islam et al., 2003). Moreover, NaDDBS surfactants are easy to remove from the side walls of CNTs, by means of annealing in air at moderatly high temperature. In other words, the electronic properties of CNTs would not be altered by the dispersion process, which is important to fabricate stable electronic devices based on CNTs with high performance.

As CNTs are bonded by Van der Waals force in bundle form, a strong force is needed to separate them to individual tubes in the dispersion process. This is achieved in general via ultra-sonication, where sound waves in the kilohertz range are used to create and destroy tiny bubbles in a liquid in a process known as cavitation. The collapse of the bubbles in the cavitation process is an energetic process, both physically and thermally, and this helps break raw CNT materials into smaller pieces and disperses them in the solvent.

In our experiments, we use a homogenizer which is more efficient than normal sonicator to achieve the dispersion of CNTs. A homogenizer is more

efficient than an ultrasonic bath, as it has a vibrating probe that is immersed into the mixture, hence allowing the sonication power to be transferred directly to the mixture. Moreover, this probe not only provides the ultrasonic sound waves to loosen CNTs, but also creates pressure waves to mix the CNT dispersive agent mixture. In our experiments, it was found that by using a homogenizer, a short duration of a few minutes was enough to disperse the CNTs homogeneously and the prepared NaDDBS dispersed CNT solution is stable long-term, as shown in Figure 2.1.

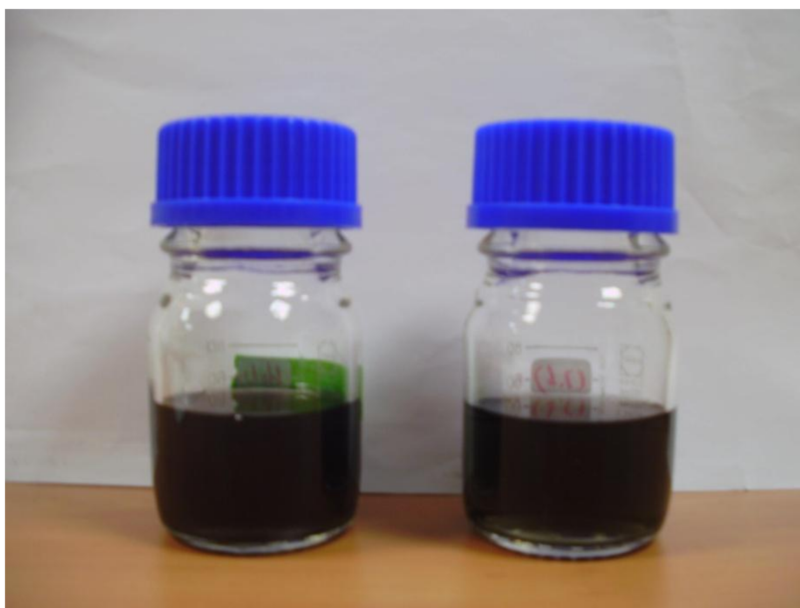

Figure 2.1: Dispersed CNT solution by NaDDBS (~ 0.1 M), after homogenization for 20 minutes (left), and after 2 weeks on storage (right).

2.1.2 Purification of carbon nanotube solutions

As-grown CNT materials generally contain metal catalyst particles, amorphous and fullerene-like carbon structures, other than CNTs. It is desirable and necessary to remove as much of these non-tube impurities in the solution as possible before the device fabrication, as these impurities could affect or even destroy the intrinsic electrical properties of the devices fabricated from the CNT solutions.

For CNT solutions, the most commonly used means to separate the suspended impurities from the CNTs in the solutions is to use high speed centrifugation (Yu et al., 2006). In the centrifuge process, most of the impurities would be left in the sediment while the CNTs would be left in the supernatant, as shown in Figure 2.2a. The centrifuge works by spinning the mixtures stored in centrifuge tubes at high speed, creating a g-force within the centrifuge tubes and separates the mixture according to their density. The impurities, which are always heavier, will stick to the bottom of the centrifuge tube, while the supernatant closer to the top contains the light weight CNTs. It should be noted that large bundles of CNTs that are heavier and bigger in size are also precipitated to the bottom of the centrifuge tube in the centrifugation process.

As shown in Figure 2.2b, after the impurities are separated from the CNT solution, the color of solution becomes lighter, near transparent, with the undesirable impurities aggregate and precipitate at the bottom of the centrifuge

tube. The supernatant is then carefully collected by a pipette and diluted for device fabrication.

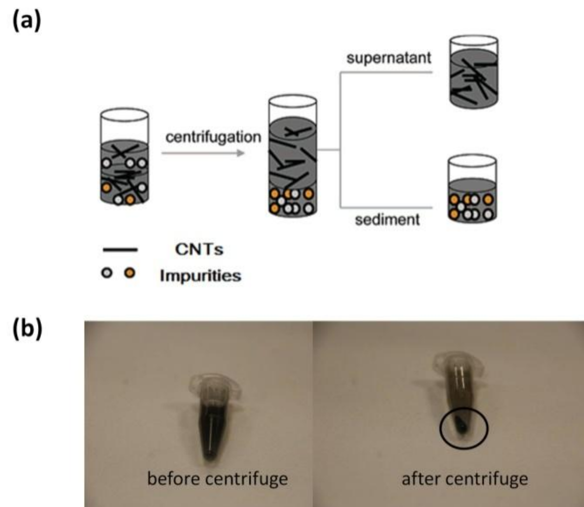

Figure 2.2: (a) Schematic diagram of the centrifugation process for removal of impurities in the CNT solution. (b) The CNT solution before and after the centrifugation process.

2.2 Fabrication procedure of individual single wall carbon nanotube field effect transistor

2.2.1 Alignment of carbon nanotubes

2.2.1.1 Floating potential AC dielectrophoresis

As discussed in Chapter 1 (Table 1.1), the alignment of CNTs remains a challenge in the fabrication of CNT based devices, owing to the ultra small scale of CNTs. As a consequence, the yield of functional devices in the fabrication of CNT devices is still low.

It has been reported that CNTs can be aligned by utilizing electrical (Chung et al., 2004), magnetic (Hone et al., 2000), mechanical forces (Lay et al., 2004) and self-assembly (Rao et al., 2003). In our work, we mainly used AC electrical field — the AC dielectrophoresis method, to manipulate the position and alignment of CNTs in the device fabrication process. This is because AC dielectrophoresis operation is simple and provides good accuracy of control and relatively high yield of device fabrication, compared to other techniques (Banerjee et al., 2006; Taeger et al., 2006; Seo et al., 2005; Stokes and Khondaker, 2008; Stokes et al., 2009). In our experiments, we used a modified AC dielectrophoresis process to fabricate our CNT devices - the floating-potential AC dielectrophoresis technology (Dong et al., 2005), as shown in Figure 2.3. By using this improved method, the individual CNT can be aligned between two opposite metal electrodes and the yield is larger compared with the normal AC

dielectrophoresis method. The mechanism of this process will be discussed in detail in following paragraphs.

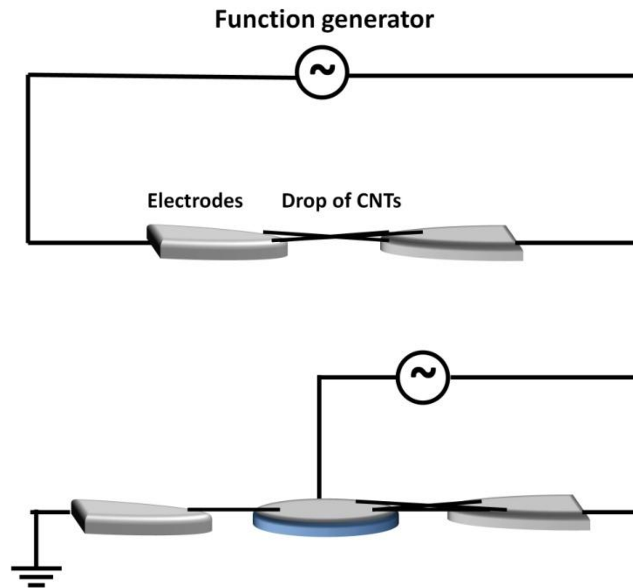

Figure 2.3: Schematic of AC dielectrophoresis setups: normal AC dielectrophoresis (top figure) and floating potential AC dielectrophoresis (bottom figure), which has additional floating electrode compared to the normal AC dielectrophoresis.

For normal AC dielectrophoresis method, it is well-understood that when uncharged dielectric or conductive matter is placed in an electric field, the electric field will induce the formation of a dipole moment inside the matter. If the field is uniform (DC electrical field), the net Coulombic force on the dipole is zero.

Otherwise, in a non-uniform (AC) electric field, the net Coulombic force is not zero. This can be depicted by equation (2.1), where *F* is the net force, *E* is the electric field, and *P* is the induced dipole moment.

$$\begin{aligned}\vec{F} &= q\vec{E}_{(\vec{r}+\vec{d})} - q\vec{E}_{(\vec{r})} \\ &= \vec{P} \bullet \nabla \vec{E}_{(\vec{r})}\end{aligned} \qquad (2.1)$$

Therefore, a polarizable CNT could be moved around in a non-uniform electric field.

The degree of alignment of CNTs in the electric field depends on the frequency of the AC electric field. It has been demonstrated that the degree of alignment of CNTs is reduced gradually with the decrease of the frequency of the electric field (Chen et al., 2001). Therefore, there is no obvious alignment in the samples in DC electric field. This is because when a DC bias is applied between two opposite metal electrodes, the CNTs would move towards the cathode or anode under the influence of the electric field as the concentration of the electric field is at the edges of the electrodes. Therefore the CNTs tend to aggregate rather than align in the DC electrical field. Moreover for CNTs aligned by an electric field with a low frequency, they are always in the form of tangled CNTs. On the other hand, electric field with a high frequency will usually straighten the CNTs.

Therefore, by using the normal AC dielectrophoresis method, both the direction and position of CNTs can be controlled by pre-defining metal electrodes

on the substrates and the applied AC electric field. However, one of the most serious drawbacks of this technology is the bad reproducibility of the fabrication of devices, e.g., the number and the property of tubes (metallic or semiconducting) cannot be precisely controlled. Therefore, the yield of devices with individual semiconducting CNTs bridging across electrodes is still low. This is because metallic CNTs are more likely than semiconducting CNTs to be attracted by the electric field between the opposite metal electrodes (Krupke et al., 2003). The net force induced by AC electrical field on CNT bundles and impurities in the purified solution would be much larger than that on individual CNTs. This is because for a particle with homogeneous and dielectric sphere, the dielectrophoresis force is given by the equation (2. 2). And therefore the CNT bundles and impurities are more likely to be attracted to the channel region than individual CNTs owing to their larger volume.

$$\vec{F} = 2\pi V \varepsilon_m K_{(\omega)} \nabla(\vec{E}_{rms}^{\,2}) \quad (2.\ 2)$$

where V is the volume of the particle, ε_m is the real part of the medium solution dielectric constant, E_{rms} is the root-mean-square value of the electric field, and K is the Clausius Mosotti factor, which depends on the particle dielectric constant ε_P and medium solution dielectric constant ε_m, given by equation 2.3:

$$K_{(\omega)} = \mathrm{Re}\left(\frac{\varepsilon_p^* - \varepsilon_m^*}{\varepsilon_P^* + 2\varepsilon_m^*}\right) \quad (2.\ 3)$$

Therefore, in the case of CNT alignment, the potential magnitude depends on (1) the volume of carbon nanotube, (2) the conductivity of the nanotube suspension, (3) the type of deposited nanotubes (semiconducting or metallic): the dipole induced by metallic CNT is much larger than that of semiconducting CNTs (Krupke et al., 2003), and (4) the magnitude of applied electric field.

The normal AC dielectrophoresis process has been optimized to a floating-potential AC dielectrophoresis (FPD) (Dong et al., 2005) to improve the yield of devices based on individual semiconducting CNTs. As reported, the yield of CNTFETs based on individual SWCNT can be up to 26% by using FPD technology. It is believed that if the purity of semiconducting tubes can be increased with the optimization of the synthesis technology in the future, this yield can be further improved.

The schematic layout of the FPD process is illustrated in Figure 2.4a. The structure has two different function regions, the controlled region (I) and floating region (II). The AC voltage is directly applied in region I and one electrode of region II is floating. Therefore, compared with region I, the electrical field of region II is much weaker. In essence, the improvement by using floating potential setup results from the modulation of distribution of electric field between the metal electrodes. Therefore, when a droplet of CNT suspension is dropped to the substrate consisting of the controlled region and the floating region, CNT bundles, having a larger volume than individual nanotubes, experience a stronger

dielectrophoretic force and are therefore deposited across the control electrodes (region I), where the larger electrical field gradient exists. In the meantime, impurities larger than individual CNTs are also deposited at region I. This is because the low conductivity of the CNT suspension causes the electrical potentials at floating regions to be much smaller than the potential at the controlled region. After a majority of the CNT bundles and impurities are attracted to regions I, there is a high probability for individual CNTs to be deposited at floating regions (II).

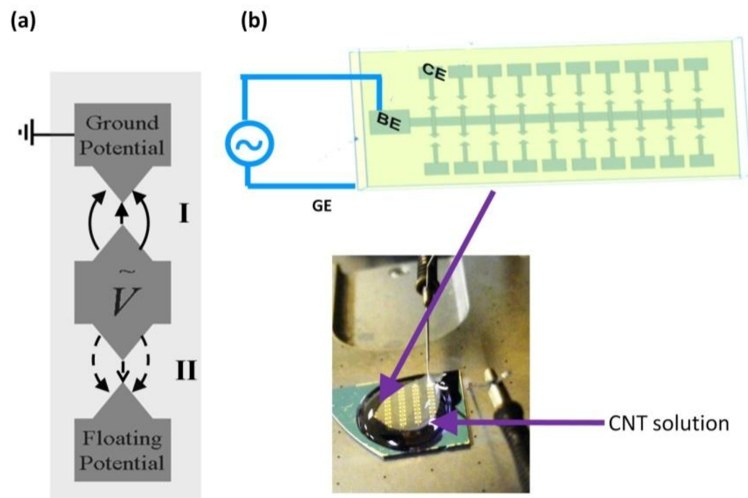

Figure 2.4: (a) The schematic layout of floating-potential AC dielectrophoresis (FPD) - region I is the controlled region and region II is the floating region. The arrows in the figure indicate the distribution of electric field in these regions. (b) Schematic layout of wafer scale floating- potential AC dielectrophoresis, and the experiment setup (top view): one probe is put on the biased electrode (BE) and another probe on the substrate of the probe station (GE).

The results of floating potential dielectrophoresis are shown in Figure. 2.5 (the SEM pictures of region I and II). It is identified that only one SWCNT is aligned across the electrodes in region II and no impurity is found in this region while in region I, tangled CNTs and impurities, e.g., amorphous carbon, are deposited. The processing conditions are as follows: amplitude of AC voltage is 12 V, frequency is 2 MHz, and the process duration is about 2 mins.

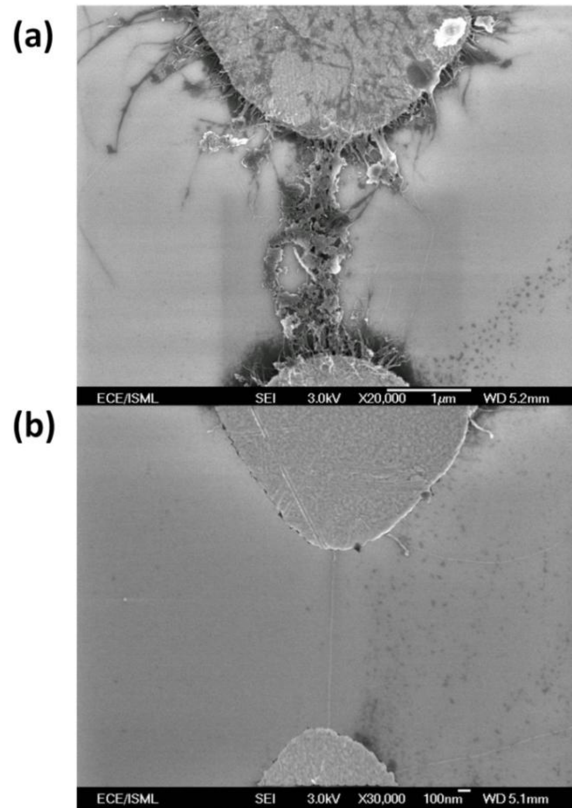

Figure 2.5: SEM pictures showing the results of floating potential dielectrophoresis: (a) the controlled region (I), where both SWCNT bundles and amorphous carbons are attracted to the electrodes, and (b) the floating region (II), where only one individual SWCNT is aligned across the electrodes.

The yield of devices with individual CNTs in our experiment is about 30%. Therefore, by using floating potential dielectrophoresis, we have found a reliable way to fabricate CNT based devices, e.g., FETs and diodes for statistical and systematical study. However, there is still one serious problem with this technology, the long processing time if a large number of devices are required.

2.2.1.2 Large scale AC dielectrophoresis

With the development of our work, it is found that although FPD is a useful means to align individual CNTs onto metal electrodes, it is not a practical technology for large scale fabrication. However in this work, the systematical study of CNT based devices is based on a large number of devices with statistical characteristics. Therefore, an AC dielectrophoresis in the wafer scale is necessary and has been achieved in our experiments.

The schematic layout of this dielectrophoresis setup is shown in Figure 2.4b, based on that proposed by Vijayaraghavan et al. (Vijayaraghavan et al., 2007). The core feature of this setup is that only one of the electrodes (biased electrode, BE) on top of the substrate is connected directly to the AC source. The other electrode of each device is set as a floating counter electrode (CE). The AC voltage is applied between the BE and the underlying silicon gate electrode (GE).

Therefore, the number of devices which can be achieved simultaneously in principle is dependent only on the design of the layout on the substrate. This is because for high electric-field frequencies (f > 100 kHz), the impedance of the CE/SiO_2/GE structure ($1/j2\pi fC_{CE\text{-}GE}$) reduces significantly. The CE is then capacitively coupled to the GE and acquires a similar potential as that of the GE. This allows us to bias all the distinct CEs without having to bond wires individually to each electrode.

In our experiments, for devices with channel length around 1 μm, the optimal parameters setting for the dielectrophoresis are determined to be: frequency $f \approx 1$ MHz, voltage amplitude $V_{p\text{-}p} \approx 8$ V, duration T ≈ 3 mins and the other processing parameter we need to adjust is the concentration of the CNT solution. The yield of devices with individual CNT is about 30~40% by using this technology. Although this value of yield is only slightly better than that of FPD discussed previously, the difficulty of device fabrication process (i.e., long processing time) is significantly reduced by using this means. It should be noted that if the control of the concentration of CNT suspension can be more accurate, the yield can be improved further. This means that in future work, there is still room for improvement of this technology. A typical working device with one individual semiconducting SWCNT fabricated by this large scale AC dielectrophoresis is shown in Figure 2.6. It is seen that the SWCNT is well straightened and no impurities appeared in the channel region.

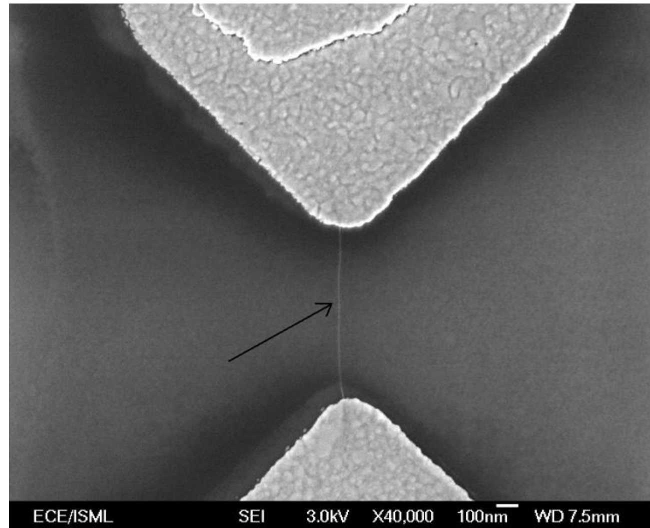

Figure 2.6: SEM picture of device based on individual SWCNT fabricated by wafer scale AC dielectrophoresis. The arrow indicate the positon of the SWCNT.

In conclusion, by using wafer scale AC dielectrophoresis, adequate number of devices based on individual CNTs can be achieved for our investigations.

2.2.2 The formation of metal and carbon nanotube contacts

Lithography is used to define the positions of the metal electrodes to form the contacts with CNTs. In this work, owing to the ultra-small size of CNTs, more accurate lithography technologies such as electron beam lithography (EBL) and

laser lithography (laser writer) rather than the conventional optical lithography are used. The electron beam lithography is done in our experiments using JEOL 5500FS, which has an accuracy in position control of about 40 nm. Another lithography technique used in our work is the laser writer (Microtech, LW 405, wave length of laser is 405 nm) with an accuracy in position control of about 100 nm. In our work, as AC dielectrophoresis is the most important way to align the CNTs, the metal electrodes are deposited on the substrate before the CNT deposition.

The metal deposition in our work is mainly by electron beam evaporation. Therefore, the metal electrodes of the CNT based devices can be gold (Au), aluminum (Al), titanium (Ti), nickel (Ni), yttrium (Y), niobium (Nb), rhodium (Rh), palladium (Pd), and silver (Ag). The vacuum of the electron beam evaporation can be as good as 10^{-7} mbar, which ensures high quality metal electrodes are achieved.

The entire fabrication process of CNTFETs with individual CNTs lying on top of metal electrodes is illustrated in Figure 2.7. The process for other devices such as random network carbon nanotube FETs and Schottky diodes is similar and will be described in the corresponding chapter in the dissertation.

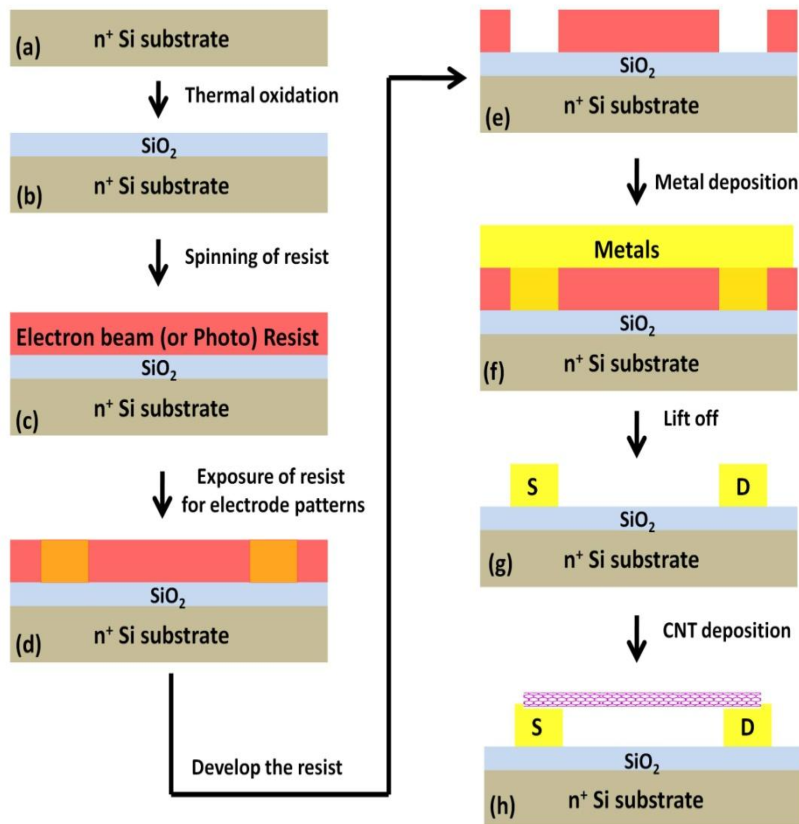

Figure 2.7: Fabrication process of CNTFETs with CNTs lying on top of metal electrodes: (a) high doping *n*-type silicon substrate is used as the back gate, (b) SiO_2 is grown as the gate insulator by means of thermal oxidation, (c) resist is spin-coated onto the surface of substrate, (d) lithography is carried out to define the shape and position of the metal electrodes, (e) exposed resist is removed by the appropriate developer, (f) metals are deposited by electron beam evaporation, g) metal lift-off is performed with the help of ultra-sonicator, h) CNTs in the solution are deposited onto the top surface of metal electrodes, and the fabricated devices are cleaned by rinsing in DI water and dried by nitrogen gas.

2.2.3 Removal of metallic carbon nanotubes

It has been discussed in chapter 1 that the synthesis of SWCNTs yields a mixture of semiconducting and metallic SWCNTs, and metallic SWCNTs are undesirable because only semiconducting SWCNTs have a significant electrical response to electric field gating effect. Furthermore, as observed in our experiments, in addition to devices with individual CNT (30~40%), there are some devices with several SWCNTs fabricated by our dielectrophoresis technology. Moreover, bundles of CNTs are also likely to appear between the metal electrodes. Therefore, the metallic tubes in the conducting channel need to be removed to increase the yield of working devices. For CNTFETs based on thin film of CNTs, which is also an important research object of our work, removing metallic tubes is extremely important to device performance, e.g., on/off current ratio. Therefore in our work, we need to develop a reliable technique to remove the metallic tubes after the fabrication of CNT devices to improve the yield of devices.

As reported, electrical breakdown is a simple process to destroy metallic tubes to achieve CNTFETs with high on/off ratio (Amlani et al., 2008; Collins et al., 2001a; Gyoung-Ho et al., 2008). This process is also commonly used in our experiments to increase the yield of working devices. It has been found that the primary factor in the breakdown initiation is the current-induced defect formation and that self-heating plays only a secondary role (Collins et al., 2001a). Therefore,

the breakdown of tubes only occurs at high bias voltage, e.g., high conducting current. In the electrical breakdown process, the semiconducting tubes can be protected once they are depleted by the gate voltage which means the current only passes through the metallic tubes. The typical results of electrical breakdown for a CNTFET with a bundle of SWCNT as the channel are shown in Figure 2.8. It can be observed that the original CNTFET exhibits very weak gate voltage dependence and after a continuous bias voltage (V_{DS}) is applied to the SWCNT bundle with the gate voltage set at a positive value, some of the metallic SWCNTs are broken. However, it is found that even though the on/off current ratio (I_{ON}/I_{OFF}) of the CNTFET after this electrical breakdown process increases to 10^2, the OFF current (I_{OFF}) of this device (~50 nA) is still substantial, which is believed to be owing to the remaining metallic SWNCTs inside the bundle. Therefore, the electrical breakdown process is applied again and finally a high performance CNTFET with I_{ON}/I_{OFF} ratio up to 10^5 (I_{OFF} ~ 1 pA) is achieved, as shown in Figure 2.8. It should be noted that the applied voltage V_{DS} in the electrical breakdown process is dependent on the size of the SWCNT bundle or the number of tubes in the channel. Therefore, the applied voltage V_{DS} for electrical breakdown is different for different devices. The above results indicate that by iterating the electrical breakdown process, all the metallic tubes can be eliminated. However, there are at least two disadvantages in this approach. Firstly the Joule heat generated by the high current passing through the metallic tubes may also

burn the adjacent semiconducting tubes. This means the unnecessary decrease of ON current (I_{ON}) of the devices is one serious drawback of this technique. Secondly, this method is almost impossible to be deployed in large scale to devices as the operation is based on an individual device. Therefore, even though this method is often used in our experiments, we continue to look for the more efficient means to remove the metallic CNTs to increase the yield of working devices.

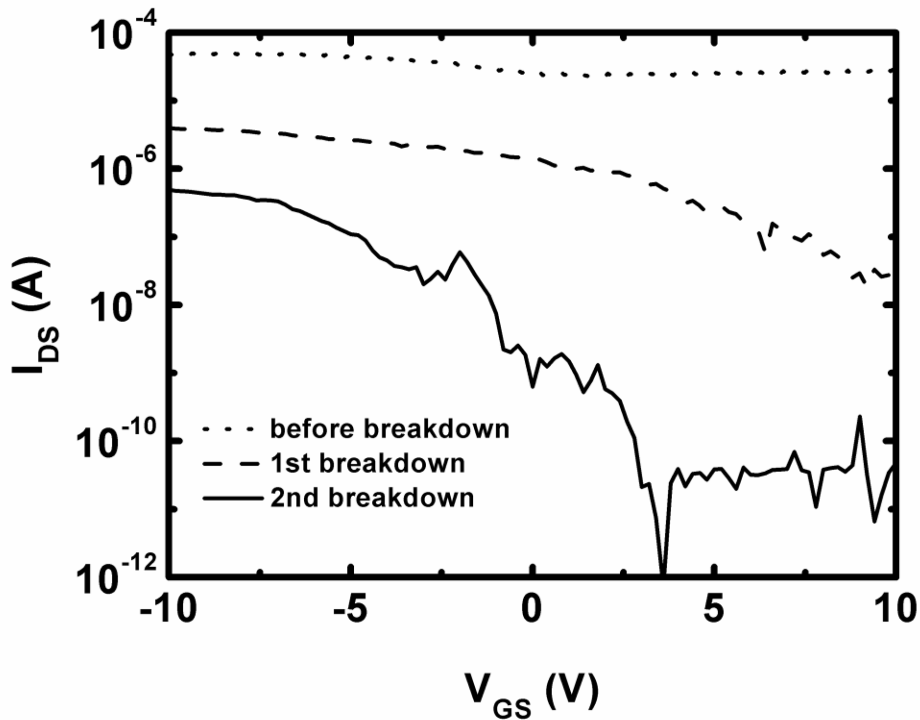

Figure 2.8: the I_{DS}-V_{GS} curves of a CNTFET with a bundle of SWCNTs as the channel, before and after the electrical breakdown process (V_{DS} = 8 V and V_{GS} = 10 V).

In addition to the electrical breakdown technique, alternative techniques have been investigated. Recently, it has been reported that electrophilic (electron-accepting) molecules (So et al., 2007) can selectively react with metallic nanotubes without gating or preconditioning and therefore, the metallic tubes would be etched while semiconducting tubes are preserved. The reaction selectivity comes from the difference between the electronic band structures of metallic and semiconducting SWCNTs. Metallic SWCNTs, contrary to semiconducting tubes, have finite electron density of states at their Fermi levels, meaning that there are electrons available to stabilize the change-transfer complex presumably formed by the electrophilic molecules at the SWCNT surface, which is suggested to facilitate the reaction. On the other hand, the absence of the electrons near the Fermi level makes semiconducting SWCNTs less likely to react with the electrophilic molecule reagent. In the experiments, it has been demonstrated that electrophilic molecules such as 2,4,6-TPPT preferentially react with metallic SWCNTs through noncovalent binding. The change of CNTFETs from non-depletable to depletable is permanent by using these molecules (So et al., 2007). Therefore in our experiments, we use 2,4,6-TPPT to optimize the yield of devices by removing the metallic tubes in the conducting channel. As shown in Figure 2.9, after several iterations, the CNTFET composed of both semiconducting and metallic tubes becomes totally depletable. This process is done simply by immersing the fabricated devices into the 2,4,6-triphenylpyrylium

tetrafluoroborate (2,4,6-TPPT) solution with stirring. This process is repeated several times to achieve the final improvement of the device performance. In our experiments, it is found the yield of conversion from non-depletable to depletable is about 50%. We believe this is owing to the existence of large size bundles of tubes which is inert to the reaction of 2,4,6-TPPT molecules. Therefore, it is believed that this technique can be further improved by improving the separation of SWCNTs in the dispersion process. More importantly, the chemical etching technique can partially overcome the challenges faced by electrical breakdown process: 1) this new technique is applied to all the devices simultaneously on the wafer, instead of individual devices as in electrical breakdown, 2) no thermal energy is generated in the chemical etching process and therefore the semiconducting tubes would not be “mis-killed”. In conclusion, our experiment results indicate that the chemical etching process using 2,4,6-TPPT molecules is a more effective way than electrical breakdown to eliminate metallic tubes, and plays an important role in the fabrication of CNT based devices.

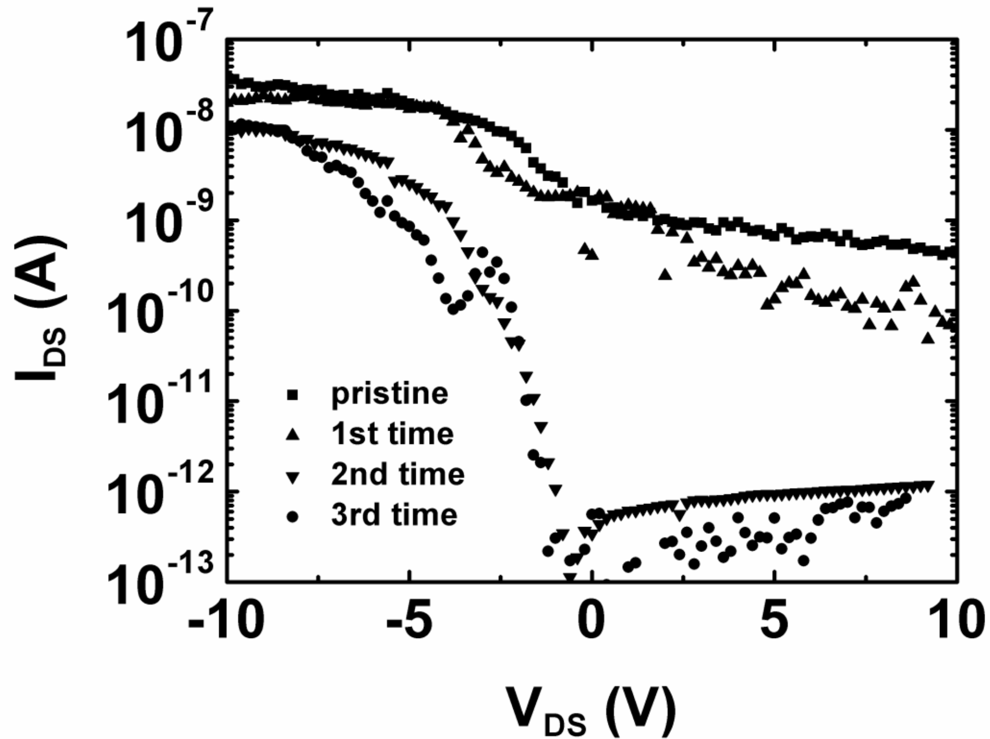

Figure 2.9: I_{DS}-V_{GS} curves of a CNTFET whose channel has both metallic and semiconducting SWCNTs, before and after the chemical etching process using 2,4,6-TPPT molecules (V_{DS} = 0.1 V).

2.3 Characterization of carbon nanotube based devices

2.3.1 Morphological characterization of carbon nanotube devices

It is obvious that the electrical characteristic of CNT devices — FET and diode — is dependent on the morphology of CNTs in the channel of the devices, e.g., the length and diameter of CNT, the number of CNTs in the channel and the alignment direction of CNT. Moreover, for random network SWCNT FET, the

density of tubes is one of the most critical parameters that affects its characteristics. In addition, impurities attached to the CNT surface or to the CNT and metal contacts can influence the electrical properties of the devices. Therefore, before any electrical characterization, the morphological information of CNT devices needs to be identified. Owing to the ultra-small scale of CNTs, scanning electron microscopy (SEM) and atomic force microscopy (AFM) are used in our work.

SEM is a powerful tool to gather almost all the morphology information of CNT devices, except the diameter of the CNT, which can be measured using an AFM. The AFM results can also help estimate whether it is an individual CNT or a CNT bundle, which is useful to understanding electrical characteristic of the devices.

In addition to AFM, Raman spectroscopy can also be used to measure the diameter of CNTs. Raman spectroscopy is a fast and non-destructive analysis technique without complicated sample preparation. The "radial breathing mode" (RBM) in Raman characterization is directly dependent on the nanotube diameter (d) through the relation: $\varpi_{RBM} = 224/d + 14$ (Rao et al., 2001), hence can be used to estimate the diameter of CNT .

2.3.2 Electrical characterization of carbon nanotube devices

In this work the electrical characterization is mainly achieved by means of a HP 4156 semiconductor analyzer and microprobe station. For FET structure (a three terminal device), the measurement setup is shown in Figure 2.10a. The bias voltage V_{DS} is applied at the two CNT and metal contacts (source and drain) and the gate bias is applied at the back-side of the substrate as the silicon substrate is highly doped. Therefore, the electrical characteristic of the CNTFET, e.g., I_{DS}-V_{DS}, I_{DS}-V_{GS}, can be readily measured. From the measurements, the electrical properties of the devices, e.g., the ON (and OFF) current, the subthreshold slope, threshold voltage and transconductance can be estimated.

For the diode structure (a two terminal device), the setup is even simpler, as shown in Figure 2.10b. Bias voltage is applied to the CNT and metal contacts to measure the *I*-*V* characteristic.

The analysis of the electrical characteristics of the devices will be discussed in the corresponding chapters.

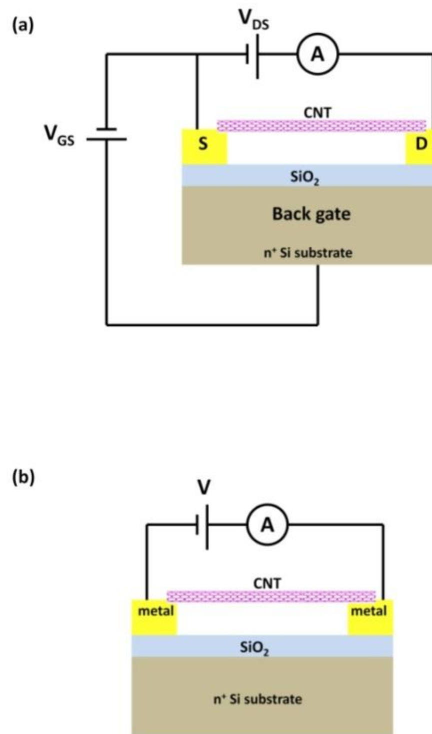

Figure 2.10: Electrical measurement setups for (a) CNTFET, and (b) CNT diode.

2.4 Summary

In conclusion, in this chapter the core steps in the fabrication of CNT based electronic devices including dispersion, purification of CNT solutions, alignment of CNTs and removal of metallic CNTs have been discussed. In our experiments, wafer scale fabrication of devices based on individual CNTs has been achieved with a yield up to 40%. It is worth noting that there is still room to

enhance the yield of working devices further by improving the existing technologies or by using new technologies. For example, the control of the electrical breakdown technology can be improved by combining automatic control using computers, which can develop this technology to wafer scale (Gyoung-Ho et al., 2008). The morphological and electrical characterization methods of CNT devices are also briefly described.

Chapter 3

High performance CNTFET with niobium carbide contact

In this chapter, the investigation on carbide contact to CNT will be presented.

3.1 Advantages of metal carbides

As discussed in chapter 1, a Schottky barrier (SB) typically exists at the metal-CNT contact interface, and when appreciable can play a critical role in limiting the current delivery capability and hindering effective switching (Chen et al., 2005b; Derycke et al., 2002; Heinze et al., 2002; Martel et al., 2001). Therefore, for CNTFET where large output current and high speed switching are required, the Schottky barrier at metal-CNT contact should be reduced as much as possible. Palladium (Pd) has been identified to be the best metal to yield a *p*-type contact to semiconducting (*s*-) SWCNTs with diameter $d > 1.6$ nm with near-zero Schottky barrier height (SBH) (Kim et al., 2005). However, for smaller diameter ($d < 1.6$ nm) SWCNT, finite SBH exists between Pd and *s*-SWCNTs, leading to a significant reduction in current flow, as a consequence of the higher bandgap ($E_g \sim 0.8/d(nm)$) of *s*-SWCNT associated with decreased diameter (Wilder et al., 1998). Therefore, Ohmic contact to small diameter *s*-SWCNTs ($d < 1.6$ nm)

remains a challenge that requires further investigations to minimize the SBH at the metal-SWCNT interface.

In earlier studies, it has been demonstrated that one type of transition metal carbide - titanium carbide (TiC) - can form near Ohmic contacts to small diameter SWCNTs with 1.2 nm ≤ d ≤ 1.4 nm (Martel et al., 2001; Nihey et al., 2001; Zhang et al., 1999). This means Ohmic contact to SWCNTs of small diameter can possibly be achieved by using transition metal carbides, which can be formed between carbon and metals by a thermal annealing process (Leroy et al., 2006; Leroy et al., 2007). In addition to being a good conductor, transition metal carbides have high melting point, high corrosive resistance, and low diffusion coefficient (reduced electromigration), thus making them suitable as interconnects in ultra-large-scale integrated circuits (Toth, 1971). However, TiC contacted SWCNT FETs normally show ambipolar characteristic owing to its low work function (3.7~3.9 eV) (Santerre et al., 1999) which makes its Fermi level aligned close to the middle of the bandgap of *s*-SWCNTs. This is a serious drawback of TiC contacts as ambipolar characteristic is not desired for high performance complementary logic circuits, where highly unipolar *p*- and *n*- FETs are required.

The material properties of many transition metal carbides have been investigated (Leroy et al., 2006; Leroy et al., 2007) and among them, niobium (Nb) carbide appears to be a potential alternative to TiC as contact to CNTFETs. In contrast to TiC, niobium carbides have high work function (NbC: 4.85~4.95 eV,

Nb_2C: ~5.2 eV) (Fujii et al., 2006; Samsonov et al., 1972) and are thermodynamically as stable as TiC. Moreover, considering the electronic structure of Nb ($4d^4 5s^1$), which has a substantial number of unfilled *d* states, stable metal carbide would be formed between carbon and Nb interface. Therefore, Nb is a promising choice for developing stable and low resistance Ohmic contact to SWCNTs (Andriotis et al., 2000).

3.2 The formation of niobium carbide at SWCNT and Niobium contacts

In our CNTFET structure, the SWCNT is laid on top of the source and drain electrodes by AC dielectrophoresis method, hence yielding a side-contact structure as shown in Figure 3.1. Moreover, the adequate overlap between SWCNT and Nb electrodes allows for sufficient interaction between the two in the carbide formation process. Electron beam evaporated Nb electrodes, with a thickness of 40 nm, were defined by means of electron beam lithography and metal lift-off technique. As shown in Figure 3.1, the Nb electrodes have a triangular tip, and the gap between the tips of adjacent electrodes is 600~800 nm. Individual SWCNTs dispersed in 1wt% sodium dodecylbenzene sulfonate (NaDDBS) solution were aligned between the gap of Nb electrodes by means of AC dielectrophoresis method, as discussed in chapter 2, using an AC voltage V_{P-P} ~ 8 V, frequency f ~ 1 MHz and duration time t ~ 1 minute. On one wafer (one

inch by one inch), we have 50 pairs of Nb electrodes for device fabrication and therefore enough number of devices can be obtained for statistical studies in our work.

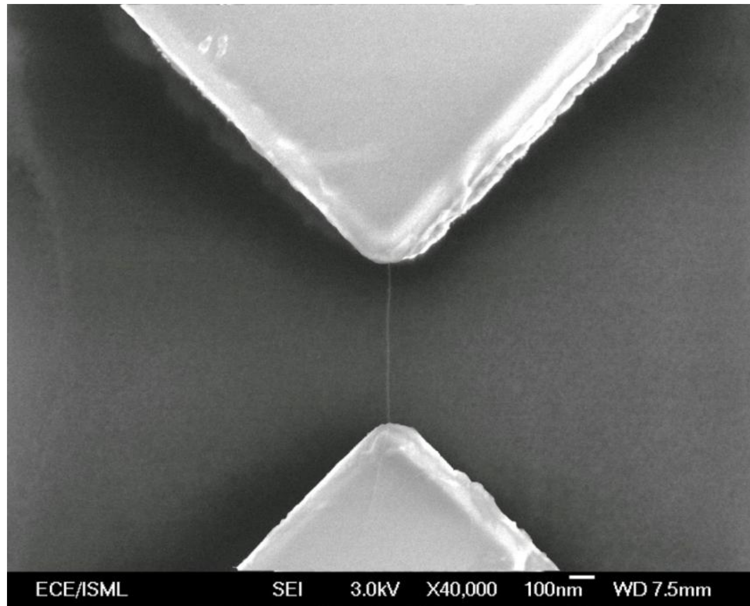

Figure 3.1: SEM picture of a typical Nb contacted SWCNT FET, the alignment of one individual SWCNT between two Nb electrodes is achieved by using AC dielectrophoresis with applied AC voltage V_{P-P} ~ 8 V, frequency f ~ 1 MHz and duration time t ~ 1 minutes.

In comparison to rectangular electrodes, the triangular tip of our Nb electrodes allows fewer individual SWCNTs being aligned in the conducting channel, which facilitates our purpose of having a single *s*-SWCNT bridging across the electrodes. The yield of devices with one individual SWCNT laid

across adjacent Nb electrodes, as shown in Figure 3.1, is between 30 to 40%. The diameters of SWCNTs used in the present work were from 1.0 to 1.5 nm, which were characterized by atomic force microscopy (AFM). After fabrication, the SWCNT FETs were given a heat treatment at ~100 ^{o}C in an oven to remove the unintentional and unavoidable contaminants in the fabrication process such as water molecules, NaDDBS (the solvent) molecules attached at the contacts interface (Islam et al., 2003).

The electrode annealing was carried out in a vacuum chamber (~3×10^{-6} *mbar*) between 400 and 900 ^{o}C to allow for reaction between Nb and SWCNT to form niobium carbides. Annealing in vacuum also avoided the formation of Nb oxides (Leroy et al., 2007), which can hinder the formation of good contacts. In order to investigate the details of change at the SWCNT/Nb interface in the process of carbide formation, 3 sets of annealing conditions were used: i) heating from room temperature to 400 ^{o}C in 90 s and holding the temperature at 400 ^{o}C for 1 hr, ii) heating from 400 to 700 ^{o}C in 90 s and holding the temperature at 700 ^{o}C for 1 hr, and iii) heating from 700 to 900 ^{o}C in 60 s and holding the temperature at 900 ^{o}C for 1 hr. As shown in Figure 3.2, at about 700 ^{o}C, the part of SWCNT on top of Nb interface disappeared, indicting the reaction between SWCNT and Nb to form niobium carbide. The characterization of the niobium carbide contact will be discussed in the following sections.

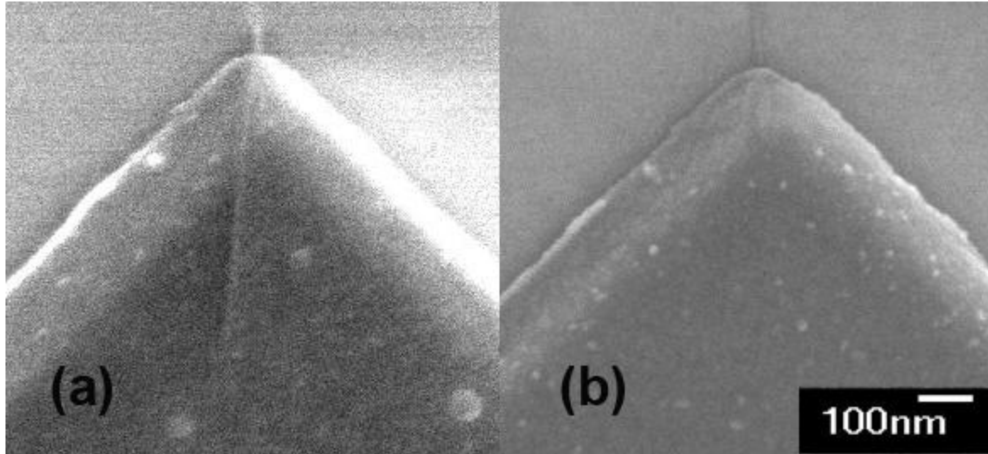

Figure 3.2: SEM pictures of a typical Nb and SWCNT contact: (a) before, and (b) after annealing in vacuum at 700 ^{o}C for 1 *hr* (resulted in the formation of niobium carbide, Nb_2C). The SWCNT lying on the Nb electrode becomes invisible after the formation of Nb_2C, signifying that the SWCNT has embedded into the electrode.

3.3 XRD characterization of niobium carbides

In order to investigate the changes happening at the contact interface between SWCNT and Nb electrodes in the niobium carbide formation process, X-ray diffraction (XRD) was employed. However, as the contact area of SWCNT and Nb electrode is one dimensional and just several hundred nanometers long, it is impossible to focus the laser beam of XRD system on the Nb contacts of the CNTFET. Therefore in this work, in order to solve this problem, we deposit a thin layer of Nb on one silicon substrate by electron beam evaporation and coated one thin layer of SWCNT film on the Nb surface. As a result, the XRD study of

SWCNT and Nb contacts can be achieved by scanning on the SWCNT thin film on the Nb layer.

To clarify the formation process of the niobium carbide, the results of XRD scanning before and after every annealing step are compared. After annealing at 400 ^{o}C, there is almost no reaction between SWCNTs and Nb and the XRD spectrum is similar to that shown in Figure 3.3a. However, after further annealing in vacuum at 700 ^{o}C for 1 hr, three peaks of Nb_2C corresponding to different lattice orientations: Nb_2C (100), Nb_2C (002) and Nb_2C (101) appear (see Figure 3.3b). If further annealing is conducted at 900 ^{o}C for 1 *hr*, an additional peak for another niobium carbide phase (NbC) is observed, as shown in Figure 3.3c, meaning the co-existence of Nb_2C and NbC after 900 ^{o}C annealing.

In conclusion, the XRD study reveals the structural change of the SWCNT and Nb contacts, which is believed to lead to changes in the electrical properties of SWCNT-Nb contacts, and this will be analyzed in detail in the following section.

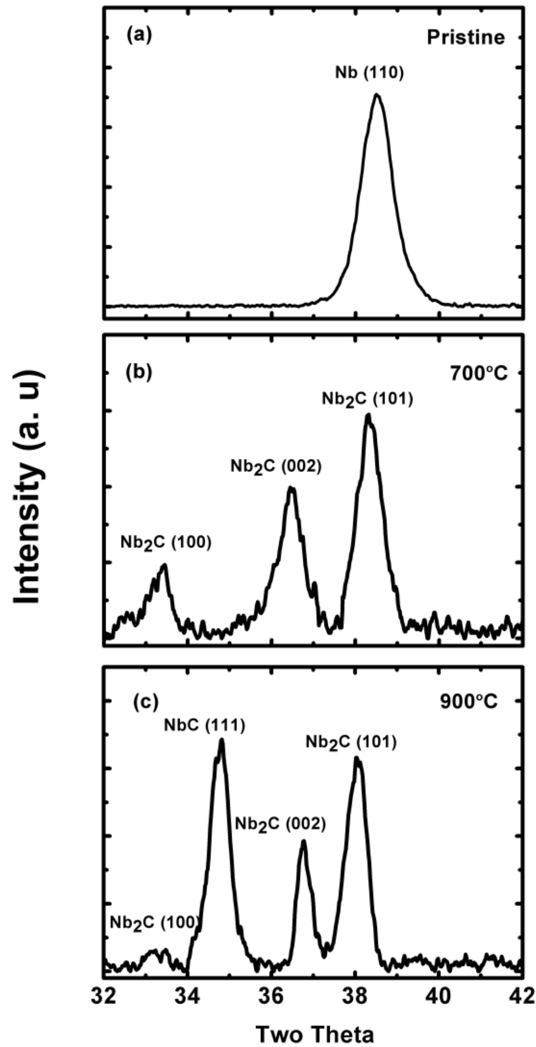

Figure 3.3: XRD spectra of SWCNT thin film deposited on 50 nm Nb layer: (a) before annealing. (b) after vacuum annealing at 700 ℃ for 1 *hr* (resulted in Nb_2C formation), and (c) after vacuum annealing at 900 ℃ for 1 *hr* (resulted in additional NbC formation). The spectrum after annealing at 400 ^{o}C is similar to that without annealing.

3.4 Electrical properties of niobium carbide in CNTFET

Owing to the good alignment effect of AC dielectrophoresis, the SWCNTs are well aligned between two adjacent electrodes (see Figure 3.1), meaning the length of the SWCNT channel is almost equal to the gap width (600~800 nm) between the tips of electrodes, and at such channel length, the transport mechanism of the fabricated devices is believed to be diffusive rather than ballistic (Durkop et al., 2003; Javey et al., 2003).

As observed in Figure 3.4, prior to annealing, almost no current was measured flowing through most of the Nb contacted SWCNT FETs. This is probably owing to the formation of a thin layer of Nb oxides (up to ~ 6 nm of NbO and Nb_2O_5) on the surface of Nb electrodes (Grundner and Halbritter, 1984; Romero et al., 2004) upon its exposure to air and to H_2O during the AC dielectrophoresis process, as a result of the high reactivity of Nb surface to the environment. These Nb oxides could lead to a tunneling barrier being formed between the SWCNT and Nb electrodes, which hinders carriers (both holes and electrons) transporting between contacts to the SWCNT channel. In addition, in the present work, as the SWCNTs are simply laid on top of Nb surface, meaning the SWCNTs are side-bonded to Nb electrodes by the Van der Waals force, our fabricated devices therefore have large parasitic contact resistance (Avouris et al., 2003). It is believed that both the presence of Nb oxides and Van der Waals

bonding between SWCNT and Nb are the reasons for the minimal carrier transport at the contacts.

After annealing in vacuum (~3×10^{-6} *mbar*) at 400 ^{o}C for 1 hr, the current flowing through the SWCNT FETs became detectable, as shown in Figure 3.4. The I_{DS}-V_{GS} characteristic, as shown in Figure 3.4a, is ambipolar with the *ON* current (I_{ON}) of the *p*- and *n*-channels of only ~ 10^{-8} A at V_{DS} = 0.1 V and the I_{ON}/I_{OFF} ratio of only ~10^{3}. This shows that near symmetrical SBHs, which are substantial, exist at the SWCNT and Nb interfaces for both hole and electron flows. The substantial SBH also results in the large subthreshold slope ~ 2.6 V/dec for the *p*-branch and ~3.2 V/dec for the *n*-branch, as shown in Figure 3.4a, and a highly nonlinear I_{DS}-V_{DS} curve (V_{GS} = 0 V), as shown in the inset of Figure 3.4b. The "improved" *I-V* characteristics, compared to those prior to annealing, are a direct result of the 400 ^{o}C thermal annealing in vacuum. This could have improved the bonding between the SWCNT and Nb electrodes and have caused the break-up of the thin layer of Nb oxides at the SWCNT and Nb interface. After 400 ^{o}C annealing, there should be no Nb carbide formation (Leroy et al., 2007), hence it is ruled out as a possible reason for any observed change in the *I-V* characteristics.

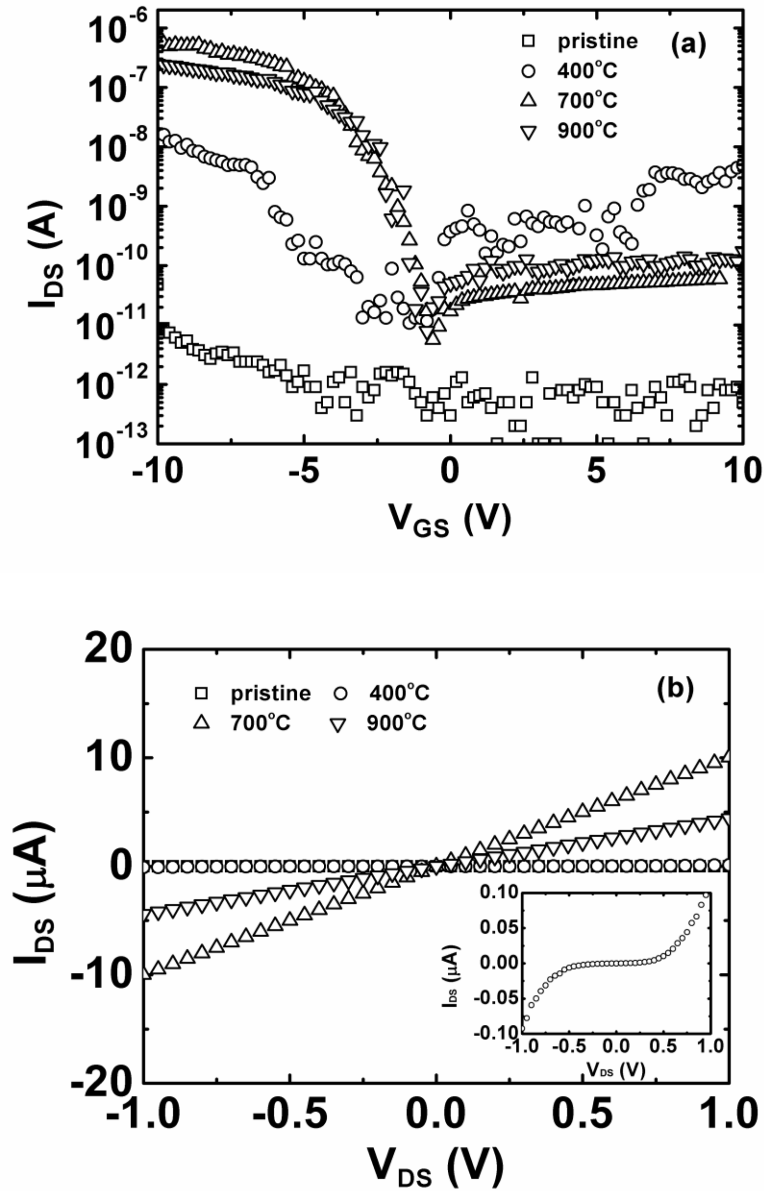

Figure 3.4: (a) I_{DS}-V_{GS} curves (V_{DS} = 0.1 V) for the SWCNT FET with Nb contacts before and after vacuum annealing at 400, 700, 900 ^{o}C for 1 hr. (b) Corresponding I_{DS}-V_{DS} curves of the SWCNT FET at V_{GS} = 0 V and the inset is an expanded curve of the SWCNT FET after vacuum annealing at 400 ^{o}C for 1 hr. The diameter of the SWCNT in the CNTFET is ~ 1.5 nm.

By further annealing at 700 ^{o}C for another 1 *hr* in vacuum, the *p*-channel *ON* current of our SWCNT FET increases by ~ 50 times (from 10^{-8} to 5×10^{-7} A), as seen in Figure 3.4a, while the current in *n*-channel decreases to < 10^{-10} A. It is also seen that the I_{ON}/I_{OFF} ratio for the *p*-channel is increased to 10^{5}, owing to the increase in I_{ON} while I_{OFF} is almost unchanged. In other words, the SWCNT FET has changed from ambipolar to unipolar *p*-type after the 700 ^{o}C annealing, signifying that the SBH for hole transport is much reduced, while that for electron transport is increased. In addition, it is seen in Figure 3.4b that the I_{DS}-V_{DS} curve of the SWCNT FET has become linear, meaning the contacts have become near Ohmic (or the SBH is very small) after the 700 ^{o}C annealing. The improvement achieved by the 700 ^{o}C annealing is believed to be owing to the formation of niobium carbide (Nb_2C) between the SWCNT and Nb (Leroy et al., 2007), which is confirmed by the XRD measurement shown in Figure 3.3. The formation of the carbide (Nb_2C) has increased the work function of the metal contact from that of Nb (Φ_m ~ 4.3 eV) to that of Nb_2C (Φ_m ~ 5.2 eV) (Samsonov et al., 1972). Consequently, the Fermi level of the contacts has shifted closer to the edge of valence band of the SWCNT, meaning the SBH for hole transport has become negligible while that for electrons has increased substantially to prevent electron transport, thus yielding a much higher *p*-channel *ON* current and highly asymmetrical, unipolar I_{DS}-V_{GS} relation, as shown in Figure 3.4a. It is also believed that the process of Nb_2C formation at high temperature breaks up the Nb

oxide layer at the contact interface, similar to the TiC formation process (Bing-Yue et al., 2006). In addition, the formation of Nb_2C could be in the form of nanorod and transform the side-bonded contact to an end-contact structure or SWCNT/Nb_2C heterostructure with well-ordered interface (Zhang et al., 1999). As shown by the SEM pictures in Figure 3.2, the SWCNT laid on the surface of the Nb electrode disappears after the 700 ^{o}C annealing. This indicates that with the formation of niobium carbide (Nb_2C), the SWCNT is entirely embedded within the electrode, thus strengthening the coupling between SWCNT and electrodes. This, coupled with a higher work function of Nb_2C, meaning the Fermi level of contacts has shifted close to the edge of valence band of SWCNT, thus leading to a negligible contact SBH for hole transport, while increasing that for electrons to prevent electron transport. It has been suggested that the effective contact area between SWCNT and Nb_2C electrodes also becomes larger (compared to that between SWCNT and Nb electrodes) with the SWCNT totally embedded in the carbide contact (Changxin et al., 2006; Zhang et al., 1999) and this can be another reason for the better electrical contacts (reduced resistance). The subthreshold slope of the SWCNT FET has also decreased to ~550 mV/dec (an improvement of about 5 times over that of the Nb contacted SWCNT FET). In addition, the transconductance (dI_{DS}/dV_{GS}) improved to 8.5×10^{-7} A/V, which is comparable to high-performance TiC-contacted SWCNT FET (Martel et al., 2001). Moreover, after the formation of Nb_2C, the contact resistance is found to

be about 100~200 kΩ, which is similar to that reported for TiC contacts (Zhang et al., 1999), suggesting that Nb_2C contacts are probably comparable to TiC contacts to SWCNT.

After further annealing at 900 ^{o}C for 1 *hr*, the *p*-channel *ON* current of SWCNT FETs decreases rather than increasing further, with respect to that after annealing at 700 ^{o}C, as shown in Figure 3.4a. From the XRD results shown in Figure 3.3c, the peak for another niobium carbide phase (NbC) is observed after 900 ^{o}C annealing, meaning the co-existence of Nb_2C and NbC, this could mean the Nb carbides (mixture of Nb_2C and NbC)/SWCNT interface may not be as well-ordered as the SWCNT/Nb_2C heterostructure, thus impeding the carrier flow. Furthermore, the work function of NbC (Φ_m ~ 4.85-4.95 eV) (Santerre et al., 1999) is slightly lower than that of Nb_2C (Φ_m ~ 5.2 eV), which probably results in a small increase in the SBH for hole transport. Therefore, the *p*-channel *ON* current of the SWCNT FET after 900 ^{o}C annealing is reduced. This signifies that the optimum annealing temperature for the formation of the Nb carbide contact for *p*-type SWCNT FET is 700 ^{o}C to form pure Nb_2C contacts and that 900 ^{o}C annealing should be avoided.

In conclusion, the change in the electrical characteristics of Nb contacted CNTFET is attributed to the formation of niobium carbide at the contacts. We will now relate that change to the change in the Schottky barrier height (SBH) of the contact. The SBH of the contacts was estimated using the usual Schottky barrier

model, as expressed by equations (3.1) and (3.2) (Hunger et al., 2004; Perello et al., 2007). As we want to investigate the pristine Schottky barrier height of metal and CNT contact, the back gate voltage is set as zero (V_{GS}=0V). As shown in Figure 3.5a, our device behaves well according to the Schottky model. The SBH at zero bias (Φ_b) is estimated by plotting the effective SHB (Φ_e), extracted from Figure 3.5a, against the square root of bias voltage ($V^{1/2}$) and fitting it linearly by equation (3.2), as shown in Figure 3.5b.

$$I \propto T^2 \cdot \exp\left(-\frac{e\Phi_e}{kT}\right) \qquad (3.1)$$

$$\Phi_e \propto \Phi_b - \left(\frac{eV}{\pi\varepsilon_1\varepsilon_0}\right)^{1/2} \qquad (3.2)$$

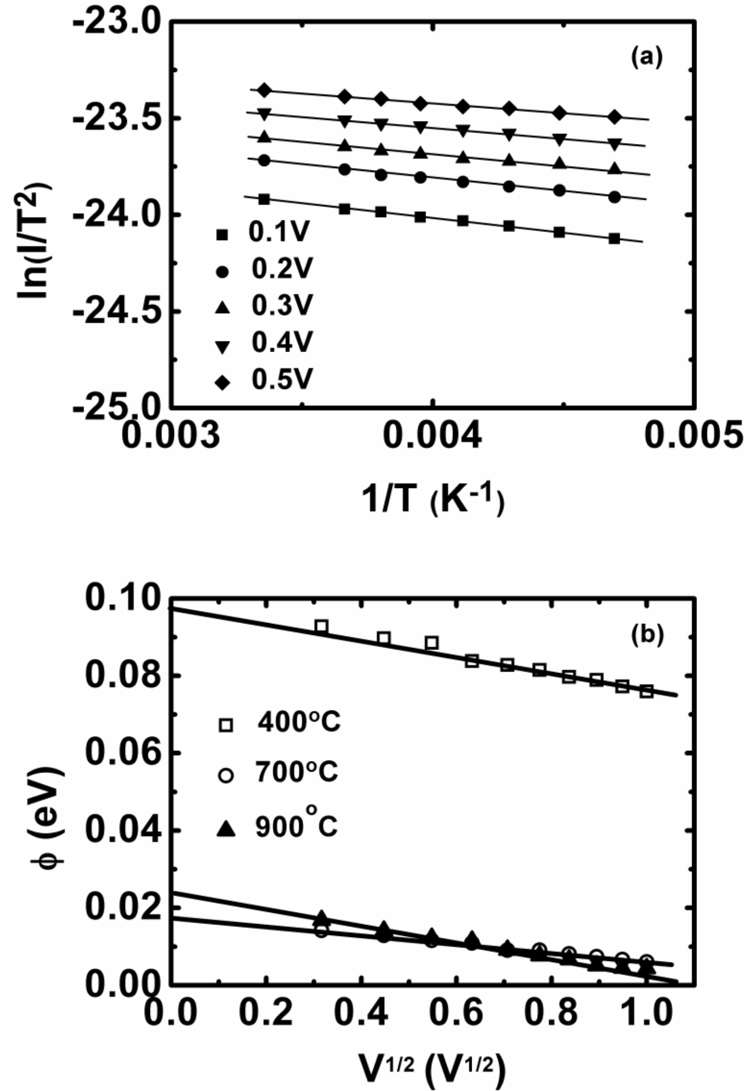

Figure 3.5: Plots of (a) $\ln(I/T^2)$ versus $1/T$ from 200 to 300 K for different bias voltages, V = 0.1 to 0.5 V in steps of 0.1 V, to determine the contact effective Schottky barrier height (Φ_e) for hole transport, gate bias V_{GS}=0V, and (b) effective SBH as a function of the square root of bias voltage ($V^{1/2}$). Schottky barriers at zero bias voltage (Φ_b) are attracted for devices after annealing at 400, 700 and 900 ^{o}C, respectively.

The SBH of the Nb/SWCNT contact after 400 ^{o}C annealing is estimated to be Φ_b~ 98 meV. After the formation of niobium carbide (Nb_2C) at 700 ^{o}C annealing, the SBH of the Nb_2C/SWCNT contact decreases significantly to Φ_b~18 meV (a decrease of > 80%), hence leading to a much higher current through the contact and resulting in the unipolar *p*-type characteristic, as shown in Figure 3.4a. With further annealing at 900 ^{o}C, the SBH of the niobium carbide and SWCNT contact increases from 18 to 24 meV, owing to the formation of an additional niobium carbide phase NbC. The variation of the contact SHB is consistent with *I-V* characteristics shown in Figure 3.4.

Finally, it has been found that after 10 days of Nb_2C formation, the electrical characteristic of our SWCNT FET with Nb_2C contacts does not change significantly (see Figure 3.6), which means the stability of Nb_2C contacted SWCNT FET is good. This is probably related to SWCNT being totally embedded in the Nb electrodes (see Figure 3.2), meaning almost no contamination in the air can impact the SWCNT/Nb interface.

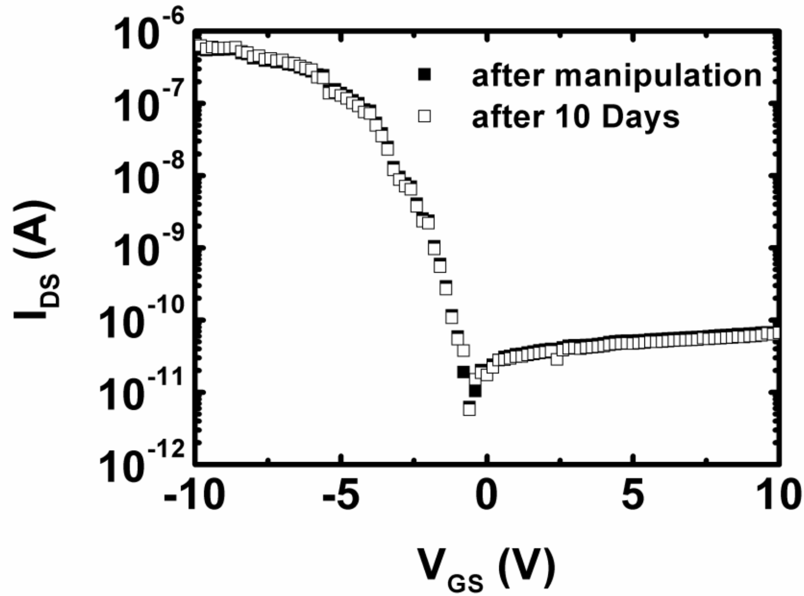

Figure 3.6: I_{DS}-V_{GS} curves (V_{DS} = 0.1 V) of Nb_2C contacted SWCNT FET immediately after the formation of Nb_2C and after exposure to air for 10 days.

3.5 Comparison of niobium carbide contacts with titanium carbide and palladium contacts

SWCNT FETs with either TiC or Pd source/drain contacts are fabricated as control devices in this work. This is because Pd is known as the best contact for *p*-type CNTFET and TiC is the only transition metal carbide that has been extensively studied as contacts for CNTFETs. The fabrication processing procedures for these two devices are similar to those described in Section 3.2, except that TiC contacts were formed by annealing Ti electrodes at 700 ^{o}C in

vacuum for 30 minutes (Leroy et al., 2006) and Pd contacts were given a general thermal annealing at 200 ^{o}C in N_2 ambient for 1 hr rather than a high temperature annealing (Javey et al., 2003). This is because for Pd and SWCNT contact, the aim of annealing is just to remove the possible contaminations at the contact interface and not for reaction between Pd and carbon atoms.

The performance of Nb_2C contacts is compared with TiC and Pd contacts to SWCNTs (d ~ 1.5 nm), as shown in Figure 3.7. It is seen that Nb_2C contacted SWCNT FET has comparable I_{ON} and subthreshold slope to those of Pd and TiC contacted devices, and shows a more unipolar p-type characteristic than TiC contacted device. The I_{DS}-V_{DS} curves of all three contacts demonstrate linear relation (see the inset of Figure 3.6). Hence, similar to Pd and TiC contacts, Ohmic characteristic can be achieved by Nb_2C contact to SWCNTs. The SBH for Pd and TiC contacts are measured to be ~17 and ~30 meV, respectively, thus Nb_2C with a SBH of ~ 18 meV is as good as Pd as contacts to SWCNTs and better than TiC. Owing to the higher work function of Nb_2C (Φ_m ~ 5.2 eV), than that of TiC (Φ_m ~ 4.33 eV), Nb_2C contacted SWCNT FET has a unipolar p-type characteristic, just like Pd contacted devices, while TiC contacted SWCNT FET has a more ambipolar characteristic. Therefore, Nb_2C is considered a better candidate than TiC as Ohmic contacts to p-type SWCNT FETs, and is as good as Pd.

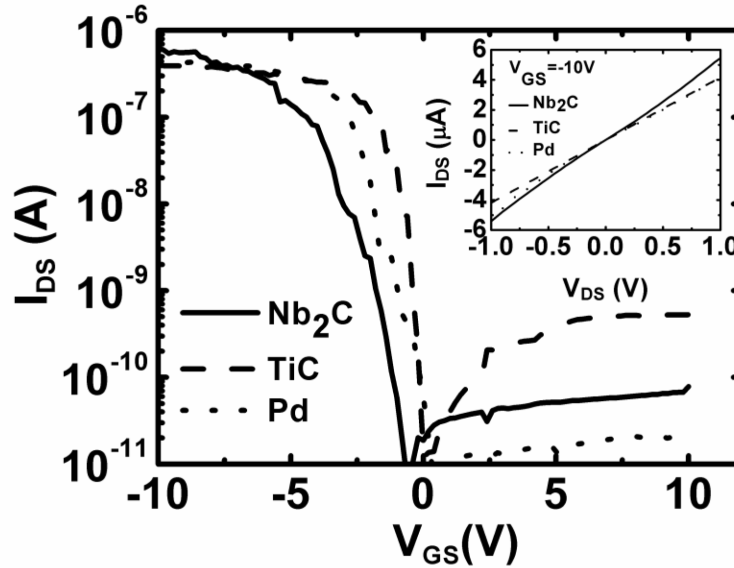

Figure 3.7: I_{DS}-V_{GS} curves (V_{DS} = 0.1V) for Nb_2C, TiC and Pd contacted SWCNT FETs (SWCNT diameter ~1.5 nm). Inset shows the corresponding I_{DS}-V_{DS} curves (V_{GS} = 0 V).

Figure 3.8 shows the I_{DS}-V_{DS} (V_{GS} = 0V) and I_{DS}-V_{GS} (V_{DS} = 0.1 V) characteristics of Pd and Nb_2C contacted SWCNT FETS with diameter of SWCNTs at ~1.5-1.6 and ~1.0 nm. It is seen that the dependence of the *I-V* characteristics on the diameter of SWCNT is significant for the former, but mild for the latter. When the diameter of SWCNT decreases to ~1.0 nm, Nb_2C can still form near Ohmic contact with SWCNTs, as manifested by the linear I_{DS}-V_{DS} relation in Figure 3.8b; while this cannot be achieved by Pd contacts, as shown in Figure 3.8a, where the I_{DS}-V_{DS} relation becomes non-linear when the diameter of

SWCNT decreases from ~1.53 nm to ~1 nm, which means the contact has changed from near Ohmic to Schottky characteristic. Our results for Pd contacts show a similar trend to that reported by Kim et al (Kim et al., 2005). The SBH of the Pd/SWCNT (d ~1 nm) contact is estimated to have increased to 78 meV (up from 17 meV for SWCNT with diameter of ~1.53 nm). This shows that the SBH of Pd contact is dependent on the bandgap (which is inversely proportional to diameter) of SWCNTs. In contrast, Nb_2C contacted devices with either large (~1.6 nm) or small (~1 nm) diameter SWCNTs exhibit similar linear I_{DS}-V_{DS} relation and near Ohmic performance, as shown in Figure 3.8b, and their SBHs remains at ~18 meV. Since the work functions of Nb_2C (~ 5.2 eV) and Pd (~ 5.12 eV) are similar, we believe the improvement of the electrical performance is related to the formation of carbide, Nb_2C, which leads to a more intimate bonding with SWCNT, regardless of the diameter of SWCNT.

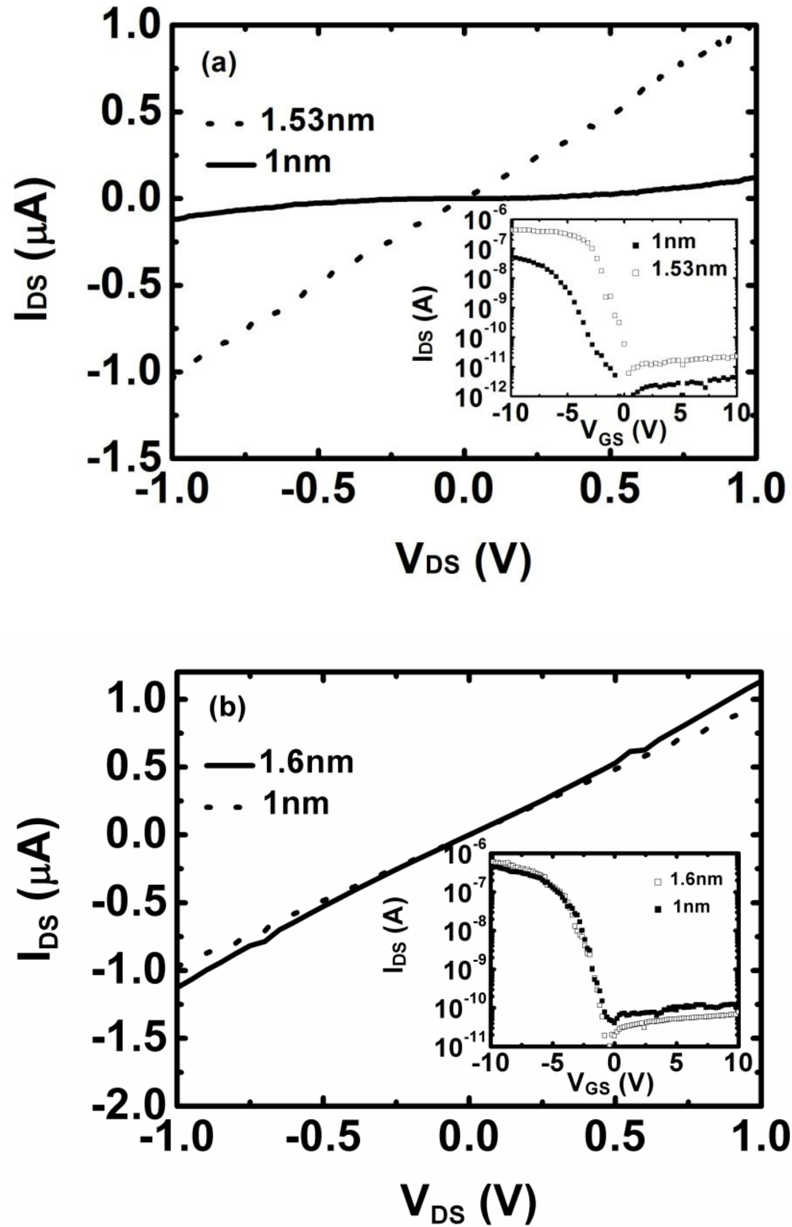

Figure 3.8: I_{DS}-V_{DS} curves (V_{GS} = 0 V) for (a) Pd contacted SWCNT FETs with 1.53 and 1 nm SWCNTs, and (b) Nb_2C contacted SWCNT FETs with 1.6 and 1 nm. Insets show the I_{DS}-V_{GS} curves (V_{DS} = 0.1 V) for SWCNT FETs.

3.6 Summary

We have fabricated and characterized SWCNT FETs with niobium contacts, which were subsequently thermally annealed in vacuum to yield niobium carbide contacts. It has been demonstrated that the formation of niobium carbide (Nb_2C) by annealing at 700 ^oC can dramatically decrease the contact resistance, which results in an increase in the *p*-channel I_{ON}, I_{ON}/I_{OFF} ratio and decrease of subthreshold slope for SWCNT FETs. This is owing to the reduction of the Schottky barrier height with the formation of Nb_2C at the interface of Nb electrode and SWCNT, as a result of the higher work function of Nb_2C and the improved bonding or better contact structure between Nb_2C and SWCNT. The performance of Nb_2C contacts to SWCNTs is shown to be as good as the Pd and TiC contacts for SWCNTs with diameter of ~1.5 nm. The Nb_2C contacts have also shown good stability. Mostly importantly, we have shown that Nb_2C can form near Ohmic *p*-type contacts to both large (> 1.6 nm) and small diameter (~1 nm) SWCNTs, while Pd can only form near Ohmic contact for large diameter SWCNT. In comparison with TiC contacts, Nb_2C contacts yield SWCNT FETs with more unipolar *p*-type characteristics, as a result of the higher work function. It should be noted that in order to exploit the niobium carbide contact for applications in SWCNT devices, thermal annealing should be conducted at 700 ^oC to yield Nb_2C only and higher annealing temperature should be avoided, e.g.,

annealing of Nb at 900 ^{o}C leads to the formation of an additional carbide phase, NbC, which degrades the contact performance.

Chapter 4

n-type random network single-wall carbon nanotube field effect transistor with Yttrium contacts

In this chapter, the investigations on Yttrium contact to *n*-type random network single-wall carbon nanotube field effect transistor (rn-SWCNT FET) will be presented.

4.1 The advantages of carbon nanotube thin film transistors

As discussed in Chapter 1, the challenges of CNTFETs based on individual SWCNT (i-SWCNT) have yet to be solved. One of the most serious problems is the poor reproducibility of device characteristics owing to the lack of precise control on the properties (chirality and diameter) of individual tubes in the synthesis. In addition, assembling individual SWCNTs on metal contacts is still technologically difficult. Furthermore, the current drive capability of individual SWCNTs (I_{MAX} ~ 25μA) is limited by the maximum conductance of SWCNT (Javey et al., 2003) and the Schottky barrier at the SWCNT and metal contacts (Heinze et al., 2002), which constrains the output current of i-SWCNT FET. On the other hand, random network SWCNTs (rn-SWCNT) FETs, where an ensemble of large number of individual tubes constituting a network (instead of individual SWCNT) is used as the channel, have shown to be promising (Seidel et

al., 2004; Snow et al., 2005; Snow et al., 2003) for applications which require large current, e.g., power transistor, flexible electronics, etc. This is because rn-SWCNT FETs have a structure, similar to the thin film transistor (TFT), with a large active area of an ensemble of SWCNTs in each device that would result in a high current drive. Moreover, the structure of rn-SWCNT FETs allows them to avoid the challenges faced by i-SWCNT FETs: (i) statistically minimizes the effects of electronic heterogeneity of individual SWCNTs, thus improving the reproducibility and uniformity of the device performance; and (ii) relaxes the process requirements of precise control of position and orientation of individual SWCNTs in the devices.

4.2 The status of *n*-type rn-SWCNT FET

To date, *p*-type rn-SWCNT FETs have been successfully fabricated (Hur et al., 2005; Izard et al., 2008; Nouchi et al., 2008; Ohishi et al., 2006; Ozel et al., 2005; Po-Wen and Chien-Hua, 2008; Seidel et al., 2004; Snow et al., 2005; Snow et al., 2003; Zavodchikova et al., 2009; Zhou et al., 2004) and have demonstrated high performance, e.g., field effect mobility as high as 150 $cm^2/(V\ s)$ (Snow et al., 2005), which is much higher than that of amorphous Si (~1 $cm^2/(V\ s)$) (Madelung, 2000), a material commonly used in commercial thin film transistors (TFT). In contrast, the research on *n*-type rn-SWCNT FETs (Hur et al., 2005; Nouchi et al., 2008; Ozel et al., 2005; Zhou et al., 2004), which is also important to rn-SWCNT

based CMOS circuits is obviously lagging behind that of the *p*-type devices. Some groups have reported *n*-type rn-SWCNT FETs achieved by means of coating rn-SWCNT with polymer polyethylene imine (PEI) (Hur et al., 2005; Nouchi et al., 2008; Zhou et al., 2004) to chemically dope the carbon nanotubes. However, the life-time of PEI coated carbon nanotube FETs is very limited as a consequence of the low air stability of PEI (Balasubramanian et al., 2008), which makes this method not suitable for practical applications. Therefore, a more reliable method is needed to fabricate *n*-type rn-SWCNT FETs. Since both individual and rn-SWCNT FETs have shown to be Schottky barrier transistors (Fukao et al., 2006; Heinze et al., 2002), it is in principle possible to achieve *n*-type characteristic by utilizing metal electrodes with ultra-low work function. It has been reported that i-SWCNT FETs with Calcium (Φ_m ~2.8 eV) (Nosho et al., 2005), Scandium (Φ_m ~3.5 eV) (Zhang et al., 2007b; Zhang et al., 2008), Gadolinium (Φ_m ~3.1 eV) (Kim et al., 2008), or Yttrium (Φ_m ~3.1 eV) (Ding et al., 2009) contacts exhibit *n*-type transport characteristic. However, to our knowledge, the idea of contact engineering has not been applied to rn-SWCNT FETs to achieve *n*-type characteristics. In our work, we explore the fabrication of rn-SWCNT FETs without using chemical doping, but by contact engineering. Yttrium (Y) is chosen in this work as the contacts not only owing to its ultra-low work function of ~3,1 eV, but also because Y/CNT contacts have shown Ohmic characteristic and relatively good stability in air (Ding et al., 2009). Moreover, its

lower commercial price than that of Sc or Gd, which makes it more cost-effective, is another advantage.

4.3 Fabrication procedure of Yttrium contacted rn-SWCNT FET

The fabrication procedure of rn-SWCNT FET is similar to that of i-SWCNT FET as discussed in Chapter 2. Highly doped silicon wafer with 200 nm dry thermal oxide (SiO_2) was used as the substrate. The silicon substrate was used as the back gate of FETs. Before depositing SWCNTs onto the substrate, the wafer was cleaned in hot Piranha solution (3:1 H_2SO_4:H_2O_2) for 45 minutes to clean the wafer surface and enhance the adhesion between SWCNTs and SiO_2. The SWCNTs were deposited onto the SiO_2 surface from the CNT solution by spin coating as no alignment is necessary, which makes the fabrication much easier.

In our work, semiconducting-rich SWCNT sample bought from *SWeNT.inc* (90% tubes are semiconducting, of which 50% have (6, 5) chirality) was used to prepare the SWCNT solution using the following recipe: 40 mg of SWCNTs powder and 1 g of sodium dodecylbenzene sulfonate (NaDDBS) were mixed with 100 ml DI water. The mixture was ultrasonicated by a homogenizer (750 Watt, 90% amplitude) for 30 mins, followed by centrifugation at 14,000 rpm for 3 hr. The supernatant (~80%) was subsequently decanted carefully to yield

only well dispersed or small bundled SWCNTs. The typical diameter and length of SWCNTs in the solution were about 1 nm and 1 μm, respectively. A few tubes of length up to ~2 μm are also observed by scanning electron microscopy (SEM). The purified solution (roughly 150 μL) was then carefully dropped via a pipette near the surface and in the center of the of the substrate (1 cm × 1 cm) spinning at 5000 rpm to deposit a thin film of SWCNTs on the SiO_2 surface. The samples were then rinsed in DI water to remove the NaDDBS residues and dried by filtered N_2 gas. As determined from SEM images, which were taken at random locations on the substrate, a monolayer of RN-SWCNTs was found to be deposited on the substrate surface (see Figure 4.1). Prior to device fabrication, the samples coated with SWCNTs were annealed at 400 ℃ to remove surfactants and water molecules to ensure good contact quality with metal. The source and drain metal electrode [Y/Au (50/30 nm)] were deposited by means of electron beam evaporation (chamber pressure~5×10^{-7} mbar). The Y layer is in direct contact with the rn-SWCNT and the Au layer was used to prevent oxidation of Y, as Y is a rare earth metal that is reactive in air. After the standard metal lift-off process, the active regions of the FETs were protected by photoresist and the extraneous SWCNTs on the substrate were removed by O_2 plasma to electrically isolate the channel region of individual transistors.

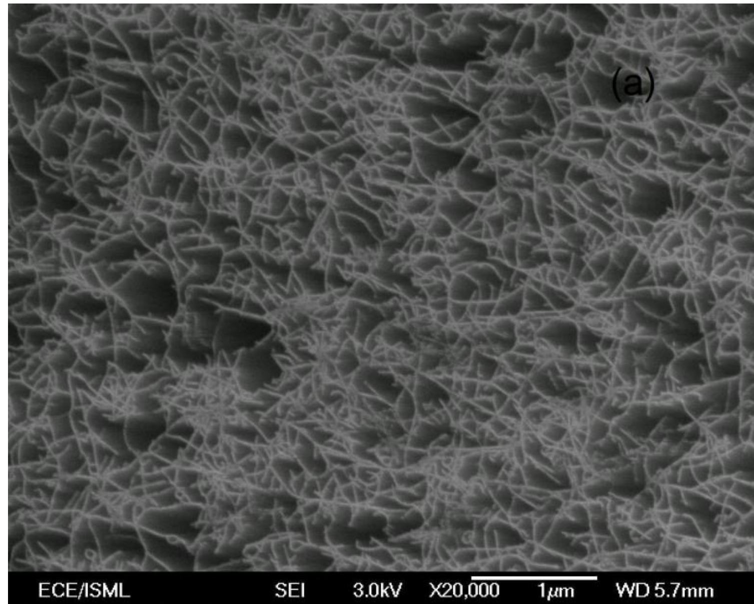

Figure 4.1: SEM picture of random network of SWCNTs on the SiO_2 substrate.

4.4 The electrical characterization of rn-SWCNT FET with Yttrium contacts

Figure 4.2a shows a typical rn-SWCNT FET and it is seen that the SWCNT strands are randomly distributed in the network of SWCNTs between the source and drain electrodes. The FET channel therefore comprises many transport routes of SWCNT strands connected to each other. As a SWCNT can be either semiconducting or metallic, depending on its chirality, and that metallic tubes can weaken the gate control effect in the carbon nanotube FET, it is essential to have the rn-SWCNTs compose of as many semiconducting SWCNTs (*s*-SWCNTs) as

possible. However, in contrast to i-SWCNT FETs, it is not necessary to remove all the metallic SWCNTs (*m*-SWCNTs) in the channel of a rn-SWCNT FET to achieve good gate control effect. This is because as long as one *s*-SWCNT exists in a transport route, it would exhibit semiconducting characteristic. As indicated in the radial breathing mode Raman characterization of the RN-SWCNT (see Figure 4.2b), there are three obvious peaks observed in the region from 150 to 400 cm^{-1}, corresponding to different chiralities of SWCNTs in the network, and the main peak is located around 275 cm^{-1}, which corresponds to a tube diameter, d = 0.86 nm ($\varpi_{RBM} = 224/d + 14$) (Rao et al., 2001). This is consistent with the (6, 5) chirality of *s*-SWCNTs in our sample. All these indicate that the channel of the FET is mainly composed of *s*-SWCNTs and hence, the devices have the potential to exhibit high on/off current ratio. Moreover, it is observed that the SWCNT strands in the network are thin and uniform, meaning the RN-SWCNTs are mainly composed of separated individual SWCNTs or small bundles of just a few SWCNTs.

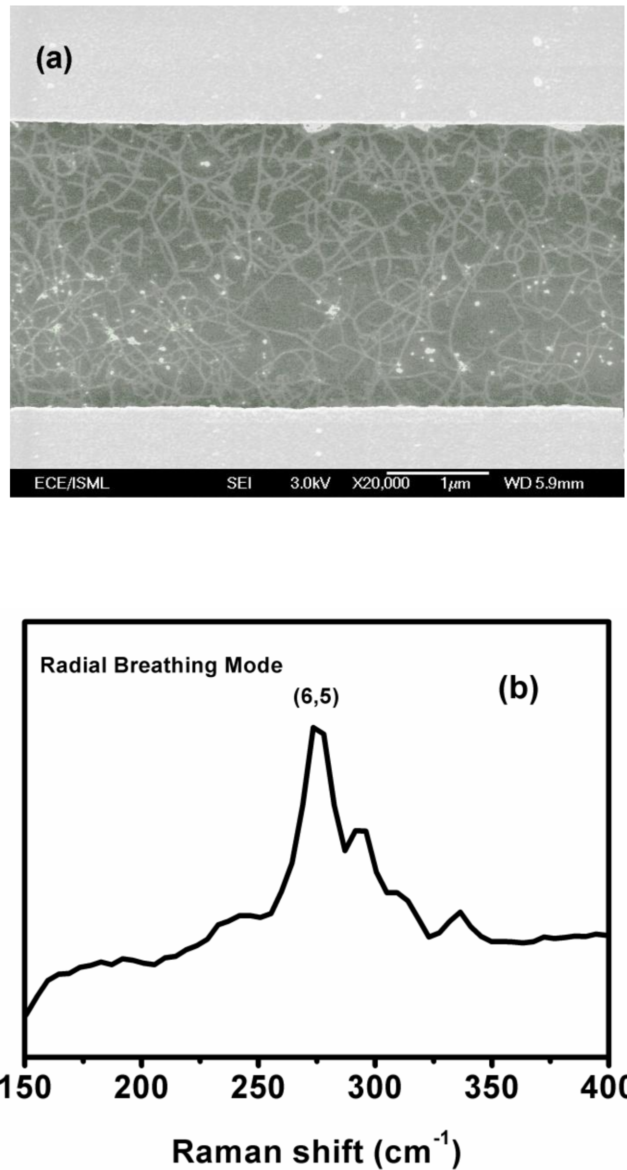

Figure 4.2: (a) SEM picture of a RN-SWCNT FET with Yttrium source and drain contacts (the lighter shade regions in figure), and (b) radial breathing mode Raman characteristic of the RN-SWCNT on the SiO_2 substrate.

Figure 4.3a depicts the linear scale I_{DS}-V_{GS} curve of one of our rn-SWCNT FETs (channel length, $L_C = 4$ μm; channel width, $W_C = 10$ μm), which obviously shows that the Y contacted rn-SWCNT FET exhibits *n*-type characteristic. The result confirms that *n*-type rn-SWCNT FET can be achieved by means of contact engineering, similar to i-SWCNT FETs. The semi-logarithmic scale I_{DS}-V_{GS} curve shown in the inset of Figure 4.3a indicates that the on/off current ratio of the RN-SWCNT FET is close to 10^4. The On-current of the transistor is defined as the current at a gate voltage, $V_{GS} = 10$ V, and the Off-current is the minimum current in the range of V_{GS} from - 10 to +10 V. From Figure 4.3b, it is noted that I_{DS} increases linearly with V_{DS} at low bias voltage, hence it can be inferred that the Y electrodes form a near Ohmic contact with the conduction band of the SWCNTs. Although our rn-SWCNT FETs exhibit *n*-type characteristic, the semi logarithmic scale I_{DS}-V_{GS} curve in the inset of Figure 4.3a reveals that the *p*-branch current (at $V_{GS} = -10$ V) of the Y contacted rn-SWCNT FET is not insignificant at ~10^{-7} A and is only just over a decade lower than the *n*-branch current, meaning the fabricated devices are more like ambipolar devices rather than pure unipolar *n*-type devices. Such ambipolar characteristic is typical of the fabricated rn-SWCNT FETs with Y contacts in this work, and is not desirable for CMOS applications.

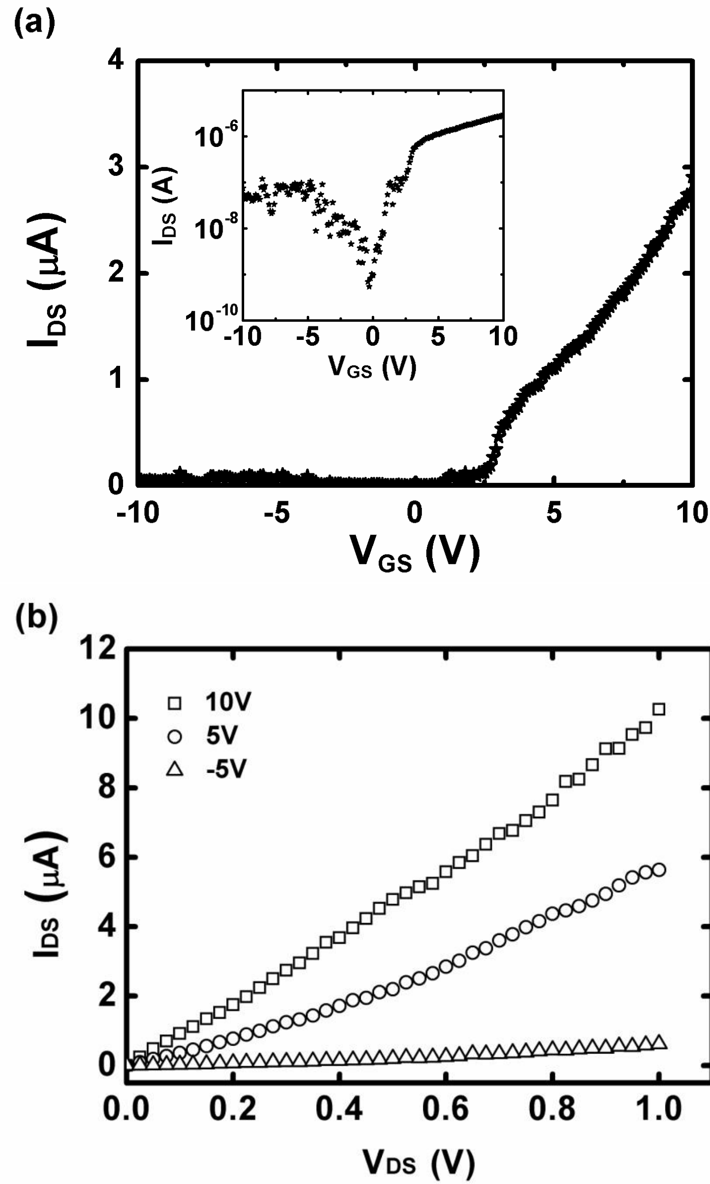

Figure 4.3: IV characteristics of a rn-SWCNT FET (channel length, $L_C = 4$ µm; channel width, $W_C = 10$ µm): (a) I_{DS}-V_{GS} curve at $V_{DS} = 0.1$ V in linear scale for V_{GS} from -10 to 10 V, and the inset shows the curve in semi logarithmic scale; and (b) I_{DS}-V_{DS} curves at $V_{GS} = 10$, 5, and -5 V for V_{DS} From 0 to 1 V.

The effects of rn-SWCNT FET channel length, L_C, on the transistor characteristics is shown in Figure 4.4. As expected, the *n*-branch On-current (I_{ON}), the Off-current (I_{OFF}), and the *p*-branch On-current (I_p) decrease with increasing L_C, since a longer channel length means a higher channel resistance and more cross-nanotube junctions along the transport routes. It is seen that although transistors with L_C = 2 μm has the highest I_{ON} ~ 10^{-5} A, the on/off current ratio (I_{ON}/I_{OFF}) is low at only ~10^2. On the other hand, for L_C = 6 or 8 μm, while I_{ON}/I_{OFF} is higher than 10^4, I_{ON} is low at just over 10^{-7} A. Consequently, we have chosen L_C = 4 μm (I_{ON} ~ 10^{-6} A, I_{ON}/I_{OFF} ~ 10^4) as the optimum channel length for further investigations.

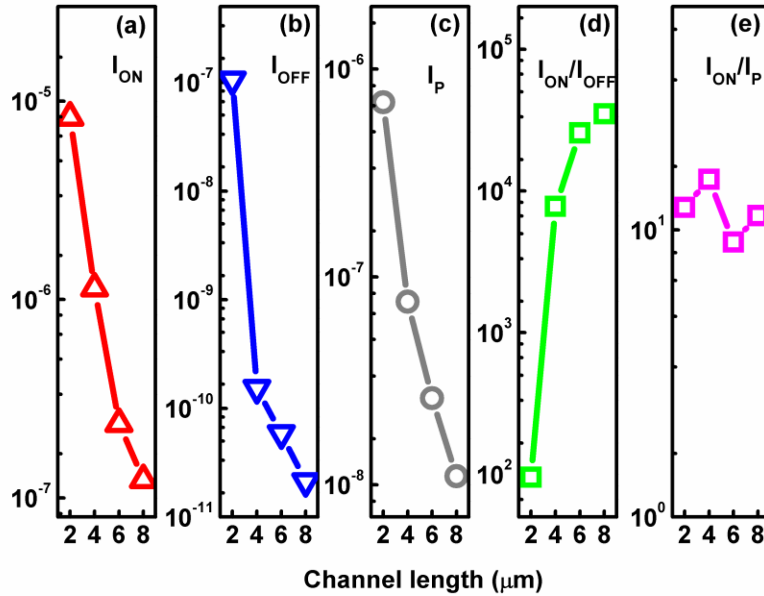

Figure 4.4: The effects of rn-SWCNT FET channel length on transistor characteristics: (a) *n*-branch On-current (I_{ON}), (b) Off-current (I_{OFF}), (c) *p*-branch on-current (I_p), (d) on/off current ratio (I_{ON}/I_{OFF}) and (e) *n*-/*p*-branch current ratio (I_{ON}/I_p). The channel width, W_C = 10 μm and the data indicated are averages of 20 devices.

As noted earlier in the inset of Figure 4.3a and in Figure 4.4e, our rn-SWCNT FETs are more ambipolar, rather than unipolar *n*-type with I_{ON}/I_p ~ 10. This is in contrast to Y contacted i-SWCNT FETs, which are more unipolar *n*-type with I_{ON}/I_p ~ 10^3 (Ding et al., 2009), achieved using contact metals of low work function. We therefore suspect that the more ambipolar characteristic of our rn-SWCNT FETs is caused by the presence of the cross-nanotube junctions in the SWCNT network, which are absent in the channel of i-SWCNT FETs. As a high I_{ON}/I_{OFF} >10^3 is observed for our RN-SWCNT FETs (see inset of Figure 4.3a and

Figure 4.3d for L_C = 4 μm), it can be confirmed that there are no pure metallic transport routes comprising entirely of *m*-SWCNTs in the transistor channel. The semiconducting transport routes in the RN-SWCNT channel can be categorized into four simplified types (see Figure 4.5). If a transport route composes entirely of *s*-SWCNTs (type I), it will exhibit *n*-type characteristic similar to a Y contacted SWCNT FET, albeit the cross-nanotube junctions will result in additional channel resistance. On the other hand, if *m*-SWCNTs are present in a transport route, the crossed *m*- and *s*-SWCNT junctions would be critical to the transport characteristic of this route. This is because the junction between crossed *m*- and *s*-SWCNT forms a rectifying Schottky barrier, while the *s*-*s* or *m*-*m* SWCNT junctions are good tunnel contacts with high conductance (Fuhrer et al., 2000). As shown in Figure 4.5, when the *m*-SWCNTs appear at the two ends of a transport route while the inner part of the route is semiconducting (type II), the transport mechanism of the route would then be subjugated by the Schottky barriers formed at the *m*- and *s*- SWNCT junctions (highlighted in Figure 4.5), as the *m*-SWCNTs form near ohmic contact with Y electrodes. The Schottky barrier at an *m*- and *s*-SWCNT junction shows *p*-type dominant behavior (Austing et al., 2007; Fuhrer et al., 2000; Yun-Hi et al., 2006), consequently hole current would probably be flowing in the Y contacted rn-SWCNT channel as well, via type II transport routes. When only one end of a transport route is *m*-SWCNT while the rest is semiconducting (type III), the transport route would behave like a Schottky diode

owing to the *n*-type near Ohmic contact formed at *s*-SWCNT/Y electrode and *p*-type Schottky contact formed at the *m*- and *s*-SWCNT junction. Therefore, electron current would conduct in this route depending on the polarity of the applied bias voltage (V_{DS}): type III on the left shown in Figure 4.5 would conduct electron current, while that on the right allows minimal current flow. Lastly, when the *m*-SWCNTs appear in the middle of a transport route (type IV), it would comprise two back-to-back Schottky *m*- and *s*-SWCNT diodes and therefore only small junction leakage current can pass through this route, which can be ignored compared with the current in other routes. In reality, additional *m*- and *s*-SWCNT junctions appear in the inner part of the type II, III and IV routes and they can be regarded as combination transport routes (e.g., type II-IV shown in figure 4.5). Since more Schottky barriers exist in such routes, the current flow would be very small.

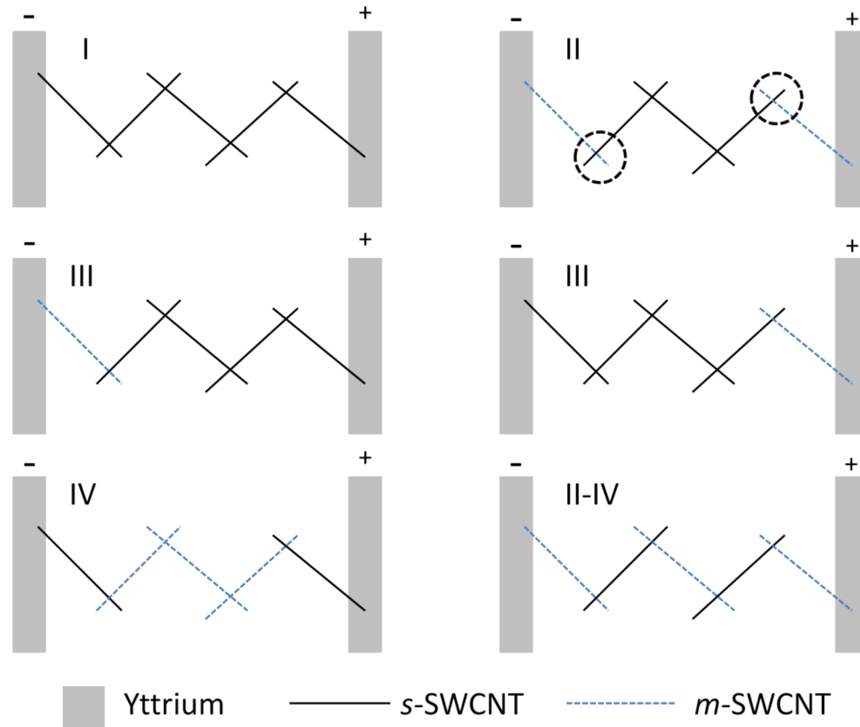

Figure 4.5: Schematics showing the 4 simplified types (I, II, III, IV) of transport routes in the RN-SWCNT FET channel. An example of combination transport route (Type II-IV) is also shown.

4.5 Optimization of rn-SWCNT FET by chemical etching

As the rn-SWCNT FETs in this work are constructed from semiconducting enriched carbon nanotube sample with 90% semiconducting nanotubes, most of the SWCNT strands in the FET channel would be semiconducting. Therefore, most of the conducting routes would compose of entirely *s*-SWCNTs and exhibit *n*-type characteristic. However, as the remaining

10% of SWCNTs in the network are of the metallic type, the hole current in type II routes shown in Figure 4.5 would possibly exist in the channel. This could explain the ambipolar I_{DS}-V_{GS} curve observed, with a smaller *p*-branch current than the *n*-branch current.

In order to improve the *n*-type unipolar characteristic of our rn-SWCNT FETs and also to verify our explanation above, the *m*-SWCNTs in the channel need to be removed to reduce the number of *m*- and *s*- SWCNT junctions in the rn-SWCNT channel. Several methods have been explored to deal with this problem. One approach that has been recently demonstrated is to lithographically pattern the channel dimensions such that the channel is long and narrow with respect to the tube lengths, which breaks the percolation in the metallic network (Qing et al., 2008). As only a single *s*-SWCNT in a multi-tube transport pathway is needed to yield an overall semiconducting behavior, it is possible to reduce significantly the possibility of metallic pathways by cutting narrow strips into the rn-SWCNT oriented along the overall transport direction. However, by using this method, the device area could be reduced, thus negating the advantage of large output current of rn-SWCNT FET. A second approach is via electrical breakdown — to deposit relatively high-density percolative SWCNT films, turn the semiconducting tubes “off” using the gate bias, and apply a large drain-source voltage pulse to burn out the metallic network, or at least a few critical metallic tubes or junctions. However by using this technology, the semiconducting

SWCNTs in the network would very likely be mis-killed by the thermal heating generated in the neighboring metallic SWCNTs. Moreover, this technique is not efficient as it has to be applied to individual devices on the wafer.

Therefore in this work, we employed the method of chemical etching to remove the metallic SWCNTs in the channel of rn-SWCNT FET. Compared with the above methods, the chemical etching is more efficient as it is applied simultaneously to all the devices on a wafer. The electrophilic molecules — 2,4,6-triphenylpyrylium tetrafluoroborate (2,4,6-TPPT) - were used to selectively etch the *m*-SWCNTs in the FET channel. The substrate was soaked and stirred in the 2,4,6-TPPT solution (~ 3 mM) for the reaction. As electrophilic (electron-accepting) molecules are believed to have stronger reactivity toward *m*-SWCNTs than *s*-SWCNT, owing to the finite electron density at the Fermi level of *m*-SWCNT (So et al., 2007), the conductance of *m*-SWCNTs in the network was found to be selectively suppressed after the etching. As shown in Figure 4.6a, the On- and Off-currents of our rn-SWCNT FET as well as the *p*-branch current decrease after the chemical etching by 2,4,6-TPPT, which means the number of transport routes is reduced as a result of broken *m*-SWCNTs in the channel. It is observed that with the decrease of current, I_{ON}/I_{OFF} increases by about two orders of magnitude, from ~10^3 to ~10^5, which confirms that the number of *m*- and *s*-SWCNTs junctions responsible for the leakage current in the FET channel has reduced. It is interesting to note that the *n*-branch current decreases by about one

order of magnitude, while the *p*-branch current decreases more significantly, by over 3 orders of magnitude, thus yielding a highly *n*-type unipolar characteristic, as shown in Figure 4.6a. This further proves the removal of *m*- and *s*-SWCNT junctions in the rn-SWCNT FET channel, consequently leaving the electron current to be dominant. It is seen that high performance *n*-type rn-SWCNT FET has been achieved by employing contact engineering with Y electrodes and its I_{ON}/I_{OFF} ~ 10^5 is comparable to the *n*-type rn-SWCNT FETs achieved by converting from originally *p*-type devices using PEI chemical doping (Nouchi et al., 2008).

As shown in Figure 4.6b, the variation in I_{ON} of 20 rn-SWCNT FETs (L_C = 4 μm, W = 10 μm) after the chemical modification process is just over one decade, which is lower than the corresponding deviation of i-SWCNT FETs of up to 3 decades, owing to the difference in nanotube diameter (Chen et al., 2005b). This is likely because rn-SWCNT FETs have many nanotubes in the channel and the effect caused by the difference in the tube diameter is significantly mitigated. Therefore, compared with i-SWCNT FETs, rn-SWCNT FETs can achieve better device reproducibility.

It should be noted that the results of the chemical etching process is dependent on the reaction time. As shown in Figure 4.6c, the reaction of metallic SWCNTs and 2,4,6-TPPT is not momentary but continuous. Therefore in the

experiment, depending on the density of SWCNTs of the network, it is important to identify the correct reaction time to optimize the device characteristics.

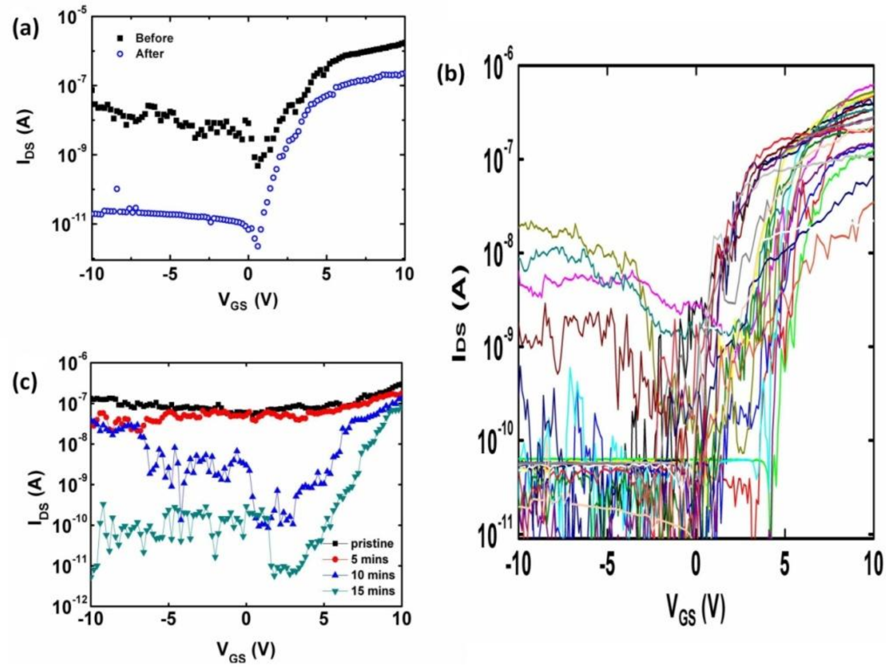

Figure 4.6: (a) I_{DS}-V_{GS} curves (V_{DS} = 0.1 V) of Y contacted rn-SWCNT FET (L_C = 4 μm, W = 10 μm) before and after the reaction with 2,4,6-TPPT, (b) I_{DS}-V_{GS} curves (V_{DS} = 0.1 V) of 20 RN-SWCNT FETs (L_C = 4 μm, W = 10 μm) after reaction with 2,4,6-TPPT, demonstrating the small deviation in the On-current of RN-SWCNT FETs, and (c) the effect of reaction time on the I_{DS}-V_{GS} curve of Y contacted rn-SWCNT FET (L_C = 2 μm, W = 10 μm).

The effects of chemical etching by 2,4,6-TPPT on the distribution of I_{ON}/I_{OFF} and I_{ON}/I_p of our rn-SWCNT FETs (L_C = 4 μm, W = 10 μm) are shown in

Figure 4.7. Prior to etching, ~85% of the fabricated RN-SWCNT FETs (L_C = 4 μm, W = 10 μm) have I_{ON}/I_{OFF} higher than 10^3 and the highest current ratio attained is 5×10^4. After etching, a still substantial ~75% of the rn-SWCNT FETs have I_{ON}/I_{OFF} higher than 10^4 and the highest current ratio achieved is 8×10^5, indicating both numbers have increased by about one order of magnitude. The change in I_{ON}/I_p is more drastic, most of the transistors have the current ratio 10-10^2 before etching, and this has up shifted to 10^3-10^4 after etching (an increase by two orders of magnitude).

The linear mobility, μ, of FETs can be estimated by the expression: $\mu = \frac{dI_{DS}}{dV_{GS}} \frac{L_C}{W} \frac{1}{V_{DS}} \frac{t_{ox}}{\varepsilon_o \varepsilon_{SiO_2}}$, where the channel length L_C = 4 μm, channel width W_C= 10 μm, bias voltage V_{DS} = 0.1 V, and gate oxide thickness t_{ox} = 200 nm (ε_o, and ε_{SiO2} are the permittivitives of free space and SiO_2, respectively). It has been found that μ of our rn-SWCNT FETs (after removing *m*-SWCNTs by 2,4,6-TPPT etching) can be up to 25 $cm^2V^{-1}s^{-1}$. This value is higher than that of other organic FETs (Fukao et al., 2006), and higher or at least comparable to that of reported *p*-type rn-SWCNT FETs with similar structures (back-gated, L: 2~μm, W~100μm) (Zhou et al., 2004). The transconductance g_m ($= \frac{dI_{DS}}{dV_{GS}}$) of our devices is about 0.12 mS/mm and this value is also comparable to that of reported *p*-type rn-SWCNT FETs (back gated, L=7μm, W=130μm) (Snow et al., 2005).

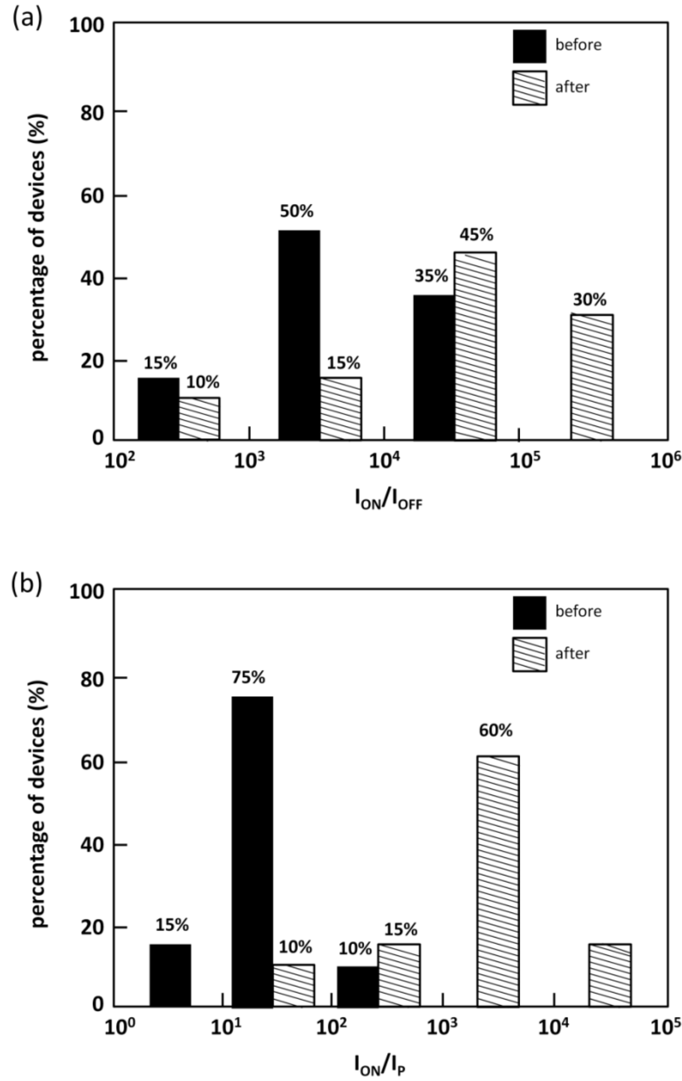

Figure 4.7: The effects of chemical etching by 2,4,6-TPPT on the distribution of (a) on/off current ratio (I_{ON}/I_{OFF}), and (b) *n-/p*-branch on-current ratio (I_{ON}/I_p) of rn-SWCNT FETs ($L_C = 4$ μm, $W = 10$ μm).

Finally, it has been found that the performance of our *n*-type rn-SWCNT FET is stable in air, as shown in Figure 4.8, where the characteristics of air-

exposed device (after 1-7 days) exhibit typical *n*-type behavior. This is believed to be due to the protection by Au layer on top of Y electrodes, which prevents Y from oxidation in the air. Therefore, it is seen that the two layer Y/Au electrode structure can achieve stable *n*-type rn-SWCNT FETs despite using a reactive rare earth metal (Y) with low work function. As shown in Figure 4.8, the I_{DS}-V_{GS} curve has a positive shift after 7 days (the shift is very small after 1 day). This is probably caused by O_2 adsorption of RN-SWCNTs in air (Kim et al., 2008), which we believe can be prevented by passivating the devices with inert material shortly after fabrication.

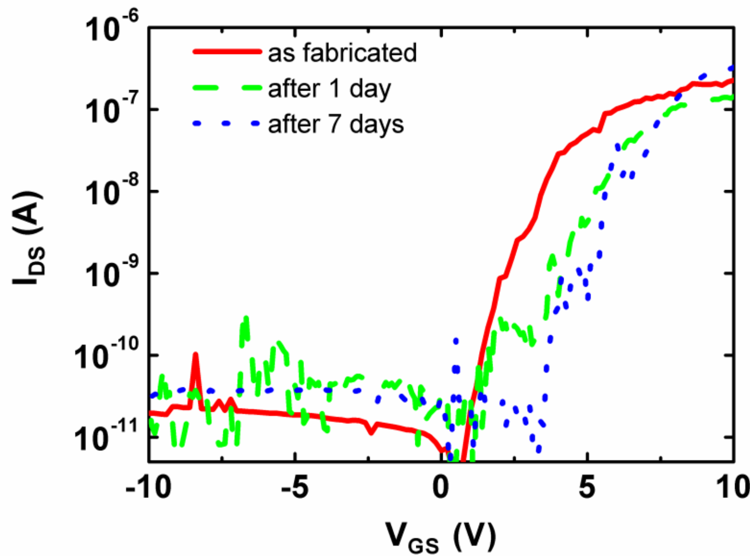

Figure 4.8: I_{DS}-V_{GS} (V_{DS} = 0.1 V) curves of a rn-SWCNT FET (L_C = 4 μm, W = 10 μm and after reaction with 2,4,6-TPPT,) with Y/Au (50/30 nm) electrodes, immediately after fabrication, and after 1 day and 7 days exposure to air.

4.6 Summary

In summary, we have successfully fabricated *n*-type rn-SWCNT FETs (L_C = 2, 4, 6 and 8 μm; W = 10 μm) with Y source and drain contacts and the *n*-type transport characteristic is attributed to the low work function of Y. It has been found that I_{ON} decreases with increasing L_C, owing to the longer channel and presence of more cross-nanotube junctions in the SWCNT network. Owing to the high percentage of semiconducting tubes (~90%) in the SWCNT sample, the as fabricated rn-SWCNT FETs exhibit good I_{ON} (~10^{-6} A) and I_{ON}/I_{OFF} current ratio (~10^4) when the channel length is 4 μm. The presence of *m*- and *s*- SWCNT Schottky junctions, as a result of the existence of ~10% metallic tubes, leads to the exhibition of undesirable ambipolar characteristic by the as fabricated rn-SWCNT FETs. By means of 2,4,6-triphenylpyrylium tetrafluoroborate (2,4,6-TPPT) modification, the *m*-SWCNTs in the rn-SWCNTs can be selectively removed, resulting in the conversion of typically ambipolar devices to unipolar *n*-type FETs with I_{ON}/I_p ~10^3-10^4. The chemical modification also improves the I_{ON}/I_{OFF} up to ~10^5, which is comparable to the *n*-type rn-SWCNT FETs achieved by converting from originally *p*-type devices using PEI chemical doping. The high value of I_{ON}/I_{OFF} is not achieved at the expense of mobility, which is estimated to be as high as 25 $cm^2V^{-1}s^{-1}$ for our unipolar *n*-type rn-SWCNT FETs. It should be noted that the mobility value is better than that of other organic FETs, and higher or at least comparable to that of reported *p*-type rn-SWCNT FETs. The

transconductance g_m of our devices is ~ 0.12 mS/mm and this is also comparable to that of reported *p*-type rn-SWCNT FETs. It has also been demonstrated that the reproducibility of rn-SWCNT FETs is better than that of i-SWCNT FETs. Moreover, our fabricated devices have demonstrated air-stable *n*-type characteristics. In summary, the achievement of uniform and stable *n*-type rn-SWCNT FETs, using low work function metal such as Y as contacts, suggests that contact engineering may be a viable and promising process for high performance *n*-type rn-SWCNT FET fabrication.

Chapter 5

The Semiconducting-Semiconducting Double-Wall Carbon Nanotube Field Effect Transistors

In this chapter, the differences between semiconducting-semiconducting double-wall carbon nanotube field effect transistors (*s-s* DWCNT FETs) and single-wall carbon nanotube field effect transistors (SWCNT FETs) will be investigated. In particular, the studies focus on the effects of inter-tube interaction of DWCNT on transistor characteristics.

5.1 The unique electrical properties of double wall carbon nanotube

Double-wall carbon nanotubes (DWCNTs) have garnered increasing attention for multiple applications because of their unique structure, which provides them with characteristics lying between those of SWCNT and multi-wall carbon nanotube (MWCNT). Depending on the chirality of the inner and outer tubes, DWCNTs can behave either like SWCNTs (both metallic and semiconducting) or semi-metallic material with very small bandgap, owing to the inter-tube interactions (Liu et al., 2009). Therefore, in addition to SWCNT, DWCNT also has the potential to be employed as a functional element for FET application. On the other hand, DWCNT has been reported to possess mechanical

properties and structural and thermal stability that are superior to those of SWCNT (Kim et al., 2004). DWCNT is hence regarded as a better candidate for applications where electronic devices have to operate under high temperature and high current environments. Moreover, compared with SWCNT, the current carrying capability of each tube of DWCNT has been experimentally demonstrated to be up to about two times that of SWCNT (Sunkyung et al., 2007; Wang et al., 2007), which means the output current of the DWCNT devices would be correspondingly larger.

5.2 The Status of DWCNT FET

Depending on the different combinations of the outer and inner tubes, there are four possible types of DWCNTs, as the two tubes can be either metallic (*m*) or semiconducting (*s*). It has been shown both *m*-*s* and *m*-*m* (with the first and second letters indicating the type of the outer and inner tube, respectively) DWCNTs, i.e, DWCNTs with metallic outer tube, exhibit metallic characteristic as their electrical properties are dominated by the outer tube (Liu et al., 2009). Therefore, both *m*-*s* and *m*-*m* DWCNTs cannot be used to make CNTFETs. On the other hand, the CNTFETs based on *s*-*m* DWCNT are found to exhibit weak gate modulation effect with very low on/off current ratio (< 10) at room temperature, owing to the inter-tube interactions (Liu et al., 2009). Therefore, *s*-*m* DWCNT is also not an ideal candidate for FET application, even though it has

been substantially studied to explore the inter-tube interactions in CNTs (Jie et al., 2007; Shidong and Grifoni, 2007; Wang et al., 2005). In conclusion, only *s*-*s* DWCNT could be used to fabricate high performance CNTFETs.

The first *s*-*s* DWCNT FET was reported in 2004 (Shimada et al., 2004), which described the ambipolar characteristic exhibited by *s*-*s* DWCNT, owing to the large diameter of the outer tube of DWCNT (Liu et al., 2009; Wang et al., 2007; Wang et al., 2005), which is similar to the characteristic of large diameter SWCNT FETs. In essence, *s*-*s* DWCNT FETs behave similar to semiconducting (*s*)-SWCNT FETs. Theoretically, the electronic properties of *s*-*s* DWCNT would be different from those of *s*-SWCNT, owing to the interactions between the inner and the outer tube in the former (Jing et al., 2005; Okada and Oshiyama, 2003). However, the effects of the inter-tube interaction on the transport characteristics of *s*-*s* DWCNT FETs have not been experimentally studied. Therefore, the main motivation of the current work is to investigate the transport characteristics of *s*-*s* DWCNT FETs, and by comparison with those of *s*-SWCNT FETs, to study the inter-tube interaction in *s*-*s* DWCNT.

5.3 The fabrication procedure of DWCNT FET

The fabrication process of back gated DWCNT FET (see Figure 5.1a) is similar to that of SWCNT FET by using AC dielectrophoresis (see Chapter 2). A typical fabricated DWCNT FET is shown in Figure 5.1b. In our work, the channel

length of DWCNT FETs was about 0.6~0.8 μm. Ti/Au (10/40 nm) electrodes were applied as the source and drain contacts. The yield of devices with only one DWCNT bridging the source and drain electrodes, as shown in Figure 5.1b, is about 30%. Therefore, our process can guarantee that there are enough devices for systematical study in our work. The TEM picture, as shown in Figure 5.1c, confirms the structure of DWCNT sample in our work.

The diameters of DWCNTs in the devices were measured by means of atomic force microscopy (AFM) and they ranged from ~1.3 to 3.7 nm. While in the control devices (SWCNT FETs), the diameter of SWCNTs was from ~ 0.9 to 2.35 nm.

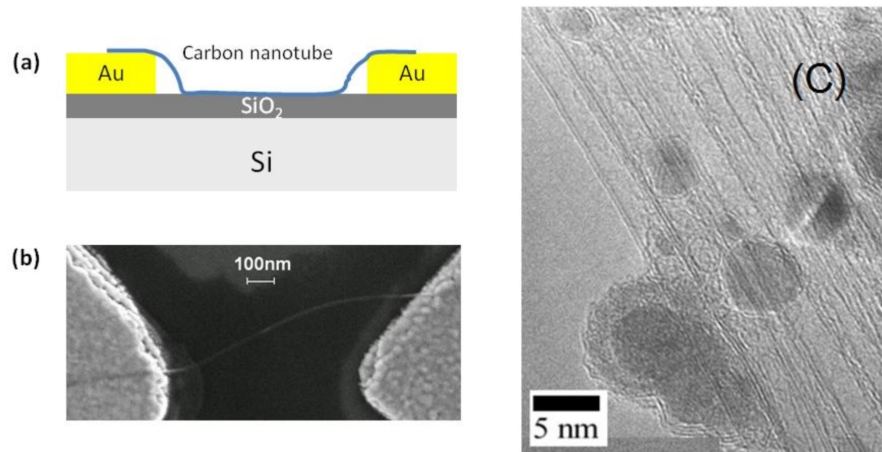

Figure 5.1: (a) Schematic layout of a back-gated carbon nanotube FET, where the carbon nanotube was deposited on the top of Ti/Au electrodes by AC dielectrophoresis, and (b) SEM picture of a typical DWCNT FET, (c) TEM picture of DWCNTs.

5.4 The electrical characteristics of DWCNT FET

5.4.1 The relationship between DWCNT FET characteristics and the structure of DWCNT

In the batch of DWCNT devices, three types of transport characteristics, i.e., metallic, semi-metallic and semiconducting have been observed, as shown in Figure 5.2a, corresponding to the *m-m*/*m-s*, *s-m* and *s-s* DWCNT channel, respectively. As for the batch of SWCNT devices, only the metallic and semiconducting characteristics are observed, as indicated in Figure 5.2b. The semi-metallic characteristic means the transport characteristic of the DWCNT FETs can be controlled by the gate voltage, like semiconducting SWCNT FETs, but the on/off current ratio (<10) is much lower than that of semiconducting FETs ($>10^3$). The semi-metallic characteristic is considered a unique feature of *s-m* DWCNT FETs. As our emphasis is the FET application of DWCNT, the following discussion will focus on *s-s* DWCNT FETs, i.e., those that exhibit on/off ratio much larger than 10.

a)

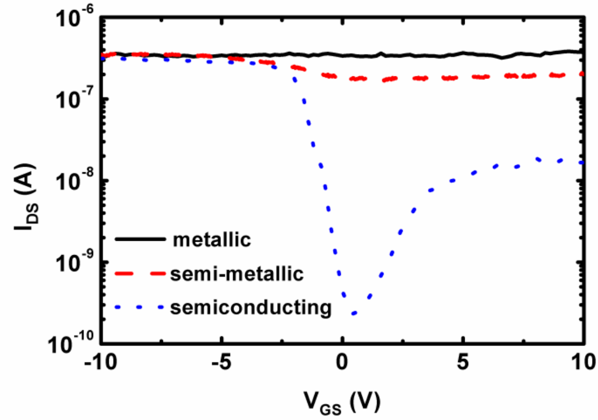

b)

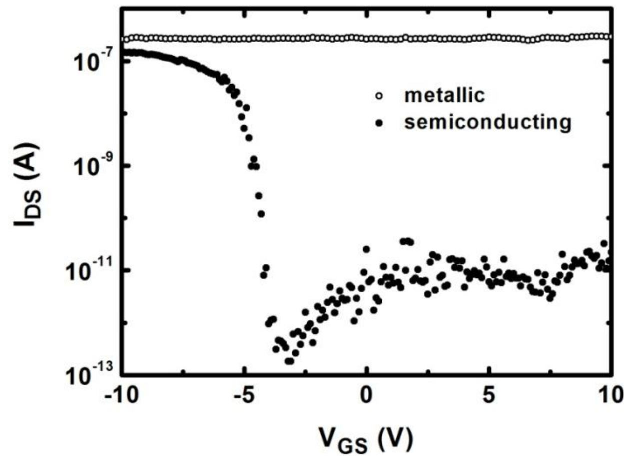

Figure 5.2: (a) I_{DS}-V_{GS} curves of three types of DWCNT-FETs: metallic (*m-m*/*m-s*), semi-metallic (*s-m*) and semiconducting (*s-s*) characteristics. The diameter of the DWCNTs exhibiting metallic, semi-metallic and semiconducting characteristics are 2.4, 2.37 and 2.34 nm, respectively. (b) I_{DS}-V_{GS} curves of two types of SWCNT-FETs: semiconducting (*s*) and metallic (*m*). The diameter of the SWCNTs exhibiting metallic and semiconducting characteristics are 1.96 and 2 nm, respectively.

5.4.2 Comparison between *s-s* DWCNT FET and *s*-SWCNT FET

In order to investigate the effects of tube-tube interactions in the *s-s* DWCNT, SWCNTs with diameter similar to that of DWCNTs (more accurately that of the outer tube) are selected to fabricate control SWCNT FETs. The comparison of transport characteristics (I_{DS}-V_{GS} curve) between the DWCNT and SWCNT FETs for various nanotube diameters is shown in Figure 5.3. In these comparisons, as the diameter of DWCNT and SWCNT are almost the same, the different performance of the two types of transistors could only result from the presence of the inner tube of DWCNT, or the inter-tube interaction in DWCNT. It is seen that the discrepancies in the electrical characteristics of these two devices vary with the nanotube diameter. This means it is the different diameters of the inner tube that results in different properties of the DWCNT.

As carbon nanotube transistors are Schottky barrier transistors (Heinze et al., 2002; Shidong and Grifoni, 2007) and high work function contacts (Ti/Au) would always lead to *p*-type characteristic (Nosho and et al., 2006), the on-state current (I_{ON}) of the DWCNT (and SWCNT) FETs in this work is defined as the source-drain current (I_{DS}) at a gate voltage, V_{GS} = -10 V, while the off-state current (I_{OFF}) is the smallest I_{DS} in the gate voltage range of -10 V < V_{GS} < 10 V. Figures 5.4 shows the I_{ON} and I_{OFF} comparison between the DWCNT and SWCNT FETs as a function of nanotube diameter.

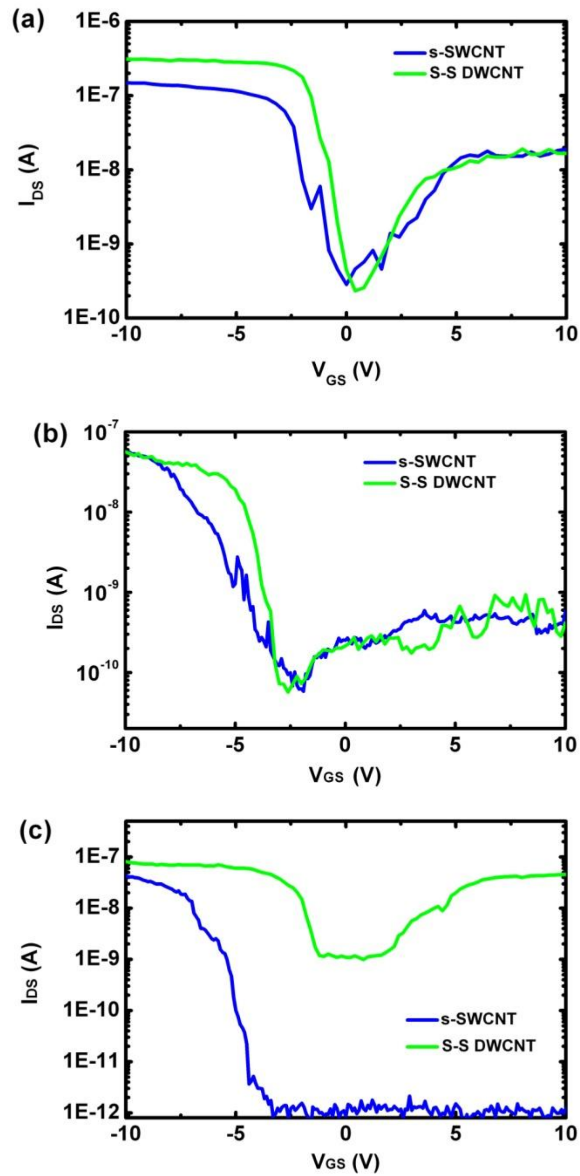

Figure 5.3: The I_{DS}-V_{GS} (V_{DS} = 0.1 V) comparison between DWCNT and SWCNT FETs. The diameters of DWCNT and SWCNT are respectively: a) 2.34 and 2.31 nm, b) 1.62 and 1.6 nm, and c) 1.38 and 1.34 nm.

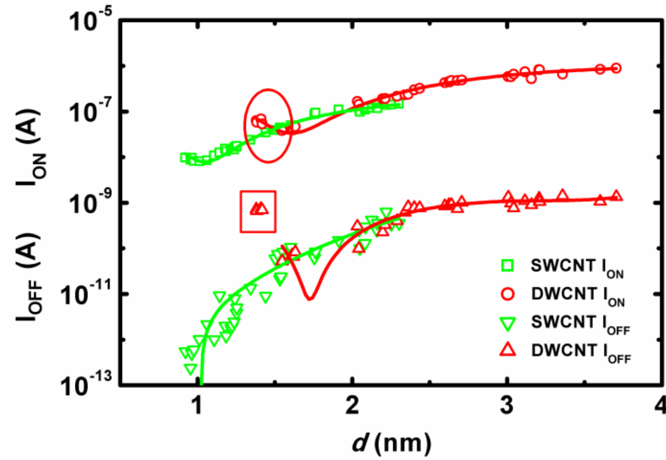

Figure 5.4: The On-current (I_{ON}) and Off-current (I_{OFF}) of DWCNT and SWCNT FETs as a function of the nanotube diameter. I_{ON} is I_{DS} at V_{GS} = -10 V and V_{DS} = 0.1 V, while I_{OFF} is the lowest I_{DS} in the range of V_{GS} from -10 to 10 V. the solid red lines are the polynomial fitted curves and the symbols are the experimental data.

5.4.2.1 For large diameter nanotubes (d ≥ 2 nm)

It is seen in Figure 5.4 that when the tube diameter is large (d ≥ 2 nm), the On-current (I_{ON}) of both DWCNT and SWCNT FETs increase monotonically with increasing tube diameter. This is attributed to the decrease of the Schottky barrier height at the DWCNT (SWCNT)/Au contacts, as a result of the increasing tube diameter. However, the values of I_{ON} are different for these two types of devices, with I_{ON} (DWCNT) > I_{ON} (SWCNT), as observed in Figure 5.4. On the other hand, the Off-current (I_{OFF}) of these two devices are almost the same. An

example of a pair of such FETs is shown in Figure 5.3a for a nanotube diameter, d~2.31-2.34 nm. It is seen that both devices exhibit ambipolar characteristic owing to the small bandgap (or large diameter) of tubes. Although they have almost the same value of *n*-branch current (~10 nA), the I_{ON} of DWCNT FET is about 2 times that of SWCNT FET. The Schottky barrier height (SBH) of both contacts were measured according to the Schottky barrier model (Sze, 1981) (see Equations 5.1 and 5.2) and are estimated, as shown in Figure 5.5:

$$I = T^2 \cdot \exp(-\frac{e\Phi_e}{kT}) \qquad (5.1)$$

$$\Phi_e \propto \Phi_b - \left(\frac{eV}{\pi\varepsilon_1\varepsilon_0}\right)^{1/2} \qquad (5.2)$$

It has been found that the SBH for DWCNT/Au contact is ~ 31 meV and that of SWCNT/Au contact is ~ 34 meV, as indicated in Figure 5.5b, which are very similar. This means the inter-tube interaction in DWCNT does not impact significantly its bandgap and work function, which determine the Schottky barrier at the DWCNT and metal contact. Therefore, the larger current of DWCNT FET can only be attributed to the current from the inner tube or the larger conductance of the outer tube of DWCNT compared with that of SWCNT of same diameter.

(a)

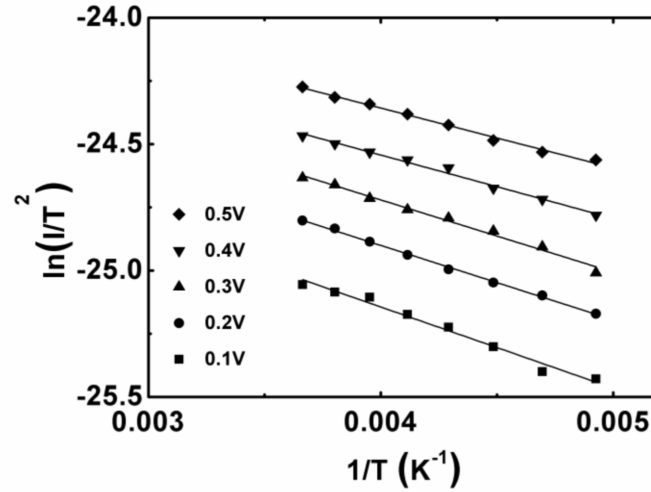

(b)

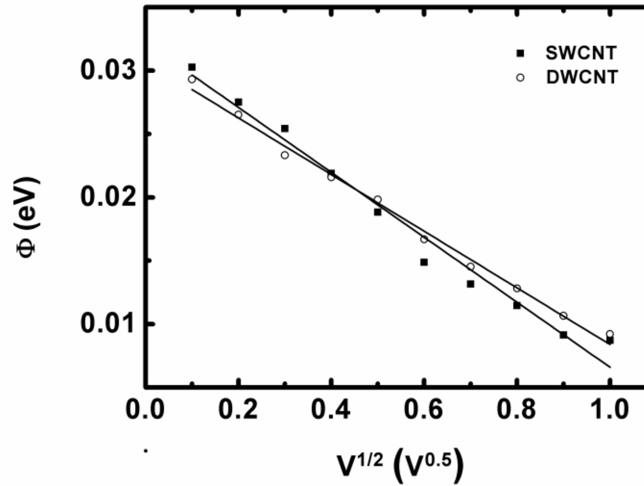

Figure 5.5: (a) Plots of $\ln(I/T^2)$ versus 1/T for T from 200 to 300 K for different bias voltages (V = 0.1 to 0.5 V in steps of 0.1 V) for DWCNT and Au Schottky contact, V_{GS}=0V. The biased dependent SBH (Φ_e) is extracted and plotted in (b) as a function of bias voltage ($V^{1/2}$) to yield the Schottky barrier height at zero bias voltage: Φ_b. The data for SWCNT and Au Schottky contact are also shown in (b).

The small Schottky barrier height of two contacts also indicates both DWCNT and SWCNT in the devices are individual tube rather than tube bundle. If the tubes in the channel are in the bundle form the diameter of each tube inside the bundle should be much smaller than 2nm which means the bandgap of them would be much larger. Therefore large schottky barrier height rather than small values would be measured for tube bundle and metal contacts. On the other hand the ambipolar characteristic of the devices also proves the devices are based on individual tubes rather than tube bundles.

The devices structure, as shown in Figure 5.1a, indicates that the DWCNT is deposited on top of Au surface, forming the side contact and therefore only the outer layer of DWCNT is in direct contact with the metal electrodes. As a result, the current mainly passes through the outer layer of DWCNT and the tunneling current from outer tube to the inner tube is almost negligible under small bias voltage (V_{DS} = 0.1 V) (Bachtold et al., 1999; Collins et al., 2001b). In our work, it has been found that the current in inner tube becomes significant to impact the electrical characteristic of the DWCNT FET when the drain bias voltage, V_{DS}, is larger than 3 V. As shown in Figure 5.6, with the increase of V_{DS} from 0.1 to 1 V (by one decade), the I_{ON} of both DWCNT and SWCNT FETs also increase by around one decade, which means the contacts are almost Ohmic (small Schottky barrier contact) and no significant tube-tube interaction happening in the DWCNT. However, when V_{DS} is increased from 1 to 3 V, it is seen that the I_{ON} of DWCNT FET increases by more than 6 times, while that of SWCNT FET increases only by around 3 times. This means at high voltage bias, the current passing through the

inner tube of DWCNT has become significant and contributed substantially to the total current even though the inner tube does not contact the Au electrodes directly. Therefore, it can be concluded that at low bias voltage (V_{DS} = 0.1 V), the current in the inner tube of DWCNT has almost no impact on the characteristics of DWCNT FET. Consequently, the larger I_{ON} of DWCNT FET observed in Figure 5.3a is attributed to the larger conductance of DWCNT.

It has been suggested (Sunkyung et al., 2007) that the electron–phonon scattering in the DWCNT might be weaker than that in SWCNT as a result of inter-tube interaction, which is obviously absent in SWCNT. We believe this may be the reason for the different conductance of these two types of tubes shown in Figure 5.3a. As the inner and outer tubes are coupled, the in-plane phonon modes are hence not well defined owing to the breaking of translational symmetry inside a nanotube, which makes the electron–phonon scattering ineffective. Although the results of Sunkyung et al (Sunkyung et al., 2007) are based on *m-m* and *m-s* DWCNTs, it is believed their explanation is also applicable to *s-s* DWCNT as this phenomenon results from the unique structure of DWCNT and does not depend on the chirality of the inner and outer tubes. Moreover, it has been reported experimentally (Green and Hersam, 2009) that, in the form of thin film, DWCNTs exhibit a larger current conductivity than SWCNTs, which is also likely to be owing to the larger conductance of individual DWCNTs composing the thin film. This further corroborates our explanation.

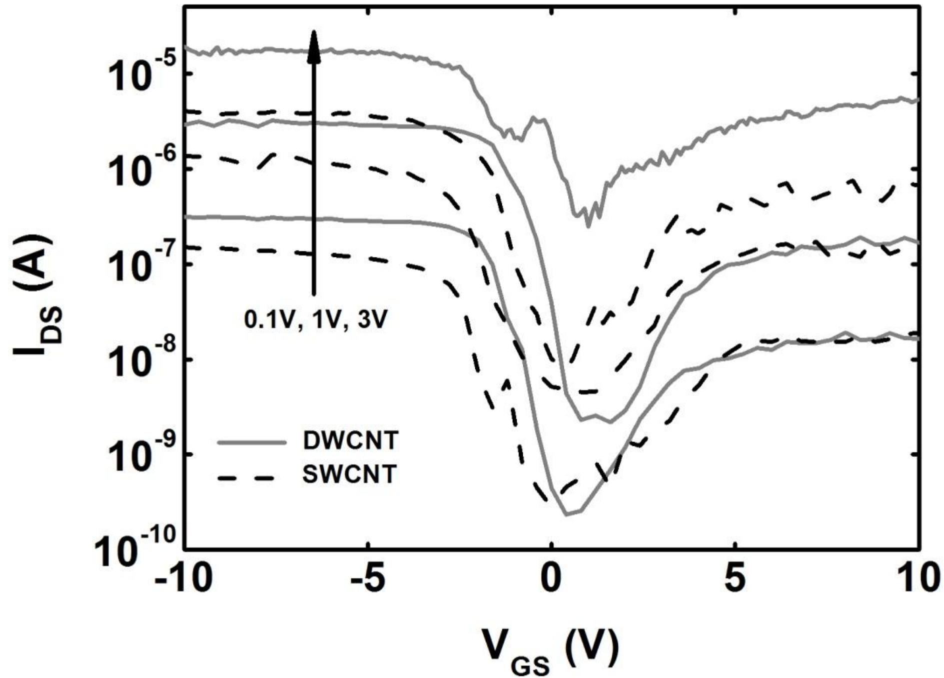

Figure 5.6: Effect of the drain field on the I_{DS}-V_{GS} characteristics of DWCNT FET and SWCNT FETs, V_{DS}= 0.1 V, 1 V and 3 V.

However, it is also observed that the *n*-branch current is almost the same for DWCNT and SWCNT FETs, as shown in Figure 5.3a, despite their different conductance. It is observed in Figure 5.3a that the *p*-branch current is always about one decade larger than the *n*-branch current. This is because the Fermi level of Ti/Au is closer to the valence band of nanotubes. Therefore, the Schottky barrier for electron transport is much higher than that for hole transport. The *n*-

branch current is hence dominated by the electron Schottky barrier which means the effect of nanotube conductance is almost negligible. As discussed earlier, the inter-tube interaction does not influence significantly the Schottky barrier of contacts under small V_{DS} bias voltage and therefore the *n*-branch currents of two devices are almost the same.

In the off state, Schottky barriers exist for both holes and electrons. Consequently, the off-state current is very sensitive to the Schottky barriers formed at the contacts. A simple model for conduction in the off-state is to include only the thermionic emission of both carriers: $I_{OFF} = AT^2 \exp(-q\Phi_e / kT) + BT^2 \exp(-q\Phi_h / kT)$, where the factors A and B are proportional to the effective mass and inversely to the diameter; Φ_e and Φ_h are respectively the Schottky barrier height for electrons and holes; T is the temperature and k is the Boltzmann constant. Such a mechanism would lead to an exponential dependence of I_{OFF} on the barrier height (Tseng et al., 2006). Therefore, I_{OFF} is not dependent on the conductance of the carbon nanotube and the same I_{OFF} is observed, as shown in Figure 5.3a.

5.4.2.2 For intermediate diameter nanotubes (2 > d ≥ 1.6 nm)

When the diameter of nanotubes decreases below 2 nm, the difference between DWCNT and SWCNT FETs changes, as shown in Figure 5.4. In fact, the

I_{ON} of DWCNT FET is no longer larger than that of SWCNT FETs. The example for a pair DWCNT and SWCNT FETs with a nanotube diameter ~1.6-1.62 nm is shown in Figure 5.3b. The smaller diameter means a larger bandgap for the nanotubes and hence, a larger Schottky barrier is formed at the nanotube/metal contacts, which results in a higher ratio of the *p*- to *n*-branch current (more than 10^2) in Figure 5.3b than that in Figure 5.3a (~ 10). By using the same methods discussed previously to estimate the SBH of this pair of devices, it is found the SBH for DWCNT/Au and SWCNT/Au contacts are 107 and 112 meV, respectively. The SBHs are still similar for the two types of nanotubes. Therefore in these devices, the large Schottky barrier dominates the transport characteristic of the carbon nanotube FETs and as a result, the difference between the conductance of DWCNT and SWCNT becomes not as important in the transport characterization, in contrast to the results shown in Figure 5.3a, where the nanotube diameter is bigger (hence a smaller contact Schottky barrier). As for I_{OFF}, as discussed previously, as long as the SBH of the carbon nanotube and metal contacts is the same, similar I_{OFF} would be achieved. It is found that the subthreshold slope of the DWCNT FET (1.24 V/dec) is smaller than that of SWCNT FET (1.36 V/dec) in this case, while they are similar in the earlier case (see Figure 5.3a). It should be noted that in this work, the difference in the subthreshold slope of DWCNT and SWCNT FETs is found to vary around 10% among all the devices. Therefore, we believe the difference of subthreshold

observed in Figure 5.3b is within experimental variation. It should be noted that as the data of DWCNT FETs are not available in the diameter range from 1.7 to 2 nm, we do not know exactly the differences between the DWCNT and SWCNT FETs in this region. However, using the data in the diameter region 1.5~1.7 nm to help establish the trends, we may conclude that with decreasing nanotube diameter in the range from 2 to 1.6 nm, the device characteristic is more dominated by the Schottky barrier rather than the properties of the tube bulk.

5.4.2.3 For small diameter nanotubes (d < 1.6 nm)

Finally, when the diameter of nanotube is small than 1.4 nm, as shown in figure 5.4, the decreasing I_{ON} and I_{OFF} of DWCNT FET suddenly turn to increase, allowing the DWCNT FETs to exhibit larger I_{ON} and I_{OFF} than those of SWCNT FETs, as shown in the example of Figure 5.3c. The On/Off current ratio of the DWCNT FET becomes less than 10^2 and it exhibits ambipolar characteristic while the corresponding SWCNT (with similar diameter) FETs exhibit high on/off current ratio (more than 10^4) and unipolar *p*-type characteristic. In principle, when the diameter of carbon nanotube is small, the large bandgap should result in highly unipolar characteristic owing to large Schottky barrier formed at the contacts, as observed for SWCNT FET. However for DWCNT FET, the observed I_{DS}-V_{GS} curve indicates that the effective bandgap of the DWCNT is very small

and hence both the Schottky barriers for hole and electron transport are small. The abnormal change of the bandgap of DWCNT is attributed to the inter-tube interaction in the DWCNT system. In theoretical studies (Jing et al., 2005; Okada and Oshiyama, 2003), it has been reported that the bandgap of *s-s* DWCNT with an ultra-small diameter inner tube would be narrowed owing to the inter-tube interaction in the *s-s* DWCNT system. In DWCNTs, it has been reported that the spacing between the inner and outer tubes is about 3.6 Å (Bandow et al., 2001), almost independent on the tube radius. Therefore, when the diameter of the outer layer of DWCNT is smaller than 1.4 nm, the diameter of inner tube is probably very small, down to 1 nm. For carbon nanotube with diameter smaller than 1 nm, the curvature of carbon nanotube would probably become significant, and the electronic structure of the DWCNT nanotubes would be significantly impacted by the different curvatures of the inner and outer tube (Jing et al., 2005; Okada and Oshiyama, 2003). This is because when a graphite sheet is rolled into a nanotube, the π states electron would be rehybridized with the σ states electron owing to its lack of mirror symmetry, which causes the downward shifts of the π and π^* electron states of the carbon nanotubes. The downward shifts of the π and π^* states of the inner tube are larger than those of the outer tube as such shift is dependent on the tube diameter. The bottom of the conduction band possessing the π^* character of the inner nanotube is thus located near or below the top of the valence band of the outer nanotube. Such overlap between the conduction band of

the inner nanotube and the valence band of the outer nanotube therefore results in the narrowing of the bandgap of *s-s* DWCNT. As a result, I_{ON} of the DWCNT FET would be larger than that of the corresponding *s*-SWCNT FET with the same diameter, as the Schottky barrier at the DWCNT/Au contacts would be significantly reduced, which also increases the off-current of the DWCNT FET. The Schottky barrier height of this DWCNT/Au contact is measured to be around 16 meV, which corroborates with the above discussion, and the Schottky barrier height for the corresponding SWCNT/Au contact is as high as 135 meV. It is interesting to find that the I_{DS}-V_{GS} curve of this DWCNT FET has a wide Off state region, about 4 V, while that for the two cases of DWCNT FETs (with larger diameter) discussed earlier is very small. This is because a small diameter DWCNT FET can never be turned off owing to the very small bandgap and hence the lowest current, composed of both hole and electron currents, is not sensitive to the shift of the Fermi level of Au in the bandgap of DWCNT.

5.5 The Ruthenium contacted DWCNT FET

In the previous chapters, it has been extensively discussed that the metal and CNT contact plays a significantly important role in the transport characteristics of CNTFET. In addition, one way to improve the contact performance has been discussed in Chapter 3, by means of carbide formation, and

another way using thiolate molecules doping will be discussed in the next chapter. In this work, in addition to investigating the unique transport characteristic of DWCNT, we would also investigate the way to optimize the metal and DWCNT contact.

Here, we would use Ruthenium (Ru) as the metal contact of *p*-type DWCNT FET, which has never been reported in literature. This is because Ru has a relatively high work function (4.7 eV) which is expected to form small Schottky barrier for hole transport in *p*-type DWCNT FET. More interestingly, oxidation or exposure to air of Ru presents no obstacle to its use as electrical contacts, because when Ru is oxidized to RuO_2, which can happen when it is heated in air at a temperature > 300°C (Sharma and Hines, 1983), it remains a good electrical conductor with a low resistivity (~50 μΩ cm). Moreover, RuO_2 has a higher work function (> 5.0 eV) than Ru and has excellent thermal stability (Jang and Lee, 2003). Therefore, it is expected that RuO_2 contact could perform as well as the best contact metals, e.g., Pd and Rh, in the CNTFET.

As shown in Figure 5.7, the I_{DS}-V_{GS} curve of Ru contacted DWNT FET does not significantly change after annealing in vacuum (at 400 ℃ for 15 mins). However, when it was annealed in O_2 gas (at 400 ℃ for 15 mins), the I_{ON} at *p*-branch increased by more than 1 decade which means the contact resistance decreased significantly. This change is attributed to the formation of RuO_2 at the Ru and DWCNT interface. As RuO_2 has a higher work function (~5.0 eV) than

Ru (~4.7 eV), the Schottky barrier height formed at DWNT/RuO_2 contact would be lower than that at DWNT/Ru contact. However, it is believed the change of the work function of metal contact is just one of the causes of the change of the contact characteristic. This is because the contact resistance of Pd (work function ~5.12 eV), despite having a slightly higher work function than RuO_2, is only several times (not decades) larger than that of Ru. Hence, we believe there are additional factors that have led to the significant improvement of contact performance (~1 decade) after the formation of RuO_2. One possibility is a better RuO_2/CNT interface formation at the contact which can result in the better quality contacts. This is because in the thermal annealing process (~400 ^oC), almost all the chemical residues attached at the Ru and DWCNT interface would evaporate. Therefore, the contact of DWCNT to the metal surface would be improved which means the surface of DWCNT would be more tightly touched with the electrode surface. In other words, the contact area could have increased after the annealing process, which can also contribute to the decrease of contact resistance.

Based on the above discussion, it can be concluded that the unique oxide of Ru, RuO_2, makes it an excellent candidate of contact to CNTFET, especially when the CNTFET is fabricated by depositing CNTs on top of metal electrodes. More importantly, Ru contacted CNTFET can be used in rich oxygen environment and high temperature condition without worry the of performance degeneration.

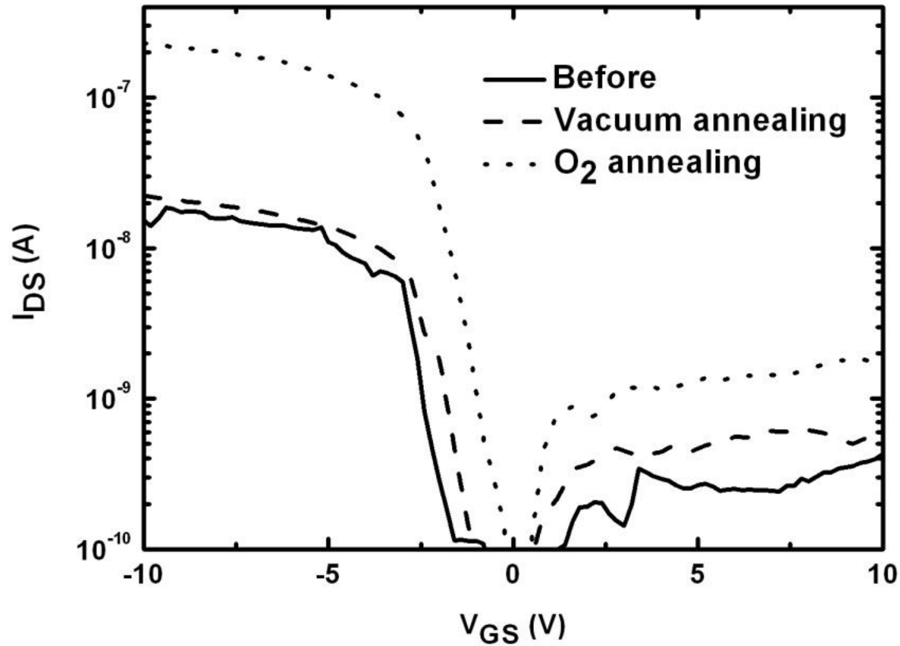

Figure 5.7: The I_{DS}-V_{GS} (V_{DS} = 10 mV) characteristics of Ru contacted DWNT FETs annealed in vacuum or O_2 ambient at 400°C for 15 mins, in comparison with that of transistor without annealing, the diameter of DWCNT is about 2.5 nm.

5.6 Summary

In summary, it has been found that in the different tube diameter regions, the characteristics of *s*-*s* DWCNT FETs can be significantly different from that of *s*-SWCNT FETs. In the diameter region, 2.0 nm > d > 1.6 nm, the DWCNT FETs behave similar to SWCNT FETs, as in this region the transistor characteristic is dominated by the Schottky barriers at the contacts. However, in the diameter

region, larger than 2 nm, where the effect of the conductance of tubes becomes important, the output current of DWCNT devices is found to be always larger than that of SWCNT devices. This is owing to the larger conductance of the DWCNT which results from its unique 2-tube structure. Finally in the diameter region, smaller than 1.6 nm, the tube-tube interaction in DWCNT becomes significant, which results in the bandgap narrowing of s-*s* DWCNT. Therefore, the transport characteristic of *s*-*s* DWCNT (d < 1.6 nm) FETs is different from that of *s*-SWCNT FETs, e.g., the output current of DWCNT transistor becomes much larger than that of SWCNT transistor and the on/off ratio of DWCNT devices is also significantly decreased. Therefore, it can be concluded that the inter-tube interaction is important to the electrical properties of *s*-*s* DWCNT. Both the conductance and bandgap of *s*-*s* DWCNT would be influenced by its inter-tube interaction. In particular, the conductance of *s*-*s* DWCNT is always larger than that of *s*-SWCNT with same diameter and the bandgap of *s*-*s* DWCNT with ultra-small diameter (< 1.6 nm) would be significantly smaller than that of the *s*-SWCNT with same diameter. Finally the application of Ruthenium contact in DWCNT FET has been investigated which shows that Ruthenium can be a good candidate as contact for high performance *p*-type CNTFET application, especially in a rich oxygen and high temperature environment, owing to the formation of its oxides (RuO_2) at the contact interface.

Chapter 6

Fabrication of single-wall carbon nanotube Schottky diode with asymmetric thiolate molecules modified gold contacts

In this chapter, investigations on the modification of gold contacts to CNT by means of thiolate molecules will be presented. Our studies have led to the successfully fabrication of SWCNT Schottky diode with asymmetric thiolate molecule modified gold contacts.

6.1 Carbon nanotube Schottky diodes

Diodes are one of the fundamental building blocks of modern semiconductor devices and they are used in rectification, switching, high frequency multiplier and photonic devices. Hence, a high performance diode characteristic is crucial to the development of electronic devices.

Nano-scale CNT diodes have already been achieved by forming either a *p–n* (Abdula and Shim, 2008; Chongwu et al., 2000; Lee et al., 2004; Zhang et al., 2007a) or metal–semiconductor Schottky junction (Jiao et al., 2008; Lu et al., 2006; Manohara et al., 2005; Yang et al., 2005). A CNT *p-n* junction can be formed through chemical doping (Chongwu et al., 2000), polymer coating (Abdula and Shim, 2008) or intramolecular junctions (Zhang et al., 2007a). In

addition, the *p-n* junction can also be manipulated by electrical gating using a pair of split gates (Lee et al., 2004).

Compared with *p-n* junction diodes, rectifying metal-semiconductor Schottky junctions have advantages owing to their higher switching speeds, lower forward resistance, lower noise level and inherent suitability for low-voltage, high-current applications (Sze 1981). In addition, the control of doping CNT is still a serious challenge and hence the electrical properties of a *p-n* junction diode demonstrated through doping of an individual nanotube always show leaky behavior owing to high doping and abrupt junction formation (Chongwu et al., 2000). Therefore in our work, we focus on CNT Schottky diodes.

In previous chapters, it has been extensively discussed that the carrier transport between carbon nanotubes (CNTs) and metal contacts is controlled predominantly by the Schottky barrier (SB) at the contact interface (Heinze et al., 2002) as the pinning effect is weak (Nosho and et al., 2006). The Schottky barrier height (SBH) between SWCNT and metal contact depends on several material parameters, e.g., the work function of metal electrode (Nosho and et al., 2006), the diameter of SWCNT (Chen et al., 2005b), and the bonding properties between SWCNT and metal electrodes (Vitale et al., 2008), of which the work function of metal electrode is deemed the most important parameter. Hence, it is possible to construct a SWCNT Schottky diode by adjusting the Fermi level alignment between the SWCNT and metal contact through engineering the work functions

of metal electrodes. This has been demonstrated by a number of research groups (Lu et al., 2006; Manohara et al., 2005; Yang et al., 2005), where Schottky diodes were fabricated by depositing two dissimilar metals at the two ends of a semiconducting SWCNT, one with a work function lower (e.g., Al or Ti) than that of SWCNTs (~4.8 eV) to yield a Schottky contact, while the other with a work function higher (e.g., Pd, Pt and Au) than that of SWCNTs to achieve an ohmic (more near ohmic) contact. These SWCNT Schottky diodes with asymmetrical metal contacts have reported good performance, e.g., the $I_{forward}/I_{reverse}$ ratio of ~10^3–10^4 and a high current carrying capacity in excess of 14 µA (Manohara et al., 2005). However, there is one possible drawback that is associated with the ease of oxidation tendency of metals (Al and Ti) with low work functions, which can pose a potential obstacle for circuit applications. For example, if the CNT is deposited on top of Al electrode to form a diode structure, the device performance would deteriorate shortly with the oxidizing of Al in the air. Therefore SWCNT Schottky diodes with asymmetrical metal electrodes cannot be fabricated by AC dielectrophoresis technology (Vijayaraghavan et al., 2007) which is one of the most powerful technologies for CNT devices fabrication.

Another way to fabricate SWCNT Schottky diodes was reported by Jiao et al. (Jiao et al., 2008), where atomic force microscopy (AFM) manipulation was used to form asymmetrical SB at the two metal/SWCNT contacts. Although the performance of such a device is air-stable, this fabrication method is not only

complex but also time consuming, which could rule it out from practical applications.

The fabrication of SWCNT Schottky diodes by means of contact engineering using thiolate molecules has been demonstrated (Kim et al., 2006). This is because thiolate molecules are known to form self-assembled monolayers (SAMs) on the surface of noble metals (e.g., Au, Ag and Pt), which can modulate the surface work function with dipole formation on the surfaces of these metals (Chun Wei et al., 2007; Rusu and Brocks, 2006). Theoretical studies have shown that the work function of Au (~5.2 eV) can be decreased or increased by more than 1 eV upon the adsorption of SAMs of the appropriate thiolate molecules (Rusu and Brocks, 2006), which means the work functions of Au electrodes can be modulated to a value not only lower than that of SWCNTs but also deep below the valence band of SWCNTs. Therefore, both Schottky and ohmic contacts with SWCNTs can be formed in principle using Au electrodes modified by the appropriate thiolate molecules. However, the potential of this SAM technology has not been extensively investigated. Therefore in this work, we would fabricate SWCNT Schottky diodes by first contacting semiconducting SWCNTs with symmetrical Au electrodes, which were subsequently modified separately by methanethiol (CH_3SH) and trifluoroethanethiol (CF_3CH_2SH). The combination of Au electrodes and these two thiolate molecules has been chosen in the present work because Au is stable in forming a good chemical bond with sulfur in the

thiolate molecules, but does not react with the carbon part of the organic molecule. Moreover, the inert property of Au makes it stable during the AC dielectrophoresis process. The two thiolate molecules were chosen because CH_3SH has been shown theoretically to decrease the work function of Au most effectively from ~5.2 to ~3.81 eV, while CF_3CH_2SH increases most effectively the work function of Au to ~6.27 eV (Rusu and Brocks, 2006). Consequently, the SBHs at the two Au/SWCNT contacts can be asymmetrically modified most effectively by CH_3SH and CF_3CH_2SH, thus leading to high performance SWCNT Schottky diodes with concurrently high $I_{forward}$ and low $I_{reverse}$.

6. 2 The fabrication procedure of SWCNT Schottky diodes with thiolate molecules

In the present work, SWCNT Schottky diodes were fabricated on a highly doped silicon substrate with 100 nm SiO_2 on its surface. Individual SWCNTs (diameter ~1.5 nm) dispersed in 1 wt% sodium dodecyl sulfate (SDS) solution were aligned between two Au electrodes, to yield the Au-SWCNT-Au structure, by means of AC dielectrophoresis. The electrodes were defined by electron-beam lithography and spaced about 800 nm apart. Using applied AC voltage $V_{P\text{–}P} = 8$ V, frequency f = 1 MHz and duration T = 1 min, we obtained a yield of 30% in

aligning an individual semiconducting SWCNT across two Au electrodes. The details of the fabrication process can also be found in Chapter 2.

The Schottky diodes are converted from the SWCNT FET by modifying the two SWCNT and Au contacts separately with thiolate molecules: methanethiol (CH_3SH) and trifluoroethanethiol (CF_3CH_2SH).

The details of the conversion process are as follows: Firstly lithography is performed to protect one of the two Au electrodes using resist (S1811), as shown in Figure 6.1a. The partially protected device structure is subsequently immersed in a 5 mM CH_3SH solution for 20 minutes to modify (decrease) the work function of the exposed Au electrode. Similar lithography steps, as shown in Figure 6.1b, are performed to expose the other Au electrode (the one protected in the previous lithography procedure) to a 5 mM CF_3CH_2SH solution for 20 minutes to increase the work function of the Au surface. By treating the two Au electrodes with different thiolate molecules, the Fermi levels of the two treated Au contacts are expected to become highly asymmetrical, owing to the formation of interface dipoles in opposite direction between Au and the absorbed self-assembled thiolate molecules, as indicated in Figure 6.1c and d. Finally, the device structure was stripped of resist and cleansed by rinsing in deionized water for 3 minutes and blown dry by filtered nitrogen gas. The electrical characteristics of our devices were tested by HP 4156C semiconductor analyzer at room temperature in air.

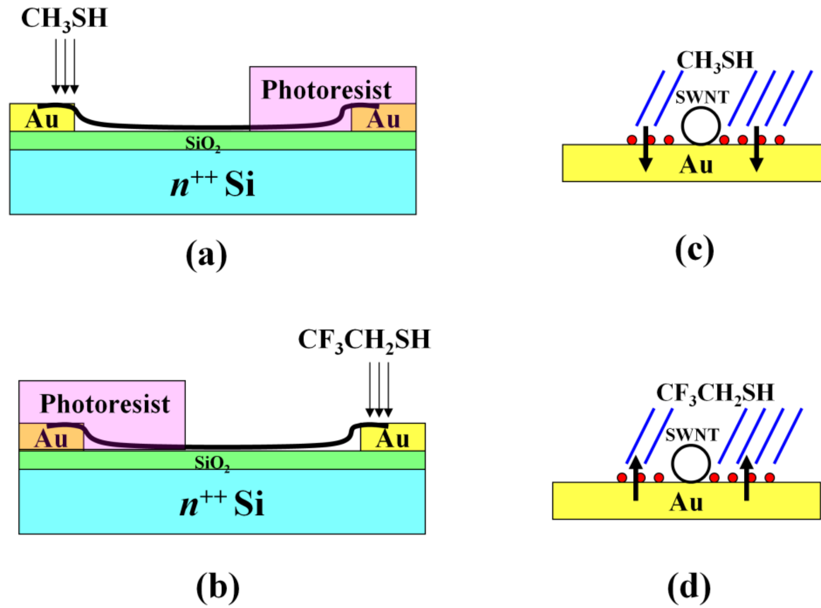

Figure 6.1: Fabrication of SWCNT Schottky diodes by asymmetrically tuning the Fermi level lineup at the two Au/SWCNT contacts using different thiolate molecules: (a) methanethiol (CH_3SH) and (b) trifluoroethanethiol (CF_3CH_2SH). The Au/SWCNT contact structure and the dipole direction (indicated by arrows) formed between Au and the absorbed self-assembled thiolate molecules are shown in (c) for CH_3SH and (d) for CF_3CH_2SH.

6.3 The electrical characteristic of the SWCNT Schottky diodes

6.3.1 The modification effect of thiolate molecules on the SWCNT and Au contacts

The effectiveness of the thiolate molecule modification of the CNT and Au contact is investigated using a back-gated SWCNT FET. The I_{DS}-V_{GS} curves ($V_{DS} = 0.1$ V) of the transistor is shown in Figure 6.2 as a function of modification duration by CH_3SH or CF_3CH_2SH. It is observed in Figure 6.2a that modification of CNT/Au contact by CH_3SH leads to a lower current at $V_{GS} < 0$ V, as a result of the lower work function of the modified Au contact and the current becomes lower with increasing duration. On the other hand, modification of CNT/Au contact by CF_3CH_2SH leads to a higher current at $V_{GS} < 0$ V, as a result of the higher work function of the modified Au contact and it becomes higher with increasing duration, as shown in Figure 6.2b. It is also seen that modification duration of 20 minutes is effective. As a long processing time is not practical, we have conducted subsequent work using modification duration of 20 minutes. As shown in Figure 6.3, the Au-SWCNT-Au structure shows a symmetrical *I*-*V* relation prior to treatment by thiolate molecules. After one of the two Au/SWCNT contacts was selectively modified by CH_3SH, the symmetrical *I*-*V* relation becomes highly asymmetrical and diode like with a high rectification $I_{forward}/I_{reverse}$ ratio of ~10^4, resulted from a drastically reduced reverse current (at negative voltage) to 100 pA, which is about 4 decades smaller than that of the pristine

device with symmetrical Au electrodes, and a forward current (at positive voltage) that is almost unchanged compared to that of the pristine device. With the second Au/SWCNT contact modified by CF_3CH_2SH, the *I-V* relation becomes more asymmetrical with an even higher $I_{forward}/I_{reverse}$ ratio, owing to an increase in the diode forward current by about 2.5 times, to ~5 μA, over the device with only one Au/SWCNT contact modified by CH_3SH. On the other hand, the reverse current remains almost unchanged with respect to the diode with only one Au electrode modified by CH_3SH.

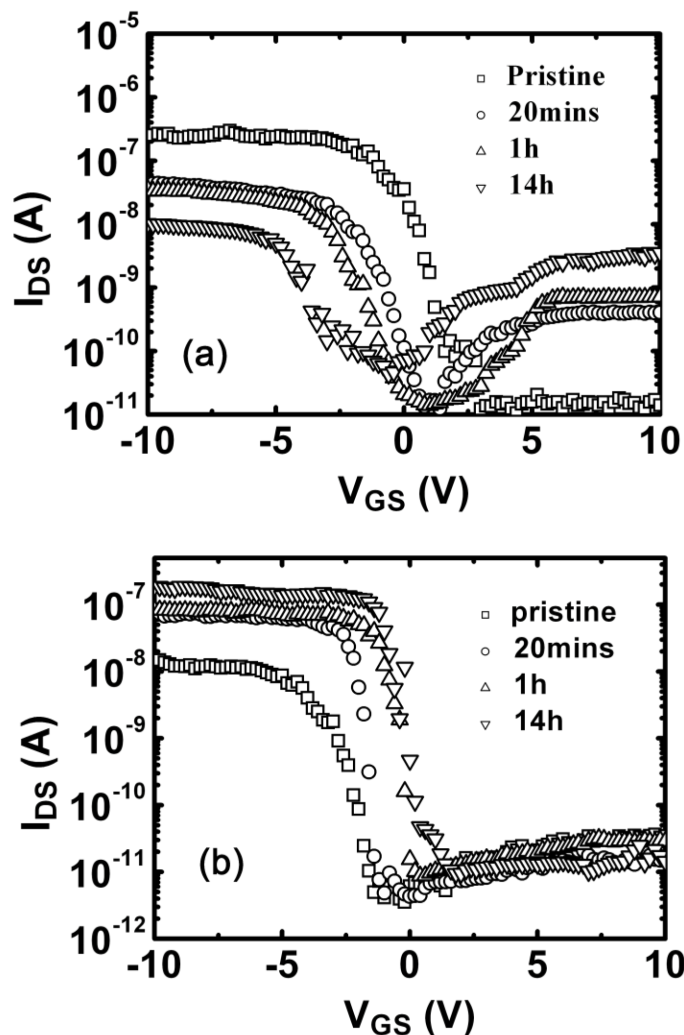

Figure 6.2: I_{DS}-V_{GS} curves (V_{DS} = 0.1 V) for back-gated SWCNT FETs as a function of modification duration by (a) methanethiol (CH_3SH) and (b) trifluoroethanethiol (CF_3CH_2SH).

It has been observed in Figure 6.3 that in fact the treatment of Au electrode by CH_3SH and CF_3CH_2SH has respectively restricted and enhanced the current flow through the Au/SWCNT contact. We also note that our device

processing depicted in Figure 6.1 would have the SWCNT exposed to the thiolate molecules as well, thus meaning the possibility of doping to the SWCNT. As the current flow through a metal/SWCNT/metal structure is determined not only by the Schottky barriers at the contact interface, but also by the doping to the SWCNT, we need to ascertain which is the main cause of the diode like characteristic as shown in Figure 6.3. As shown in Figure 6.2a, when the entire FET (i.e., including both the two Au contacts and the SWCNT channel) is modified by CH_3SH for 20 minutes, the *p*-channel ON current (I_{ON}), i.e., I_{DS} at V_{GS} = -10 V, of the FET decreases by almost one decade with respect to that of the untreated FET. There are two possible reasons for these observations: i) an increased in the SBHs at the CH_3SH modified Au/SWCNT contacts, and ii) the electron doping to the SWCNT channel by CH_3SH. The subthreshold slope, $S = dV_{GS}/d(\log I_{DS})$ is seen in Figure 6.2a to increase with the decrease in I_{ON}, hence one can conclude that the SBHs at the contacts have increased after modification by CH_3SH, as doping effect does not induce a change in the subthreshold slope. On the other hand, as the threshold voltage (V_{TH}) of FET is also observed to be slightly shifted by 1~2 V, as shown in Figure 6.2a, this indicates that the electron doping to the SWCNT has also happened. By selectively doping only the SWCNT channel with CH_3SH (with both the Au contacts protected by resist), we observe in Figure 6.4a that V_{TH} of the SWCNT FET shifts in the same way and by about the same amount as in Figure 6.2a, but not with a simultaneous substantial

decrease in the ON current and an increase in the subthreshold slope. This shows that the main effect of electron doping to the SWCNT is in the shift of the V_{TH}, and it does not change the ON current of the FET significantly. Therefore, one can conclude that after CH_3SH treatment, the decrease in the ON current of the FET (Figure 6.2a) is mainly attributed to the increase of the SBHs caused by CH_3SH modification of the Au/SWCNT contacts.

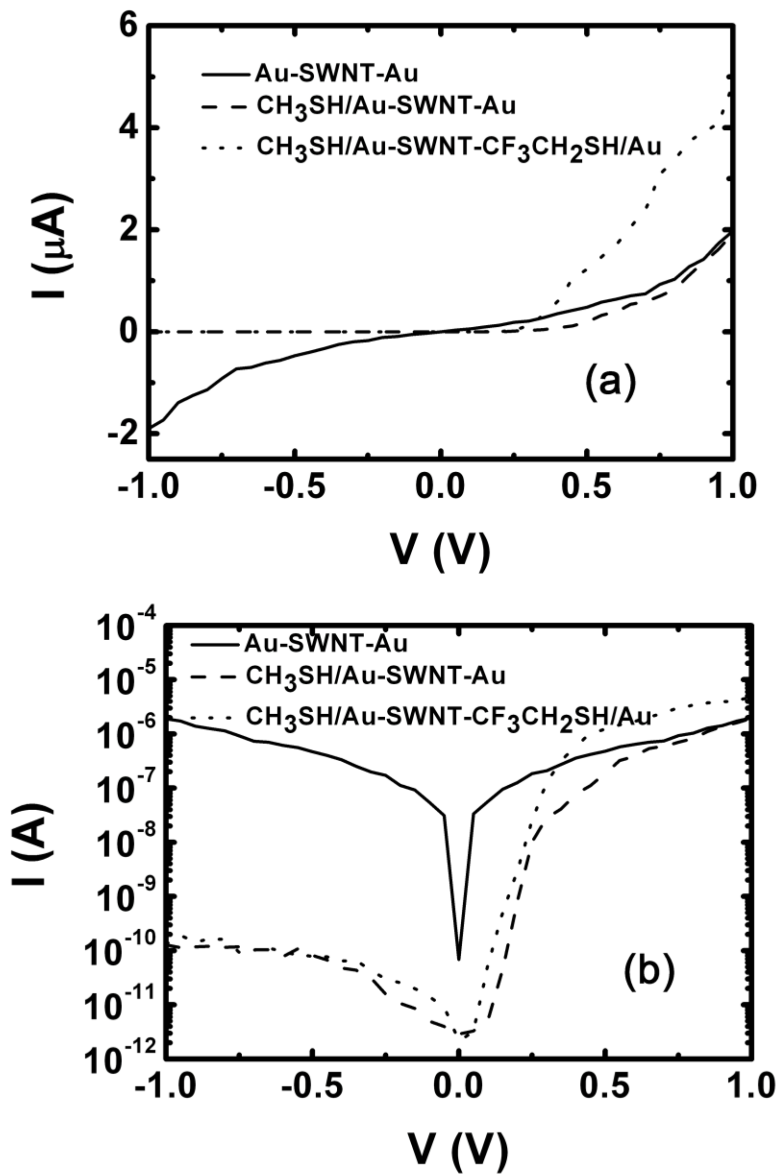

Figure 6.3: I-V curves of Au-SWCNT-Au structures before and after modification by different thiolate molecules: methanethiol (CH_3SH) and trifluoroethanethiol (CF_3CH_2SH) in (a) linear scale; (b) semi-log scale.

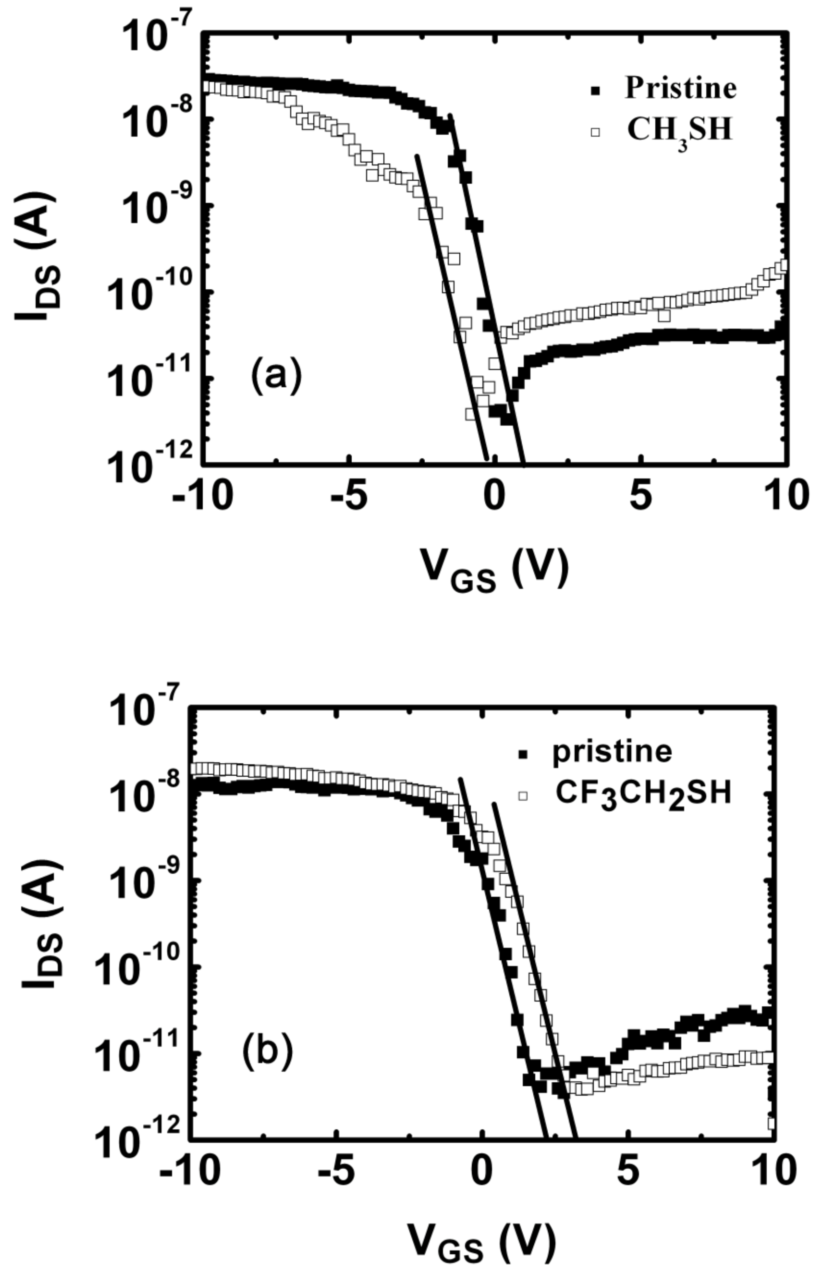

Figure 6.4: I_{DS}-V_{GS} curves (V_{DS} = 0.1 V) for SWCNT FETs with only SWCNT channels modified by thiolate molecules and SWCNT/Au contacts are protected by resist: (a) by CH_3SH; (b) by CF_3CH_2SH.

On the other hand, the influence of the other thiolate molecules (CF_3CH_2SH) on the Au/SWCNT contact is opposite to that of CH_3SH, as shown in Figures 6.2b and Figures 6.4b, where the *p*-channel ON current of the FET is increased mainly as a result of a lower SBH at the CF_3CH_2SH modified Au/SWCNT contacts, as indicated by a lower *p*-channel subthreshold slope shown in Figure 6.2b. Although CF_3CH_2SH does lead to hole doping of the SWCNT, as indicated by the positive shift in V_{TH} in Figures 6.2b and Figures 6.4b, it does not increase the *p*-channel ON current significantly, as shown in Figure 6.4b. In conclusion, CH_3SH and CF_3CH_2SH modifications have respectively caused a decrease and increase in the work function of Au surface, which in turn result in a higher and lower contact SBH for hole transport. The asymmetric change in SBH at the two Au/SWCNT contacts are the main reasons that lead to the diode like I-V curves observed in Figure 6.3. Although CH_3SH and CF_3CH_2SH treatments will also dope the carbon nanotube, the hole current is not significantly affected, as shown in Figures 6.2b and Figures 6.4b.

6.3.2 The working mechanism of the SWCNT Schottky diodes

Figure 6.5 shows the energy band diagrams of our Au-SWCNT-Au structure at forward and reverse biases. Before modification, as shown in Figures 6.5a and b, both Au electrodes have the same work function, thus resulting in

similar SBHs at the two Au/SWCNT contacts. As a result, holes transport through the Au-SWCNT-Au structure is similar regardless of the polarity of the bias and a symmetrical *I-V* curve is observed. It should be noted that there are two current components flowing through the Au/SWCNT contacts, owing to thermionic emission and tunneling (indicated by the solid and dashed arrows in Figure 6.5). The tunneling component is much smaller than the emission component as the Schottky barrier width is thick with pristine Au contacts. However, after both Au electrodes are modified by thiolate molecules, both the height and width of the SB at CH_3SH modified Au/SWCNT contact are increased while those at the CF_3CH_2SH modified Au/SWCNT contact are decreased, as shown in Figure 6.5c and d. Consequently, thermionic emission of holes across the CH_3SH modified Au/SWCNT contact is much reduced as a result of the higher SB when a negative bias voltage is applied. Therefore, only tunneling current flows across the contact, which has also been reduced owing the broader SB, thus leading to a small reverse current (~ 100 pA). On the other hand, holes can flow easily through the lower SB at the CF_3CH_2SH modified Au/SWCNT contact under forward bias. Hence, highly asymmetrical *I-V* curves are achieved in SWCNT Schottky diodes with Au electrodes asymmetrically modified by thiolate molecules.

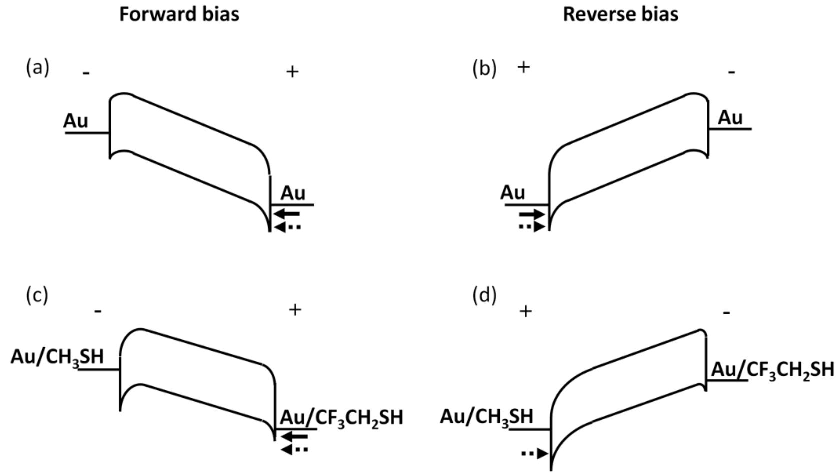

Figure 6.5: Energy band diagrams of Au-SWCNT-Au structure under forward and reverse bias: (a), (b) before modification; (c), (d) after modification by thiolate molecules, CH_3SH and CF_3CH_2SH. In the Figure, solid arrow indicates thermionic emission current and dashed arrow indicates tunnelling current.

Using the following equations (Sze, 1981),

$$I \propto T^2 \cdot \exp\left(-\frac{e\Phi_e}{kT}\right) \qquad (6.1)$$

$$\Phi_e \propto \Phi_b - \left(\frac{eV}{\pi\varepsilon_1\varepsilon_0}\right)^{1/2} \qquad (6.2)$$

the SBH of the untreated Au/SWCNT contact at zero bias, $V = 0$, is estimated to be Φ_b~110 meV, by plotting $\ln(I/T^2)$ versus $1/T$ from 200 to 300 K to determine

the bias dependent Schottky barrier height, Φ_e, at various bias voltage *V* (0.1 to 0.5 V in steps of 0.1V) and subsequently extracting Φ_b, as shown in Figure 6.6a and b. After modification by CH_3SH, the SBH of the Au/SWCNT contact increases to Φ_b~190 meV (an increase of >70%), hence leading to a much reduced current through the contact and resulting in the asymmetrical diode characteristics shown in Figure 6.3.

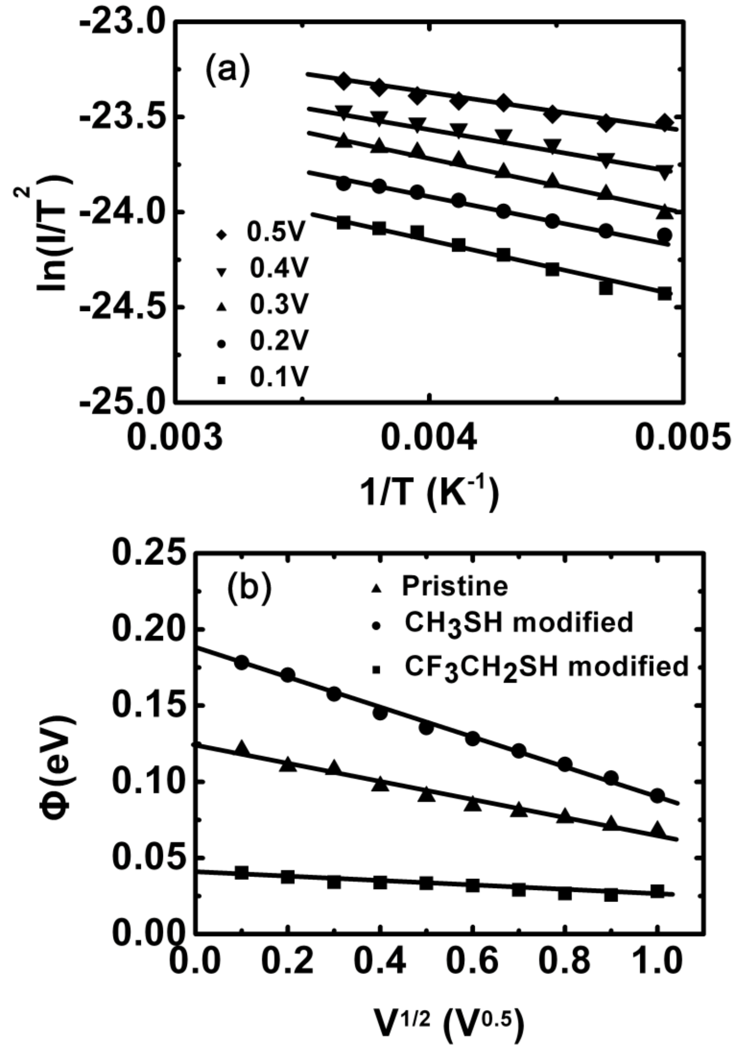

Figure 6.6: (a) Plots of ln (I/T^2) versus 1/T for T from 200 to 300 K for different bias voltages (V = 0.1 to 0.5 V in steps of 0.1 V) for SWCNT and Au Schottky contact. V_{GS}=0V. The biased dependent SBH (Φ_e) is extracted and plotted in (b) as a function of bias voltage ($V^{1/2}$) to yield the Schottky barrier height at zero bias voltage: Φ_b.

6.3.3 Enhancing SWCNT Schottky diode performance using asymmetric thiolate molecules modified gold contacts

We have used two types of thiolate molecules to achieve the diode structure because one serious drawback of the diode structure with only one of the Au/SWCNT contact modified by thiolate molecules is its low forward current. This was also observed in the work of Kim et al (Kim et al., 2006) where only one of the two Au/SWCNT contacts was modified by another type of thiolate molecule, 2-aminoethanethiol ($HSCH_2CH_2NH$), to increase the SBH at one Au/SWCNT contact. On the other hand, compared with the forward current of SWCNT Schottky diodes fabricated with asymmetric metal electrodes (Manohara et al., 2005; Yang et al., 2005), the value of our device with just one Au/SWCNT contact modified by CH_3SH is only 1~2 μA, which is several times smaller. This is because the other untreated Au/SWCNT contact remains non-ohmic and has a substantial SBH of Φ_b ~110 meV. As a result, the forward current is limited. In order to overcome this obstacle, we therefore use a second thiolate molecule, CF_3CH_2SH, in the current work to modify the other Au/SWCNT contact so as to increase the work function of the Au electrode. This results in the reducing of the SBH at Au/SWCNT contact and brings it closer to an ohmic characteristic. As shown in Figure 6.6b, the SBH after CF_3CH_2SH modification is decreased to Φ_b ~40 meV (by >60% compared to the pristine Au/SWCNT contact) and this has led to an increase in the diode forward current by about 2.5 times to ~5 μA, as

shown in Figure 6.3. This forward current value is closer to that reported for SWCNT Schottky diodes with asymmetrical metal electrodes (using high work function metal Pd or Pt as ohmic contacts) (Manohara et al., 2005; Yang et al., 2005) and as expected, much higher than that of the diodes reported by Kim et al (Kim et al., 2006) with only one Au/SWCNT contact modified by thiolate molecules.

Although theoretical studies have indicated that the work function of Au which is modified by CF_3CH_2SH is expected to be 6.27 eV (Rusu and Brocks, 2006), which is much higher than that of either Pd (~5.2 eV) or Pt (~5.6 eV), the forward current of our diodes is not better than that of diodes with Pd (Pt) contacts (Manohara et al., 2005; Yang et al., 2005). One reason is probably that the 20 minute duration of CF_3CH_2SH treatment to the Au/SWCNT contact is not sufficiently long to yield the expected work function of Au of 6.27 eV, but results only in a lower value. As shown in Figure 6.2b, an extended 14 hour treatment will lead to a higher I_{ON} which shows that a 20 minutes treatment by CF_3CH_2SH may be not long enough to induce the maximum increase in the work function of Au surface. This could also explain the moderate SBH, Φ_b ~40 meV, of the Au/SWCNT contact modified by CF_3CH_2SH for 20 minutes. The imperfect chemical bonding between the SWCNT and Au, which may not have been improved by CF_3CH_2SH treatment, could probably be another cause for the moderate SBH Φ_b ~40 meV. It is known that despite Au and Pd having similar

work function, Au/SWCNT contact has a larger SBH than Pd/SWCNT contact because the chemical bonding between Au and SWCNT is worse than that between Pd and SWCNT (Vitale et al., 2008). We had also fabricated SWCNT FETs with Pd contacts and the SBH of the Pd/SWCNT contact was measured as Φ_b ~17 meV, which is less than half the SBH of Au/SWCNT contact modified by CF_3CH_2SH. The third possible reason is the side-contact structure (SWCNTs lying on top of metal electrodes and bonding with Van der Waals force) used in our diodes which has led to a larger contact resistance, in contrast to the embedded-contact structure used in the works of Yang et al (Yang et al., 2005) and Manohara et al (Manohara et al., 2005).

The reverse current of our diodes is at least one decade smaller (~100 pA) in comparison to that of the SWCNT Schottky diodes with asymmetrical metal electrodes (Lu et al., 2006; Manohara et al., 2005). One possible reason is the low work function of Au electrode modified by CH_3SH (expected to ~3.8 eV (Rusu and Brocks, 2006)) which is lower than that of the low work function metals (Al ~ 4.1 eV, Ti ~ 4.3 eV). The side-contact structure of our diodes may also be a contributing factor. Based on the results shown in Figure 6.2a, it can be concluded that the 20 minute modification by CH_3SH has not attained the lowest possible work function, since a much longer 14 hour treatment will induce a lower I_{ON}. This also means that it is possible to reduce the reverse current of our diodes

further by extending the CH_3SH treatment to the Au/SWCNT contact to a longer duration to restrict more the hole injection through the contact.

Using the diode current equation: $I = I_s\left[e^{q(V-IR_S)/nkT} - 1\right]$, the current ideality factor, n, of our SWCNT Schottky diodes is estimated to be ~1.42-1.8, which is a bit better than that reported for SWCNT Schottky diodes with asymmetrically metal electrodes (ranging from 1.5 to 1.9) (Manohara et al., 2005). In the current equation, I_s is the reverse saturation current, q is the electron charge, V is the bias voltage, R_S is the lumped series resistance, k is Boltzmann constant, and T is the absolute temperature. In summary and based on preceding discussion, we can conclude that high performance SWCNT Schottky diodes can be fabricated by the SAM technology with more ideal *I-V* characteristics, lower reverse current, higher rectification $I_{forward}/I_{reverse}$ ratio and similarly high forward current compared to SWCNT Schottky diodes fabricated with asymmetrical metal electrodes (Lu et al., 2006; Manohara et al., 2005; Yang et al., 2005).

6.3.4 The effect of back gate voltage on the electrical characteristic of the SWCNT Schottky diodes

Figure 6.7 shows the *I-V* characteristics of our SWCNT Schottky diodes at different back-gate bias (V_{GS}), where it is seen that the forward and reverse currents of the diodes are gate bias dependent. This is not unexpected as the

applied gate voltage will modulate the SB of the Au/SWCNT contacts of diodes by 'pushing' the valence band of the SWCNT up and down at negative and positive gate bias, respectively. In reverse bias, the diode current is mainly determined by the hole current flowing through the contact with a higher SBH (the Au/SWCNT contact modified by CH_3SH) and is mainly the tunneling current as the thermionic emission current is blocked mostly by the large SBH, as shown in Figure 6.5d. As the tunneling current is sensitive to the Schottky barrier width, the reverse current is increased significantly when the gate voltage is changed from 0 to -10 V, as seen in Figure 6.7, owing to the decrease in the Schottky barrier width at negative gate bias. On the other hand, when the gate voltage is changed from 0 to +10 V, the Schottky barrier width is broadened and leads to a lower reverse current for the diode. However, the decrease is only marginal, as seen in Figure 6.7. This could signify that positive gate voltage does not modulate the width of Schottky barrier as effectively as negative gate voltage.

The forward current of the diode is determined by the hole current flowing through the contact with a lower SBH (the Au/SWCNT contact modified by CF_3CH_2SH), as seen in Figure 6.5c, and its dependence on gate voltage shows that in addition to the expected thermal emission component, the tunneling component could be substantial as well as the gate voltage primarily modulates the width of Schottky barrier, but not its height. Negative and positive gate voltages lead to a narrower and broader Schottky barrier, respectively, hence

resulting a higher and lower forward current, as observed in Figure 6.7. The gate voltage dependence of the diode forward current also means the SBH of the Au/SWCNT contact which is modified by CF_3CH_2SH is not low enough to yield an ohmic contact and this agrees well with the measured SBH Φ_b~40 meV, which is a moderate height. If the contact is ohmic, the forward current should have only minimal dependence on the gate voltage.

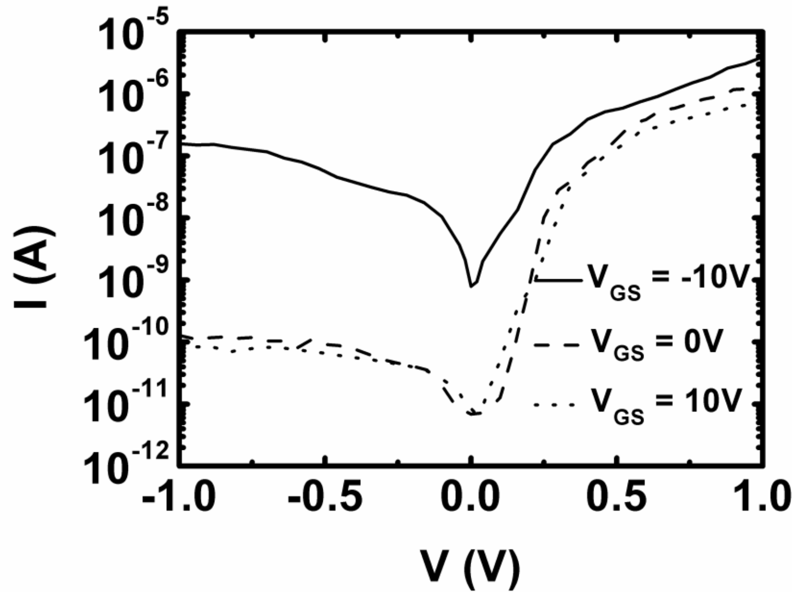

Figure 6.7: I-V characteristics of SWCNT Schottky diode at different gate voltages (V_{GS}= -10, 0 and 10 V) in semi-log scale.

6.3.5 The stability of SWCNT Schottky diodes by thiolate molecules

Finally, it has been found that SWCNT Schottky diodes fabricated by the SAM technology are not stable in air when left unpassivated. After exposure to air

for several days, the highly asymmetrical *I-V* characteristic degrades and becomes more symmetrical, as shown in Figure 6.8. This is probably owing to the oxidation of SAM, which means the dipole induced by thiolate molecules will be damaged by oxidation after several days and the work function of Au surface will revert to its pristine value (Cortes et al., 2009; Yang et al., 2004). One possible way to overcome this problem and to improve the stability of SAM technology is probably to deposit a layer of oxygenless insulator such as SiN_x to protect the devices to prevent the SAM formed at the Au surface from reacting with O_2 molecules.

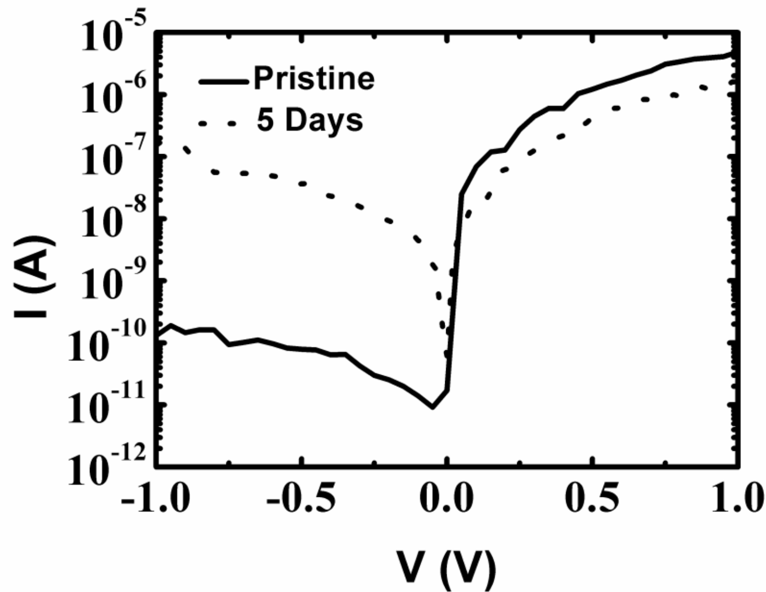

Figure 6.8: *I-V* curves of SWCNT Schottky diode fabricated by SAM technology after fabrication and after 5 days of exposure to air.

6. 4 Summary

We have demonstrated experimentally the effectiveness of thiolate molecules, CH_3SH and CF_3CH_2SH, in tuning the work function of Au surface asymmetrically and have applied it to the fabrication of SWCNT Schottky diodes. Symmetrical Au-SWCNT-Au structures have been converted to Schottky diodes by asymmetrically modifying the two Au/SWCNT contacts using CH_3SH and CF_3CH_2SH, which respectively decreases and increases the work function of Au surface, resulting in a higher and lower SBH at Au/SWCNT contacts. The Au/SWCNT contacts modified by CH_3SH and CF_3CH_2SH have SBHs of ~190 and ~40 meV, increased by over 70 % and decreased by over 60% respectively with respect to that of pristine Au/SWCNT contact of ~110 meV. Our SWCNT Schottky diodes have a forward and reverse current ratio ($I_{forward}/I_{reverse}$) higher than 10^4, a forward current as high as ~5 μA, a reverse leakage current as low as ~100 pA and a current ideality factor as low as ~1.42. In conclusion, the performance of SWCNT Schottky diodes fabricated by asymmetrically modifying Au contacts using different thiolate molecules is shown to be at least comparable to, if not better than those fabricated with asymmetrical metal electrodes, which suggests that this technique could be a useful method to fabricate high performance carbon nanotube Schottky diodes.

Chapter 7

Conclusions and Suggested Future Work

7.1 Conclusion

In this thesis, we have fabricated and characterized several types of CNT based devices: individual SWCNT FETs (i-SWCNT FETs), random network SWCNT FETs (rn-SWCNT FETs), DWCNT FETs, and SWCNT Schottky diodes. This has led to a better understanding of the operation of such devices. Emphasis was placed on the CNT/metal contact and that has allowed us to fabricate high performance p-type i-SWCNT FETs with niobium carbide end contacts, n-type rn-SWCNT FETs with Yttrium contacts, and SWCNT Schottky diodes with asymmetric thiolate molecules modified gold contacts. We have also identified that RuO_2 could make an excellent contact to CNT. In the following sections, more details will be presented.

7.1.1 High performance CNTFET with niobium carbide contact

Application of metal carbide as contacts is a potential way to achieve stable Ohmic contacts in CNTFETs. In our work, SWCNT FETs with Nb carbide (Nb_2C) contacts have been fabricated by annealing in vacuum at 700 ^oC for 1 hr. The Nb_2C/SWCNT contacts demonstrate very small Schottky barrier height of

~18 meV to *p*-type transport. This is attributed to the higher work function of Nb_2C (~5.2 eV) and/or improved bonding between Nb_2C and SWCNTs, e.g., end-contact structure formed at SWCNT and Nb_2C interface. Therefore, the Nb_2C contacted SWCNT FETs exhibit performance as good as those with Pd contacts: the *p*-channel ON current is as high as 0.5 μA at V_{DS} = 0.1 V, I_{ON}/I_{OFF} ratio is up to ~10^5, and the subthreshold slope is ~550 mV/dec. Moreover, compared with another well studied metal carbide contact — titanium carbide, Nb_2C contacts yield more unipolar *p*-type SWCNT FETs, as a result of the higher work function of Nb_2C. This suggests Nb_2C surpasses TiC as a candidate as contact for CNTFET application. More importantly, the application of Nb_2C carbide can overcome the challenge of the metal contact in CNTFET — Nb_2C contacts can form near Ohmic contacts to small diameter (~1 nm) SWCNTs which cannot be achieved by Pd contacts.

7.1.2 *n*-type random network single-wall carbon nanotube field effect transistor with Yttrium contacts

High performance *n*-type rn-SWCNT FET is critically important to CMOS applications of CNT based thin film FET. In our work, it has been achieved by means of contact engineering, where a low work function metal, Yttrium (Y), is used for the source and drain contacts.

In our work, it has been found that Yttrium electrodes lead to *n*-type characteristic for rn-SWCNT FETs owing to its ultra-low work function while ambipolar characteristic is also observed. The ambipolar transport characteristic is believed to be due to the presence of crossed metallic (*m*-) and semiconducting (*s*-) SWCNT junctions in the channel of rn-SWCNT FETs, which form *p*-type rectifying Schottky barrier and introduce non-negligible hole current. By applying chemical etching using 2,4,6-triphenylpyrylium tetrafluoroborate (2,4,6-TPPT), we have successfully converted the ambipolar rn-SWCNT FETs to highly unipolar *n*-type devices by selectively removing the *m*-SWCNTs in the FET channel and hence, eliminating the *m-s* tube junctions.

The typical characteristics of our unipolar *n*-type rn-SWCNT FETs are as follows: I_{ON}/I_{OFF} ratio up to ~10^5, mobility as high as 25 $cm^2V^{-1}s^{-1}$, and transconductance of 0.12 μS/μm, and they have demonstrated air-stable *n*-type characteristics. More importantly, the rn-SWCNT FETs have better reproducibility than FETs based on individual SWCNT.

7.1.3 Fabrication of single-wall carbon nanotube Schottky diode with gold contacts modified by asymmetric thiolate molecules

We have fabricated SWCNT Schottky diodes by asymmetrically modifying the two Au/SWCNT contacts using different thiolate molecules, methanethiol (CH_3SH) and trifluoroethanethiol (CF_3CH_2SH). Characterization

has revealed that highly asymmetrical contacts with Schottky barrier heights of ~190 and ~40 meV (increased by over 70% and decreased by over 60%, respectively with respect to that of pristine Au/SWCNT contact of ~110 meV) were achieved for the CH_3SH and CF_3CH_2SH modified Au/SWCNT contacts.

The performance of our SWCNT Schottky diodes was as follows: the forward and reverse current ratio ($I_{forward}/I_{reverse}$) higher than 10^4, a forward current as high as ~5 μA, a reverse leakage current as low as ~100 pA, and a current ideality factor as low as ~1.42. This is at least comparable to, if not better than SWCNT Schottky diodes fabricated with asymmetrical metals.

In our work, we have optimized the electrical characteristic of CNT Schottky diodes fabricated by thiolate molecules, and the results suggest that this may be a viable way to achieve practical CNT Schottky diodes.

7.1.4 Semiconducting-Semiconducting Double-Wall Carbon Nanotube Field Effect Transistors

In our work, it has been found the *s-s* DWCNT can also be used for CNTFET application, and the tube-tube interaction is important in the transport characteristic of DWCNT, as the *s-s* DWCNT FET can behave differently from *s*-SWCNT FET, depending on the nanotube diameter.

The conductance of DWCNT is found to be always larger than that of SWCNT owing to the inter-tube interaction in the DWCNT, e.g., less electron-

phonon scattering in DWCNTs. In addition, we have also shown that the Schottky barrier height (SBH) at the CNT/metal contact is similar for SWCNT and DWCNT with the same diameter. In other words, the inter-tube interaction in DWCNT does not have a significant effect on the SBH at the CNT/metal contact.

When the diameter of DWCNT and SWCNT is large (> 2 nm), i.e., when the SBH at the CNT/metal contact is low, the transport characteristic of CNTFET is mainly controlled by the bulk nanotube resistance and the output current of the DWCNT FETs is always larger than that of SWCNT FETs. However, when the tube diameter of DWCNT and SWCNT is intermediate (1.4 nm < d < 2 nm), i.e., when the SBH at the CNT/metal contact becomes substantial, the transport characteristic of CNTFET is dominated by the Schottky barrier at the contacts, and the DWCNT FET behaves similar to SWCNT FET. This is because the difference in nanotube resistance becomes insignificant in comparison to the contact resistance. It is interesting to find that when the tube diameter is smaller than 1.4 nm, the tube-tube interaction in DWCNT results in the bandgap narrowing of the *s-s* DWCNT. The output current of DWCNT transistor then becomes much larger that of SWCNT transistor and the on/off ratio of DWCNT devices is also significantly decreased.

And in the study of DWCNT FETs, it has also been found that the unique oxide of Ru, RuO_2, is an excellent candidate for contact to *p*-type CNTFET, especially when the CNTFET is fabricated by depositing CNTs on top of metal

electrodes. This is not only because of the high work function of RuO_2 (~5.0 eV) which leads to small Schottky barriers for hole transport but also due to the good contact interface formed between RuO_2 and DWCNT. Moreover Ru contacted CNTFET can be used in rich oxygen environment and high temperature condition without worry of the performance degeneration due to the formation of RuO_2 in such conditions.

7.2 Suggested Future Work on carbon nanotube electronics

7.2.1 Other metal carbide contacts for CNTFET application

In our experiment, even though high performance *p*-type CNTFET with Ohmic contact has been achieved by using Nb electrodes with the formation of Nb_2C, it is still of interest to investigate other metal carbides, e.g., Co and Mo.

As has been discussed, a major hurdle to the widespread application of CNTs in FETs is the control of the position and orientation of CNT ensembles. To date, the direct synthesis of CNTs at desired positions has been identified as one promising way to overcome this challenge (Jing et al., 1998; Woong et al., 2002). In this method, transition metals such as Co, Fe and Mo are used as the catalyst islands. Therefore, it may be possible to form directly the transition metal carbide between these metal islands and CNTs during synthesis, i.e., an in-situ process.

Consequently, the investigation of the characteristic of these metal carbide/CNT contacts can be of relevance.

Another meaningful future work is to look for metal carbides that can form unipolar *n*-type contacts with CNTs. This will be important to the CMOS application of CNTFETs. To our knowledge, such results have not been reported.

7.2.2 Metal gate engineering

In this dissertation, the study of CNTFETs is mainly focused on the CNT and metal contact. However, there is another important application of metal in CNTFET structure — metal gate. This is because for a CNTFET, the metal gate is important to the control of threshold voltage (V_{TH}) — the switching control of CNTFET. However, compared with the CNT and metal contact, the study on metal gate of CNTFET is still preliminary (Chen et al., 2007).

As mentioned in chapter 1, the precise control of threshold voltage of CNTFET is still a challenge. For a given undoped CNTFET with a fixed energy gap (tube diameter) and oxide thickness, tuning the work function of the gate metal is the only way to control the threshold voltage. This is because the gate work function acts like an extra voltage source in addition to the applied gate voltage. However, unfortunately, the accurate relationship of the work function of gate metal to V_{TH} of CNTFET is still not clear. In addition to the work function,

the impact of metal and insulator interface on V_{TH} also warrants investigations. Therefore, it is necessary to understand the working mechanism of the metal gate in CNTFET and to optimize it for both *p*- and *n*- type CNTFETs,

7.2.3 Graphene FETs

7.2.3.1 Brief comparison between graphene and CNT

In 2004, Novoselov, Geim, and co-workers at the University of Manchester used a simple mechanical exfoliation technique to obtain supported single layer graphene and study its electrical properties (Novoselov et al., 2004; Novoselov et al., 2005). This study has generated enormous interest and intense activity in graphene research (Allen et al., 2009; Castro Neto et al., 2009; Geim, 2009; Geim and Novoselov, 2007). And it has been found the electrical, optical, mechanical, and thermal properties of graphene achieve extreme values that are hardly met by any other materials, e.g., the π electrons in graphene provide an ideal 2D system: single atom thickness with the π and π^* states non-interacting.

Nowadays, many researchers who used to work on CNT electronics have moved to work with graphene. Does this mean graphene is a better material than CNT? And is there a future for CNT based electronic devices? In order to answer these questions, in this section we would like to do a brief comparison between

graphene FET (GFET) and CNTFET and investigate the possible future work on GFET.

Comparing the transport properties of graphene and carbon nanotubes, we find that they are, in many respects, similar. For example, in both cases the carriers can have very high mobilities (Bolotin et al., 2008; Du et al., 2008) and ambipolar transport (Novoselov et al., 2004). However, there are also differences, the most important, from the device point of view, being the difference in dimensionality (1D vs 2D). And there is the presence of a band gap in semiconducting nanotubes while graphene is a zero-bandgap semiconductor (Novoselov et al., 2004). Moreover from the practical point of view, nanotubes, with their many different chiralities, pose a problem in producing a well-defined starting material for technology. Graphene, on the other hand, is well-defined and its planar geometry allows the use of the highly advanced techniques already developed in the semiconductor industry.

7.2.3.2 Comparison between graphene FET and CNTFET

Semiconducting nanotubes which have band gaps that scale inversely with their diameter allow for excellent gate switching with current on/off ratios of the order of 10^4-10^7, appropriate for digital switches. Graphene, on the other hand, does not have a band gap which means it does not turn off completely, even

though the density of states (DOS) = 0 at E_{Dirac}. Experimentally, most studies of graphene FETs (GFETs) obtain I_{ON}/I_{OFF} ratios $\leq$ 10 (Novoselov et al., 2004). Therefore GFETs are not appropriate for digital switches.

Then why is there such a strong interest in graphene electronics? The key attractions of graphene are its outstanding carrier mobility, the good transconductance of graphene devices, and the ultimate thinness and stability of the material. These characteristics suggest that graphene may be an ideal material for radio frequency (rf) analog electronics. This is because in analog rf operation, completes switch-off of the device is not necessary. The key performance metric of these high-frequency transistors is their cut-off frequency, f_T ($f_T = g_m/2\pi C$, where g_m and C are the transconductance and capacitance of the device, respectively (Schwierz, 2010)), which is defined as the frequency at which the current gain of the device becomes 1 and signifies the maximum frequency at which signals can be propagated in the transistor. Therefore graphene FET with high transconductance can exhibit high f_T. Currently, the highest published f_T value for an rf GFET is 100 GHz for 240 nm gate length transistors (Lin et al., 2010).

Recently researchers are looking for a way to open a bandgap in graphene to make it possible for digital switch application. An approach to open a bandgap in graphene is to reduce the dimensionality of graphene from 2D to 1D by cutting graphene into narrow ribbons, graphene nanoribbons (GNRs) (Li et al., 2008). If

the GNR is narrow enough, 1D confined states are formed similar to those of a particle in a narrow, long quantum box. The gap opened is inversely proportional to the width of the GNR. For a substantial gap, ≥0.5 eV, which can allow room temperature operation of devices, GNRs with a constant width of 2-3 nm are required. Unfortunately, current lithographic techniques cannot deliver such performance. Furthermore, problems with ribbon width reproducibility, edge roughness control, and production scale limit the usability of the existing techniques in technology.

In conclusion, both GFET and CNTFET are important for nano-electronics devices in the future but for different applications, e.g., CNTFET for digital switches and GFET for rf analog electronics. It is therefore unfair to predict there is no future development space for CNT electronic devices with the appearance of graphene. Especially to date CNTFET is still considered as the most promising candidate to replace Si in digital switch devices.

7.2.3.3 Future work on graphene and metal contact

As same as CNTFET, even though graphene itself has excellent electrical properties, if there is no good contact developed between graphene and metal contact, none of the excellent electrical properties can be fully utilized in practical

devices. This is because carriers have to be injected into graphene and then collected through metal contacts.

One key problem that needs to be addressed for GFET is that of the contact resistance, which limits f_T and therefore must be reduced, especially for scaled devices operating near the ballistic limit (Schwierz, 2010). Therefore in order to improve the performance of GFET, ultra-low contact resistance needs to be developed. In addition the transport mechanism between graphene and metal, e.g., from a pure 2D system to a 3D system, is still not clear which becomes a challenge not only to the practical application of graphene devices but also to the understanding of physical properties of graphene.

Therefore in our future work when we move to graphene FET, a possible focus can be the graphene and metal contact which is not only extremely important to the practical application of GFET but also a good connection of our present work.

References:

Abdula, D., and Shim, M. (2008). Performance and Photovoltaic Response of Polymer-Doped Carbon Nanotube p−n Diodes. ACS Nano *2*, 2154-2159.

Allen, M.J., Tung, V.C., and Kaner, R.B. (2009). Honeycomb Carbon: A Review of Graphene. Chemical Reviews *110*, 132-145.

Amlani, I., Pimparkar, N., Nordquist, K., Lim, D., Clavijo, S., Zhengfang, Q., and Emrick, R. (2008). Automated removal of metallic carbon nanotubes in a nanotube ensemble by electrical breakdown. Paper presented at: 2008 8th IEEE Conference on Nanotechnology (NANO), 18-21 Aug 2008 (Piscataway, NJ, USA, IEEE).

An, L., Fu, Q., Lu, C., and Liu, J. (2004). A simple chemical route to selectively eliminate metallic carbon nanotubes in nanotube network devices. Journal of the American Chemical Society *126*, 10520-10521.

Andriotis, A.N., Menon, M., and Froudakis, G.E. (2000). Various bonding configurations of transition-metal atoms on carbon nanotubes: Their effect on contact resistance. Applied Physics Letters *76*, 3890-3892.

Appenzeller, J., Lin, Y.M., Knoch, J., and Avouris, P. (2004). Band-to-band tunneling in carbon nanotube field-effect transistors. Physical Review Letters *93*, 196805-196801.

Austing, D.G., Lefebvre, J., Bond, J., and Finnie, P. (2007). Carbon contacted nanotube field effect transistors. Applied Physics Letters *90*, 103112-103111.

Avouris, P., Appenzeller, J., Martel, R., and Wind, S.J. (2003). Carbon nanotube electronics. Proceedings of the IEEE *91*, 1772-1784.

Avouris, P., Chen, Z., and Perebeinos, V. (2007). Carbon-based electronics Nature Nanotechnology *2*, 605 - 615.

Bachtold, A., Strunk, C., Salvetat, J.-P., Bonard, J.-M., Forro, L., Nussbaumer, T., and Schonenberger, C. (1999). Aharonov-Bohm oscillations in carbon nanotubes. Nature *397*, 673-675.

Balasubramanian, K., Eduardo Lee, J.H., Weitz, R.T., Burghard, M., and Kern, K. (2008). Carbon nanotube transistors - chemical functionalization and device characterization. Physica Status Solidi (A) Applications and Materials *205*, 633-646.

Bandow, S., Takizawa, M., Hirahara, K., Yudasaka, M., and Iijima, S. (2001). Raman scattering study of double-wall carbon nanotubes derived from the chains of fullerenes in single-wall carbon nanotubes. Chemical Physics Letters *337*, 48-54.

Banerjee, S., White, B.E., Huang, L., Rego, B.J., O'Brien, S., and Herman, I.P. (2006). Precise positioning of single-walled carbon nanotubes by ac dielectrophoresis. J. Vac. Sci. Technol. B *24*, 3173.

Banhart, F. (2009). Interactions between metals and carbon nanotubes: at the interface between old and new materials Nanoscale *1*, 201-213.

Bing-Yue, T., Chien-Li, W., Jeng-Hua, W., and Ming-Jinn, T. (2006). Effect of oxygen absorption on contact resistance between metal and carbon nano tubes (CNTs). Paper presented at: 2006 International Symposium on VLSI Technology, Systems and Applications (VLSI-TSA), 24-26 April 2006 (Piscataway, NJ, USA, IEEE).

Bolotin, K.I., Sikes, K.J., Jiang, Z., Klima, M., Fudenberg, G., Hone, J., Kim, P., and Stormer, H.L. (2008). Ultrahigh electron mobility in suspended graphene. Solid State Communications *146*, 351-355.

Buttiker, M. (1988). Symmetry of electrical conduction. IBM Journal of Research and Development *32*, 317-334.

Castro Neto, A.H., Guinea, F., Peres, N.M.R., Novoselov, K.S., and Geim, A.K. (2009). The electronic properties of graphene. Reviews of Modern Physics *81*, 109-162.

Changxin, C., Lijun, Y., Kong, E.S.W., and Yafei, Z. (2006). Ultrasonic nanowelding of carbon nanotubes to metal electrodes. Nanotechnology *17*, 2192-2197.

Chen, C., Liu, L., Lu, Y., Eric Kong, S-W., Zhang, Y., Sheng, X., and Ding, H. (2006). A method for creating reliable and low-resistance contacts between carbon nanotubes and microelectrodes. Carbon *45*, 436–442.

Chen, J., Freitag, M., Klinke, C., Afzali, A., Tsang, J., and Avouris, P. (2005a). Charge transferred doping and electroluminescence in carbon nanotube transistors. Paper presented at: 2005 5th IEEE Conference on Nanotechnology, July 11, 2005 - July 15, 2005 (Nagoya, Japan, Institute of Electrical and Electronics Engineers Computer Society).

Chen, X.Q., Saito, T., Yamada, H., and Matsushige, K. (2001). Aligning single-wall carbon nanotubes with an alternating-current electric field. Applied Physics Letters *78*, 3714-3716.

Chen, Z., Appenzeller, J., Knoch, J., Lin, Y.-m., and Avouris, P. (2005b). The Role of Metal−Nanotube Contact in the Performance of Carbon Nanotube Field-Effect Transistors. Nano Letters *5*, 1497-1502.

Chen, Z., Appenzeller, J., Solomon, P.M., Lin, Y.-M., and Avouris, P. (2007). Gate work function engineering for nanotube-based circuits. Paper presented at: 54th IEEE International Solid-State Circuits Conference, ISSCC 2007, Febrary 11, 2007 - Febrary 15, 2007 (San Francisco, CA, United states, Institute of Electrical and Electronics Engineers Inc.).

Choi, H.C., and Lim, H. (2008). Mass transport of lithium ions intercalated in pyrene-functionalized single-walled carbon nanotubes: a facile way to Schottky diode (San Diego, CA, USA, SPIE).

Chongwu, Z., Jing, K., Yenilmez, E., and Hongjie, D. (2000). Modulated chemical doping of individual carbon nanotubes. Science *290*, 1552-1555.

Chun Wei, L., Keke, Z., Tantang, H., Lohani, A., Mhaisalkar, S.G., Lain-Jong, L., Nagahiro, T., Tamada, K., and Chen, Y. (2007). Tuning of electrical characteristics in networked carbon nanotube field-effect transistors using thiolated molecules. Applied Physics Letters *91*, 103515-103511.

Chung, J., Lee, K.-H., Lee, J., and Ruoff, R.S. (2004). Toward Large-Scale Integration of Carbon Nanotubes. Langmuir *20*, 3011-3017.

Collins, P.G., Arnold, M.S., and Avouris, P. (2001a). Engineering Carbon Nanotubes and Nanotube Circuits Using Electrical Breakdown. Science *292*, 706-709.

Collins, P.G., Hersam, M., Arnold, M., Martel, R., and Avouris, P. (2001b). Current Saturation and Electrical Breakdown in Multiwalled Carbon Nanotubes. Physical Review Letters *86*, 3128.

Derycke, V., Martel, R., Appenzeller, J., and Avouris, P. (2002). Controlling doping and carrier injection in carbon nanotube transistors. Applied Physics Letters *80*, 2773-2775.

Ding, L., Wang, S., Zhang, Z., Zeng, Q., Wang, Z., Pei, T., Yang, L., Liang, X., Shen, J., Chen, Q., *et al.* (2009). Y-contacted high-performance n-type single-walled carbon nanotube field-effect transistosrs: Scaling and comparison with Sc-contacted devices. Nano Letters *9*, 4209-4214.

Dong, L., Chirayos, V., Bush, J., Jiao, J., Dubin, V.M., Chebian, R.V., Ono, Y., Conley, J.F., and Ulrich, B.D. (2005). Floating-Potential Dielectrophoresis-Controlled Fabrication of Single-Carbon-Nanotube Transistors and Their Electrical Properties. The Journal of Physical Chemistry B *109*, 13148-13153.

Donghun, K., and et al. (2005). Oxygen-induced p-type doping of a long individual single-walled carbon nanotube. Nanotechnology *16*, 1048.

Du, X., Skachko, I., Barker, A., and Andrei, E.Y. (2008). Approaching ballistic transport in suspended graphene. Nat Nano *3*, 491-495.

Durkop, T., Getty, S.A., Cobas, E., and Fuhrer, M.S. (2003). Extraordinary Mobility in Semiconducting Carbon Nanotubes. Nano Letters *4*, 35-39.

Cortes, E., Rubert, A.A, Benitez, G., Carro, P., Vela, M.E., and Salvarezza, R.C. (2009) Enhanced Stability of Thiolate Self-Assembled Monolayers (SAMs) on Nanostructured Gold Substrates. Langmuir, *25*, 5661, (2009)

Engel, M., Small, J.P., Steiner, M., Freitag, M., Green, A.A., Hersam, M.C., and Avouris, P. (2008). Thin film nanotube transistors based on self-assembled, aligned, semiconducting carbon nanotube arrays. ACS Nano *2*, 2445-2452.

Fuhrer, M.S., Nyg, aring, rd, J., Shih, L., Forero, M., Yoon, Y.-G., Mazzoni, M.S., nbsp, C.*, et al.* (2000). Crossed Nanotube Junctions. Science *288*, 494-497.

Fujii, R., Gotoh, Y., Liao, M.Y., Tsuji, H., and Ishikawa, J. (2006). Work function measurement of transition metal nitride and carbide thin films. Vacuum *80*, 832-835.

Fukao, T., Nakamura, S., Kataura, H., and Shiraishi, M. (2006). Solution-processed single-walled carbon nanotube transistors with high mobility and large on/off ratio. Japanese Journal of Applied Physics, Part 1 (Regular Papers, Short Notes & Review Papers) *45*, 6524-6527.

Geim, A.K. (2009). Graphene: Status and Prospects. Science *324*, 1530-1534.

Geim, A.K., and Novoselov, K.S. (2007). The rise of graphene. Nature Materials *6*, 183-191.

Green, A.A., and Hersam, M.C. (2009). Processing and properties of highly enriched double-wall carbon nanotubes. Nat Nano *4*, 64-70.

Grundner, M., and Halbritter, J. (1984). On the natural Nb2O5 growth on Nb at room temperature. Surface Science *136*, 144-154.

Gyoung-Ho, B., Jea-Ho, H., Eun-Kyoung, J., Hye-Mi, S., Jeong, O.L., Ki-jeong, K., and Hyunju, C. (2008). On-chip electrical breakdown of metallic nanotubes for mass fabrication of carbon-nanotube-based electronic devices. IEEE Transactions on Nanotechnology *7*, 624-627.

Heinze, S., Radosavljevic, M., Tersoff, J., and Avouris, P. (2003). Unexpected scaling of the performance of carbon nanotube Schottky-barrier transistors. Physical Review B (Condensed Matter and Materials Physics) *68*, 235418-235411.

Heinze, S., Tersoff, J., Martel, R., Derycke, V., Appenzeller, J., and Avouris, P. (2002). Carbon Nanotubes as Schottky Barrier Transistors. Physical Review Letters *89*, 106801.

Hone, J., Llaguno, M.C., Nemes, N.M., Johnson, A.T., Fischer, J.E., Walters, D.A., Casavant, M.J., Schmidt, J., and Smalley, R.E. (2000). Electrical and thermal transport properties of magnetically aligned single wall carbon nanotube films. Applied Physics Letters *77*, 666-668.

Hunger, T., Lengeler, B., and Appenzeller, J. (2004). Transport in ropes of carbon nanotubes: contact barriers and Luttinger liquid theory. Physical Review B (Condensed Matter and Materials Physics) *69*, 195406-195401.

Hur, S.-H., Yoon, M.-H., Gaur, A., Shim, M., Facchetti, A., Marks, T.J., and Rogers, J.A. (2005). Organic nanodielectrics for low voltage carbon nanotube thin film transistors and complementary logic gates. Journal of the American Chemical Society *127*, 13808-13809.

Islam, M.F., Rojas, E., Bergey, D.M., Johnson, A.T., and Yodh, A.G. (2003). High Weight Fraction Surfactant Solubilization of Single-Wall Carbon Nanotubes in Water. Nano Letters *3*, 269-273.

Izard, N., Kazaoui, S., Hata, K., Okazaki, T., Saito, T., Iijima, S., and Minami, N. (2008). Semiconductor-enriched single wall carbon nanotube networks applied to field effect transistors. Applied Physics Letters *92*, 243112.

Izumida, T., Hatakeyama, R., Neo, Y., Mimura, H., Omote, K., and Kasama, Y. (2006). Electronic transport properties of Cs-encapsulated single-walled carbon nanotubes created by plasma ion irradiation. Applied Physics Letters *89*, 093121-093123.

Jang, H.W., and Lee, J.-L. (2003). Transparent Ohmic contacts of oxidized Ru and Ir on p-type GaN. Journal of Applied Physics *93*, 5416-5421.

Javey, A., Guo, J., Farmer, D.B., Wang, Q., Yenilmez, E., Gordon, R.G., Lundstrom, M., and Dai, H. (2004a). Self-Aligned Ballistic Molecular Transistors and Electrically Parallel Nanotube Arrays. Nano Letters *4*, 1319-1322.

Javey, A., Guo, J., Wang, Q., Lundstrom, M., and Dai, H. (2003). Ballistic carbon nanotube field-effect transistors. Nature *424*, 654-657.

Javey, A., Jing, G., Paulsson, M., Qian, W., Mann, D., Lundstrom, M., and Hongjie, D. (2004b). High-field quasiballistic transport in short carbon nanotubes. Physical Review Letters *92*, 106804-106801.

Javey, A., Shim, M., and Dai, H. (2002). Electrical properties and devices of large-diameter single-walled carbon nanotubes. Applied Physics Letters *80*, 1064-1066.

Javey, A., Tu, R., Farmer, D.B., Guo, J., Gordon, R.G., and Dai, H. (2005). High Performance n-Type Carbon Nanotube Field-Effect Transistors with Chemically Doped Contacts. Nano Letters *5*, 345-348.

Ji-Yong, P., Rosenblatt, S., Yaish, Y., Sazonova, V., Ustunel, H., Braig, S., Arias, T.A., Brouwer, P.W., and McEuen, P.L. (2004). Electron-phonon scattering in metallic single-walled carbon nanotubes. Nano Letters *4*, 517-520.

Jia, C., Klinke, C., Afzali, A., and Avouris, P. (2005). Self-aligned carbon nanotube transistors with charge transfer doping. Applied Physics Letters *86*, 123108-123101.

Jiao, L., Xian, X., Fan, B., Wu, Z., Zhang, J., and Liu, Z. (2008). Fabrication of Carbon Nanotube Diode with Atomic Force Microscopy Manipulation. The Journal of Physical Chemistry C *112*, 7544-7546.

Jie, L., Sun, Y., Peng, L.M., Sun, Z.Z., and Wang, X.R. (2007). Proximity and anomalous field-effect characteristics in double-wall carbon nanotubes. Applied Physics Letters *90*, 52109-52101.

Jing, K., Soh, H.T., Cassell, A.M., Quate, C.F., and Hongjie, D. (1998). Synthesis of individual single-walled carbon nanotubes on patterned silicon wafers. Nature *395*, 878-881.

Jing, L., Zhengxiang, G., Wei, S., Ming, N., Nagase, S., Dapeng, Y., Hengqiang, Y., and Xinwei, Z. (2005). Electronic structures of semiconducting double-walled carbon nanotubes: Important effect of interlay interaction. Chemical Physics Letters *414*, 429-433.

Kajiura, H., Nandyala, A., Coskun, U.C., Bezryadin, A., Shiraishi, M., and Ata, M. (2005). Electronic mean free path in as-produced and purified single-wall carbon nanotubes. Applied Physics Letters *86*, 122106-122101.

Kaminishi, D., Ozaki, H., Ohno, Y., Maehashi, K., Inoue, K., Matsumoto, K., Seri, Y., Masuda, A., and Matsumura, H. (2005). Air-stable n-type carbon nanotube field-effect transistors with Si[sub 3]N[sub 4] passivation films fabricated by catalytic chemical vapor deposition. Applied Physics Letters *86*, 113115-113113.

Kim, B.-K., Kim, J.-J., So, H.-M., Kong, K.-j., Chang, H., Lee, J.-O., and Park, N. (2006). Carbon nanotube diode fabricated by contact engineering with self-assembled molecules. Applied Physics Letters *89*, 243115-243113.

Kim, H.-S., Jeon, E.-K., Kim, J.-J., So, H.-M., Chang, H., Lee, J.-O., and Park, N. (2008). Air-stable n-type operation of Gd-contacted carbon nanotube field effect transistors. Applied Physics Letters *93*, 123106-123103.

Kim, W., Javey, A., Tu, R., Cao, J., Wang, Q., and Dai, H. (2005). Electrical contacts to carbon nanotubes down to 1 nm in diameter. Applied Physics Letters *87*, 173101-173103.

Kim, Y.A., Muramatsu, H., Hayashi, T., Endo, M., Terrenes, M., and Dresselhaus, M.S. (2004). Thermal stability and structural changes of double-walled carbon nanotubes by heat treatment. Chemical Physics Letters *398*, 87-92.

Kitiyanan, B., Alvarez, W.E., Harwell, J.H., and Resasco, D.E. (2000). Controlled production of single-wall carbon nanotubes by catalytic decomposition of CO on bimetallic Co-Mo catalysts. Chemical Physics Letters *317*, 497-503.

Kodama, Y., Sato, R., Inami, N., Shikoh, E., Yamamoto, Y., Hori, H., Kataura, H., and Fujiwara, A. (2007). Field-effect modulation of contact resistance between carbon nanotubes. Applied Physics Letters *91*, 133515-133513.

Kong, J., Zhou, C., Yenilmez, E., and Dai, H. (2000). Alkaline metal-doped n-type semiconducting nanotubes as quantum dots. Applied Physics Letters *77*, 3977-3979.

Krupke, R., Hennrich, F., Weber, H.B., Kappes, M.M., and Lohneysen, H. (2003). Simultaneous deposition of metallic bundles of single-walled carbon nanotubes using ac-dielectrophoresis. Nano Letters *3*, 1019-1023.

Landauer, R. (1996). Spatial variation of currents and fields due to localized scatterers in metallic conduction (and comment). Journal of Mathematical Physics *37*, 5259-5268.

Lay, M.D., Novak, J.P., and Snow, E.S. (2004). Simple Route to Large-Scale Ordered Arrays of Liquid-Deposited Carbon Nanotubes. Nano Letters *4*, 603-606.
Lee, J.U., Gipp, P.P., and Heller, C.M. (2004). Carbon nanotube p-n junction diodes. Applied Physics Letters *85*, 145-147.

Leonard, F., and Tersoff, J. (2000). Role of Fermi-level pinning in nanotube Schottky diodes. Physical Review Letters *84*, 4693-4696.

Leroy, W.P., Detavernier, C., Van Meirhaeghe, R.L., Kellock, A.J., and Lavoie, C. (2006). Solid-state formation of titanium carbide and molybdenum carbide as contacts for carbon-containing semiconductors. Journal of Applied Physics *99*, 063704-063705.

Leroy, W.P., Detavernier, C., Van Meirhaeghe, R.L., and Lavoie, C. (2007). Thin film solid-state reactions forming carbides as contact materials for carbon-containing semiconductors. Journal of Applied Physics *101*, 053714-053710.

Li, X., Wang, X., Zhang, L., Lee, S., and Dai, H. (2008). Chemically Derived, Ultrasmooth Graphene Nanoribbon Semiconductors. Science *319*, 1229-1232.

Li, Y.F., Hatakeyama, R., and Kaneko, T. (2007). n-type and p-type double-walled carbon nanotube field-effect transistors based on charge-transfer modulation. Applied Physics A: Materials Science and Processing *88*, 745-749.

Liang, Y.X., and Wang, T.H. (2004). A double-walled carbon nanotube field-effect transistor using the inner shell as its gate. Physica E: Low-Dimensional Systems and Nanostructures *23*, 232-236.

Lim, H., Shin, H.S., Shin, H.-J., and Choi, H.C. (2008). Lithium Ions Intercalated into Pyrene-Functionalized Carbon Nanotubes and Their Mass Transport: A Chemical Route to Carbon Nanotube Schottky Diode. Journal of the American Chemical Society *130*, 2160-2161.

Lin, Y.-M., Dimitrakopoulos, C., Jenkins, K.A., Farmer, D.B., Chiu, H.-Y., Grill, A., and Avouris, P. (2010). 100-GHz Transistors from Wafer-Scale Epitaxial Graphene. Science *327*, 662.

Liu, K., Wang, W., Xu, Z., Bai, X., Wang, E., Yao, Y., Zhang, J., and Liu, Z. (2009). Chirality-dependent transport properties of double-walled nanotubes measured in situ on their field-effect transistors. Journal of the American Chemical Society *131*, 62-63.

Lu, C., An, L., Fu, Q., Liu, J., Zhang, H., and Murduck, J. (2006). Schottky diodes from asymmetric metal-nanotube contacts. Applied Physics Letters *88*, 133501-133503.

Lu, J., Yin, S., Peng, L.M., Sun, Z.Z., and Wang, X.R. (2007). Proximity and anomalous field-effect characteristics in double-wall carbon nanotubes. Applied Physics Letters *90*, 052109.

M, S.S. (1981). Physics of Semiconductor Devices.

Madelung, O., ed. (2000). Technology and Applications of Amorphous Silicon (Springer, Berlin).

Maiti, A., and Ricca, A. (2004). Metal-nanotube interactions - binding energies and wetting properties. Chemical Physics Letters *395*, 7-11.

Mann, D., Javey, A., Jing, K., Qian, W., and Hongjie, D. (2003). Ballistic transport in metallic nanotubes with reliable Pd ohmic contacts. Nano Letters *3*, 1541-1544.

Manohara, H.M., Wong, E.W., Schlecht, E., Hunt, B.D., and Siegel, P.H. (2005). Carbon Nanotube Schottky Diodes Using Ti−Schottky and Pt−Ohmic Contacts for High Frequency Applications. Nano Letters *5*, 1469-1474.

Martel, R., Derycke, V., Lavoie, C., Appenzeller, J., Chan, K.K., Tersoff, J., and Avouris, P. (2001). Ambipolar Electrical Transport in Semiconducting Single-Wall Carbon Nanotubes. Physical Review Letters *87*, 256805.

Martel, R., Schmidt, T., Shea, H.R., Hertel, T., and Avouris, P. (1998). Single- and multi-wall carbon nanotube field-effect transistors. Applied Physics Letters *73*, 2447-2449.

Matsuoka, K., Kataura, H., and Shiraishi, M. (2006). Ambipolar single electron transistors using side-contacted single-walled carbon nanotubes. Chemical Physics Letters *417*, 540-544.

Merchant, C.A., and Markovic, N. (2009). The photoresponse of spray-coated and free-standing carbon nanotube films with Schottky contacts. Nanotechnology *20*,175202.

Nemec, N., Tomanek, D., and Cuniberti, G. (2006). Contact Dependence of Carrier Injection in Carbon Nanotubes: An Ab Initio Study. Physical Review Letters *96*, 076802-076804.

Nihey, F., Ichihashi, T., Yudasaka, M., and Iijima, S. (2001). Electrical contact with titanium carbide to an individual single-walled carbon nanotube. Paper presented at: Nanonetwork Materials: Fullerenes, Nanotubes, and Related Systems, 15-18 Jan 2001 (USA, AIP).

Nosho, Y., and et al. (2006). Relation between conduction property and work function of contact metal in carbon nanotube field-effect transistors. Nanotechnology *17*, 3412.

Nosho, Y., Ohno, Y., Kishimoto, S., and Mizutani, T. (2005). n-type carbon nanotube field-effect transistors fabricated by using Ca contact electrodes. Applied Physics Letters *86*, 073105-073103.

Nouchi, R., Tomita, H., Ogura, A., Kataura, H., and Shiraishi, M. (2008). Logic circuits using solution-processed single-walled carbon nanotube transistors. Applied Physics Letters *92*, 253507.

Nougaret, L., Happy, H., Dambrine, G., Derycke, V., Bourgoin, J.P., Green, A.A., and Hersam, M.C. (2009). 80 GHz field-effect transistors produced using high purity semiconducting single-walled carbon nanotubes. Applied Physics Letters *94*, 243505.

Novoselov, K.S., Geim, A.K., Morozov, S.V., Jiang, D., Zhang, Y., Dubonos, S.V., Grigorieva, I.V., and Firsov, A.A. (2004). Electric Field Effect in Atomically Thin Carbon Films. Science *306*, 666-669.

Novoselov, K.S., Jiang, D., Schedin, F., Booth, T.J., Khotkevich, V.V., Morozov, S.V., and Geim, A.K. (2005). Two-dimensional atomic crystals. Proceedings of the National Academy of Sciences of the United States of America *102*, 10451-10453.

Ohishi, M., Shiraishi, M., Ochi, K., Kubozono, Y., and Kataura, H. (2006). Improvements in the device characteristics of random-network single-walled carbon nanotube transistors by using high- k gate insulators. Applied Physics Letters *89*, 203505.

Okada, S., and Oshiyama, A. (2003). Curvature-induced metallization of double-walled semiconducting zigzag carbon nanotubes. Physical Review Letters *91*, 216801.

Ozel, T., Gaur, A., Rogers, J.A., and Shim, M. (2005). Polymer electrolyte gating of carbon nanotube network transistors. Nano Letters *5*, 905-911.

Patil, N., Deng, J., Lin, A., Wong, H.S.P., and Mitra, S. (2008a). Design methods for misaligned and mispositioned carbon-nanotube immune circuits. IEEE Transactions on Computer-Aided Design of Integrated Circuits and Systems *27*, 1725-1736.

Patil, N., Lin, A., Myers, E.R., Wong, H.S.P., and Mitra, S. (2008b). Integrated wafer-scale growth and transfer of directional carbon nanotubes and misaligned-carbon-nanotube-immune logic structures. Paper presented at: 2008 Symposium on VLSI Technology, 17-20 June 2008 (Piscataway, NJ, USA, IEEE).

Perello, D., Kim, M.J., Cha, D., Han, G.H., Bae, D.J., Jeong, S.Y., Lee, Y.H., and Yun, M. (2007). Schottky barrier engineering in carbon nanotube with various metal electrodes. Paper presented at: 2007 7th IEEE International Conference on Nanotechnology - IEEE-NANO 2007, August 2, 2007 - August 5, 2007 (Hong Kong, China, Inst. of Elec. and Elec. Eng. Computer Society).

Po-Wen, C., and Chien-Hua, C. (2008). High-performance carbon nanotube network transistors for logic applications. Applied Physics Letters *92*, 063511.

Qing, C., Hoon-sik, K., Pimparkar, N., Kulkarni, J.P., Congjun, W., Moonsub, S., Roy, K., Alam, M.A., and Rogers, J.A. (2008). Medium-scale carbon nanotube thin-film integrated circuits on flexible plastic substrates. Nature *454*, 495-500.

Rao, A.M., Chen, J., Richter, E., Schlecht, U., Eklund, P.C., Haddon, R.C., Venkateswaran, U.D., Kwon, Y.K., and Tománek, D. (2001). Effect of van der Waals Interactions on the Raman Modes in Single Walled Carbon Nanotubes. Physical Review Letters *86*, 3895.

Rao, S.G., Huang, L., Setyawan, W., and Hong, S. (2003). Nanotube electronics: Large-scale assembly of carbon nanotubes. Nature *425*, 36-37.

Romero, R., Ramos-Barrado, J.R., Martin, F., and Leinen, D. (2004). Nb_2O_5 thin films obtained by chemical spray pyrolysis. Surface and Interface Analysis *36*, 888-891.

Rusu, P.C., and Brocks, G. (2006). Work functions of self-assembled monolayers on metal surfaces by first-principles calculations. Physical Review B (Condensed Matter and Materials Physics) *74*, 073414.

Samsonov, G.V., Podchernyaeva, I.A., Fomenko, V.S., Lovrenko, V.A., Okhremchuk, L.N., and Protsenko, T.G. (1972). Correlation between the work functions of transition metal carbides in their homogeneity regions and surface recombination of hydrogen atoms. Powder Metallurgy and Metal Ceramics *11*, 389-392.

Santerre, F., El Khakani, M.A., Chaker, M., and Dodelet, J.P. (1999). Properties of TiC thin films grown by pulsed laser deposition. Applied Surface Science *148*, 24-33.

Schwierz, F. (2010). Graphene transistors. Nat Nano *5*, 487-496.

Sebastian Taeger, Daniel Sickert, Petar Atanasov, Gerald Eckstein, and Michael Mertig (2006). Self-assembly of carbon nanotube field-effect transistors by ac-dielectrophoresis. physica status solidi (b) *243*, 3355-3358.

Seidel, R., Graham, A.P., Unger, E., Duesberg, G.S., Liebau, M., Steinhoegl, W., Kreupl, F., Hoenlein, W., and Pompe, W. (2004). High-current nanotube transistors. Nano Letters *4*, 831-834.

Seo, H.-W., Han, C.-S., Choi, D.-G., Kim, K.-S., and Lee, Y.-H. (2005). Controlled assembly of single SWNTs bundle using dielectrophoresis. Microelectronic Engineering *81*, 83-89.

Shan, B., Cho, K. (2004). *Ab initio* study of Schottky barriers at metal-nanotube contacts. Physical Review B *70*, 233405.

Sharma, S.P., and Hines, L.L. (1983). OXIDATION OF RUTHENIUM. IEEE transactions on components, hybrids, and manufacturing technology *CHMT-6*, 89-92.

Shidong, W., and Grifoni, M. (2005). Helicity and electron-correlation effects on transport properties of double-walled carbon nanotubes. Physical Review Letters *95*, 266802-266801.

Shidong, W., and Grifoni, M. (2007). Schottky-barrier double-walled carbon-nanotube field-effect transistors. Physical Review B (Condensed Matter and Materials Physics) *76*, 33413-33411.

Shim, M., Javey, A., Shi Kam, N.W., and Dai, H. (2001). Polymer Functionalization for Air-Stable n-Type Carbon Nanotube Field-Effect Transistors. Journal of the American Chemical Society *123*, 11512-11513.

Shimada, T., Sugai, T., Ohno, Y., Kishimoto, S., Mizutani, T., Yoshida, H., Okazaki, T., and Shinohara, H. (2004). Double-wall carbon nanotube field-effect

transistors: ambipolar transport characteristics. Applied Physics Letters *84*, 2412-2414.

Slava V. Rotkin, S.S., ed. (2005). Applied Physics of Carbon Nanotubes (Springer).

Snow, E.S., Campbell, P.M., Ancona, M.G., and Novak, J.P. (2005). High-mobility carbon-nanotube thin-film transistors on a polymeric substrate. Applied Physics Letters *86*, 33105-33101.

Snow, E.S., Novak, J.P., Campbell, P.M., and Park, D. (2003). Random networks of carbon nanotubes as an electronic material. Applied Physics Letters *82*, 2145-2147.

So, H.-M., Kim, B.-K., Park, D.-W., Beom, S.K., Kim, J.-J., Kong, K.-J., Chang, H., and Lee, J.-O. (2007). Selective suppression of conductance in metallic carbon nanotubes. Journal of the American Chemical Society *129*, 4866-4867.

Stadermann, M., Papadakis, S.J., Falvo, M.R., Novak, J., Snow, E., Fu, Q., Liu, J., Fridman, Y., Boland, J.J., Superfine, R., *et al.* (2004). Nanoscale study of conduction through carbon nanotube networks. Physical Review B *69*, 201402.

Stokes, P., and Khondaker, S.I. (2008). Local-gated single-walled carbon nanotube field effect transistors assembled by AC dielectrophoresis. Nanotechnology *19*, 175202.

Stokes, P., Silbar, E., Zayas, Y.M., and Khondaker, S.I. (2009). Solution processed large area field effect transistors from dielectrophoreticly aligned arrays of carbon nanotubes. Applied Physics Letters *94*, 113104.

Sumanasekera, G.U., Adu, C.K.W., Fang, S., and Eklund, P.C. (2000). Effects of Gas Adsorption and Collisions on Electrical Transport in Single-Walled Carbon Nanotubes. Physical Review Letters *85*, 1096.

Sunkyung, M., Woon, S., Nam, K., Joon Sung, L., Pil Sun, N., Soon-Gul, L., Jongwan, P., Myung-Hwa, J., Hyun-Woo, L., Kicheon, K., *et al.* (2007). Current-carrying capacity of double-wall carbon nanotubes. Nanotechnology *18*, 235201.

Tans, S.J., Verschueren, A.R.M., and Dekker, C. (1998). Room-temperature transistor based on a single carbon nanotube. Nature *393*, 49-52.

Toth, L.E., ed. (1971). Transition Metal Carbides and Nitrides (Academic Press, New York and London).

Tseng, Y.-C., Phoa, K., Carlton, D., and Bokor, J. (2006). Effect of Diameter Variation in a Large Set of Carbon Nanotube Transistors. Nano Letters *6*, 1364-1368.

Vijayaraghavan, A., Blatt, S., Weissenberger, D., Oron-Carl, M., Hennrich, F., Gerthsen, D., Hahn, H., and Krupke, R. (2007). Ultra-Large-Scale Directed Assembly of Single-Walled Carbon Nanotube Devices. Nano Letters *7*, 1556-1560.

Vitale, V., Curioni, A., and Andreoni, W. (2008). Metal−Carbon Nanotube Contacts: The Link between Schottky Barrier and Chemical Bonding. Journal of the American Chemical Society *130*, 5848-5849.

Wang, S., Liang, X.L., Chen, Q., Yao, K., and Peng, L.M. (2007). High-field electrical transport and breakdown behavior of double-walled carbon nanotube field-effect transistors. Carbon *45*, 760-765.

Wang, S., Liang, X.L., Chen, Q., Zhang, Z.Y., and Peng, L.M. (2005). Field-effect characteristics and screening in double-walled carbon nanotube field-effect transistors. Journal of Physical Chemistry B *109*, 17361-17365.

White, C.T., and Todorov, T.N. (1998). Carbon nanotubes as long ballistic conductors. Nature *393*, 240-242.

Wilder, J.W.G., Venema, L.C., Rinzler, A.G., Smalley, R.E., and Dekker, C. (1998). Electronic structure of atomically resolved carbon nanotubes. Nature *391*, 59-62.

Woong, K., Hee Cheul, C., Moonsub, S., Yiming, L., Dunwei, W., and Hongjie, D. (2002). Synthesis of ultralong and high percentage of semiconducting single-walled carbon nanotubes. Nano Letters *2*, 703-708.

Yang, G., Amro, N.A., Starkewolfe, Z.B., Liu, G. (2004). Molecular-Level Approach To Inhibit Degradations of Alkanethiol Self-Assembled Monolayers in Aqueous Media. Langmuir, *20*, 3995.

Yang, M.H., Teo, K.B.K., Milne, W.I., and Hasko, D.G. (2005). Carbon nanotube Schottky diode and directionally dependent field-effect transistor using asymmetrical contacts. Applied Physics Letters *87*, 253116-253113.

Yu-Ming, L., Appenzeller, J., Knoch, J., and Avouris, P. (2005a). High-performance carbon nanotube field-effect transistor with tunable polarities. IEEE Transactions on Nanotechnology *4*, 481-489.

Yu-Ming, L., Appenzeller, J., Zhihong, C., Zhi-Gang, C., Hui-Ming, C., and Avouris, P. (2005b). High-performance dual-gate carbon nanotube FETs with 40-nm gate length. IEEE Electron Device Letters *26*, 823-825.

Yu, A., Bekyarova, E., Itkis, M.E., Fakhrutdinov, D., Webster, R., and Haddon, R.C. (2006). Application of centrifugation to the large-scale purification of electric arc-produced single-walled carbon nanotubes. Journal of the American Chemical Society *128*, 9902-9908.

Yuegang, Z., Aileen, C., Jien, C., Qian, W., Woong, K., Yiming, L., Morris, N., Yenilmez, E., Jing, K., and Hongjie, D. (2001). Electric-field-directed growth of aligned single-walled carbon nanotubes. Applied Physics Letters *79*, 3155-3157.

Yun-Hi, L., Jong-Hee, L., Chung, S.J., Lee, S., and Ju, B.K. (2006). Carrier carrying capacity of one-step grown suspended carbon nanotube bridge with carbon nanotube contact electrodes: for practical one-dimensional electronics. Applied Physics Letters *89*, 73109-73101.

Yung-Fu, C., and Fuhrer, M.S. (2005). Electric-field-dependent charge-carrier velocity in semiconducting carbon nanotubes. Physical Review Letters *95*, 236803-236801.

Zavodchikova, M.Y., Kulmala, T., Nasibulin, A.G., Ermolov, V., Franssila, S., Grigoras, K., and Kauppinen, E.I. (2009). Carbon nanotube thin film transistors based on aerosol methods. Nanotechnology *20*, 085201.

Zhang, W.J., Zhang, Q.F., Chai, Y., Shen, X., and Wu, J.L. (2007a). Gate voltage dependent characteristics of p-n diodes and bipolar transistors based on multiwall CNx/carbon nanotube intramolecular junctions. Nanotechnology *18*, 395205-395201.

Zhang, Y., Franklin, N.W., Chen, R.J., and Dai, H. (2000). Metal coating on suspended carbon nanotubes and its implication to metal-tube interaction. Chemical Physics Letters *331*, 35-41.

Zhang, Y., Ichihashi, T., Landree, E., Nihey, F., and Iijima, S. (1999). Heterostructures of Single-Walled Carbon Nanotubes and Carbide Nanorods. Science *285*, 1719-1722.

Zhang, Z., Liang, X., Wang, S., Yao, K., Hu, Y., Zhu, Y., Chen, Q., Zhou, W., Li, Y., Yao, Y., *et al.* (2007b). Doping-Free Fabrication of Carbon Nanotube Based Ballistic CMOS Devices and Circuits. Nano Letters *7*, 3603-3607.

Zhang, Z. B., Zhang, S. L., Campbell, E. B. E. (2006). All-around contact for carbon nanotube field-effect transistors made by ac dielectrophoresis. J. Vac. Sci. Technol. *B* ***24***, 131.

Zhang, Z.Y., Wang, S., Ding, L., Liang, X.L., Xu, H.L., Shen, J., Chen, Q., Cui, R.L., Li, Y., and Peng, L.M. (2008). High-performance n-type carbon nanotube field-effect transistors with estimated sub-10-ps gate delay. Applied Physics Letters *92*, 133117-133113.

Zhen, Y., Kane, C.L., and Dekker, C. (2000). High-field electrical transport in single-wall carbon nanotubes. Physical Review Letters *84*, 2941-2944.

Zhou, Y., Gaur, A., Hur, S.-H., Kocabas, C., Meitl, M.A., Shim, M., and Rogers, J.A. (2004). p-Channel, n-Channel Thin Film Transistors and p−n Diodes Based on Single Wall Carbon Nanotube Networks. Nano Letters *4*, 2031-2035.

List of Publications
Referred Journal Papers

Huang. L, Chor. E. F, Wu. Y, and Guo. Z, Fabrication of single-walled carbon nanotube Schottky diode with gold contacts modified by asymmetric thiolate molecules, Carbon, 48, 1298, (2010).

Huang. L, Chor. E. F, Wu. Y, and Guo. Z, Investigations of niobium carbide contact for carbon-nanotube-based devices, Nanotechnology, 21, 095201, (2010).

Zhang. C, Wang. Y, ***Huang. L***, Wu. Y, Electrical transport study of magnetomechanical nanocontact in ultrahigh vacuum using carbon nanowalls, Applied Physics Letters, 97, 062102, (2010).

Huang. L, Chor. E. F and Wu. Y, Doping-free fabrication of *n*-type random network single-walled carbon nanotube field effect transistor with Yttrium contacts, Physica E, 43, 1365, (2011).

Huang. L, Chor. E. F and Wu. Y, The Semiconducting-Semiconducting Double-Wall Carbon Nanotube Field Effect Transistors, submitted to Fullerenes, Nanotubes and Carbon Nanostructures.

Conference Presentations

L. Huang, E. F. Chor, Y. Wu, and Z. Guo. Z, Comparison between SWNT and DWNT field effect transistors with Ru contacts, International Conferences on Materials for Advanced Technologies (ICMAT) 2007, Singapore.

L. Huang, E. F. Chor, Y. Wu, and Z. Guo, Niobium Carbide (Nb_2C) Contact for Carbon Nanotube Based Devices, International Conferences on Materials for Advanced Technologies (ICMAT) 2009, Singapore.

L. Huang, E. F. Chor, Y. Wu, and Z. Guo, Comparison Between Double- and Single-Wall Carbon Nanotube Field Effect Transistors, International Conferences on Materials for Advanced Technologies (ICMAT) 2009, Singapore.

L. Huang, E. F. Chor, Y. Wu, and Z. Guo, Fabrication of Single Wall Carbon Nanotube Schottky Diodes by Controlling Energy-Level Alignment at Carbon Nanotube/Au Contacts with Self-Assembled Molecules, Tenth International Conference on the Science and Application of Nanotubes (NT09) 2009, China.